

Physik Department
der Technischen Universität München
Lehrstuhl für Biophysik E22

**Electrochemical Sensing of Surface Reactions on Gallium
Arsenide-based Semiconductor Devices Functionalized with
Bio-organic Molecular Systems**

Daniel Gassull

Vollständiger Abdruck der von der Fakultät für Physik der Technischen Universität München zur Erlangung des akademischen Grades eines

Doktors der Naturwissenschaften (Dr. rer. nat.)

genehmigten Dissertation.

Vorsitzender: Univ.-Prof. Dr. Roland Netz

Prüfer der Dissertation: 1. Univ.-Prof. Dr. Matthias Rief
2. Univ.-Prof. Dr. Motomu Tanaka,
Ruprecht-Karls-Universität Heidelberg.

Die Dissertation wurde am 03.07.2007 bei der Technischen Universität München eingereicht und durch die Fakultät für Physik am 24.07.2007 angenommen.

Als meus pares

Maria Àngels i Miquel Àngel,

i al meu germà

Abel

Zusammenfassung

Das Ziel dieser Arbeit ist die elektrochemische Charakterisierung von mit (bio)organischen Systemen funktionalisierten GaAs Oberflächen, vor dem Hintergrund einer Anwendung als chemisch/biochemischer Sensor. Die Beschichtung mit monomolekularen Mercaptobiphenyl-Schichten (MBPs) via kovalente Arsenid-Sulfid Bindungen verhindert die elektrochemische Degradation von GaAs in physiologischen Elektrolyten für länger als einen Tag. Wie im Hauptteil dieser Arbeit gezeigt wird, bieten Impedanzspektroskopie-Messungen (über einen weiten Frequenzbereich und bei verschiedenen Vorspannungen) einzigartige Möglichkeiten zur quantitativen Identifizierung verschiedener elektrochemischer Schichten.

Im Kapitel 5 wird die pH-Empfindlichkeit von GaAs Elektroden untersucht, welche mit hydrophoben CH₃-MBP Monolagen beschichtet sind. Der Widerstand R_p der funktionalisierten GaAs- Grenzfläche ist proportional zum pH-Wert des Elektrolyten und der externen Vorspannung U_{bias} , woraus man die beobachtete pH-Empfindlichkeit des funktionalisierten GaAs zu **35 mVpH⁻¹** berechnen kann. Die Modellierung mit vereinfachten Ersatzschaltkreisen erlaubt es, aus mehreren möglichen Modellen für Mechanismus der pH-Empfindlichkeit ein Modell auszuwählen, dass als Erklärung die Adsorption von OH⁻-Ionen an die hydrophoben CH₃-MBP Monolagen identifizieren.

Kapitel 5.2 beinhaltet die Funktionalisierung von AlGaAs/GaAs Heterostrukturen mit CH₃-MBP Monolagen. Unter Beibehaltung der etablierten Funktionalisierungs-Protokolle zeigt der mit CH₃-MBP Monolagen funktionalisierte 2DEG-Baustein eine ausgezeichnete elektrochemische Stabilität. Darüber hinaus zeigt der Flächenwiderstand, welcher der Ladungsträgerkonzentration in der 2DEG Schicht entspricht, ähnlich wie bei reinem GaAs eine deutliche Abhängigkeit vom pH-Wert des Elektrolyten. Bemerkenswert ist zudem, dass die pH-Empfindlichkeit von **36 mVpH⁻¹** des funktionalisierten 2DEG vergleichbar mit der von reinem GaAs ist, was auf den gleichen molekularen Mechanismus schließen lässt.

Um ein tieferes Verständnis über den Mechanismus der pH-Empfindlichkeit von hydro-

phobem GaAs zu erlangen, wurde der Einfluss verschiedener Ionen im Rahmen der Hofmeister-Serie untersucht. Dies ist Gegenstand von Kapitel 6. Dort wird die pH-Abhängigkeit anhand von reinen GaAs-Elektroden untersucht, welche wiederum mit CH₃-MBP Monolagen funktionalisiert sind. Im Vergleich zu I⁻ gibt es bei Cl⁻-Anionen eine höhere pH-Abhängigkeit, wobei die Interpretation ist, dass I⁻-Anionen eine höhere Adsorptionskraft an die Oberfläche besitzen als Cl⁻ Ionen (Hofmeister-Serie).

Im letzten Kapitel (Kapitel 7) wird eine mögliche Anwendung von Oberflächen-gestützten Lipid-Monolagen auf MBP-funktionalisiertem GaAs als elektrochemischer Biosensor untersucht. Unter Verwendung eines leicht veränderten Ersatzschaltkreises, der die Eigenschaften von Lipidmembranen als Diffusionsbarrieren berücksichtigt, wird demonstriert, dass das System in der Lage ist, sowohl die Kinetik der Membranbildung als auch mit einer solchen Kompositmembran das Oberflächenpotential der Membran zu detektieren. Darüber hinaus kann die enzymatische Aktivität der Phospholipase A₂, nämlich das Abschneiden einer Fettsäure von einem Phospholipidmolekül, durch Impedanzspektroskopie in einem großen Frequenzbereich erfolgreich beobachtet werden.

Die erzielten Resultate demonstrieren, dass mit (bio)organischen molekularen Systemen funktionalisiertes GaAs sich gut eignet, Veränderungen von Oberflächenpotentialen in wässrigen Lösungen zu detektieren, welche durch verschiedene chemische/biochemische Stimuli verursacht werden, wie beispielsweise pH Veränderungen, Adsorption von Ionen, oder enzymatische Reaktionen. Aufgrund der durch die Beschichtung mit organischen Monolayern erzielten exzellenten elektrochemischen Stabilität können mit Hilfe der Impedanzspektroskopie über einen weiten Frequenzbereich verschiedene elektrochemische Schichten quantitativ unterschieden werden. Die Tatsache, dass die beobachtete pH Empfindlichkeit von reinem GaAs vergleichbar ist zu der von 2DEG Bausteinen, ist ein überzeugendes Indiz dafür, dass die quantitative Auswertung einer funktionalisierten Oberfläche ein Punkt von kritischer Bedeutung für eine hohe elektrochemische Empfindlichkeit ist.

Summary

The general aim of the present work is the electrochemical characterization of GaAs surfaces functionalized with bioorganic molecular systems towards chemical/biochemical sensor applications. Deposition of monomolecular films of mercaprobiphenyls (MBPs) via covalent arsenide-sulfide bonding prevents the electrochemical degradation of GaAs in physiological electrolytes for more than a day. As demonstrated in the main part of the thesis, measurements of impedance spectroscopy in a wide frequency range and at various bias potentials offer a unique advantage to identify different electrochemical layers in a quantitative manner.

In Chapter 5, pH sensitivity of GaAs electrodes coated with hydrophobic CH₃-MBP monolayers is reported. The interface resistance of the functionalized GaAs (R_p) is proportional to the electrolyte pH and external potential U_{bias} from which the apparent pH sensitivity of the functionalized GaAs can be calculated to be **35 mVpH⁻¹**. Among several possible scenarios, simplified equivalent circuit models enable one to account for the mechanism of pH sensitivity in terms of the adsorption of OH⁻ ions on hydrophobic CH₃-MBP monolayers.

In Chapter 5.2, two-dimensional electron gas (2DEG) devices based on AlGaAs/GaAs heterostructures are functionalized with CH₃-MBP monolayers. Following the same functionalization protocols, the 2DEG device functionalized with CH₃-MBP monolayers shows an excellent electrochemical stability. Furthermore, similar to that found on bulk GaAs, the sheet resistance, i.e. the carrier concentration in the 2DEG layer, shows a clear sensitivity to the electrolyte pH. Interestingly, the pH sensitivity of the functionalized 2DEG, **36 mVpH⁻¹**, is comparable to that of bulk GaAs with the same monolayer, implying that the obtained sensitivity is governed by the same molecular mechanism.

To gain a deeper insight into the mechanism of pH sensitivity of hydrophobic GaAs, the influence of different counter anions on the pH sensitivity is studied in Chapter 6 within the framework of Hofmeister series. Here, the sensitivity is evaluated by impedance spectroscopy of bulk GaAs electrodes with CH₃-MBP monolayers.

In comparison to I^- , a higher pH sensitivity can be found in the presence of Cl^- , which can be understood as a higher adsorption strength of I^- anions on the surface with respect to Cl^- anions (Hofmeister series).

In the last chapter (Chapter 7), a potential application of supported lipid monolayers on MBP-functionalized GaAs as electrochemical biosensors is exploited. Using a slightly modified equivalent circuit model that takes the diffusion barrier properties of lipid membranes, the kinetics of membrane formation as well as the capability of such composite membranes to detect the membrane surface potential is quantitatively demonstrated. Furthermore, the enzymatic activity of phospholipase A_2 , i.e. cleavage of a fatty acid from a phospholipids molecule, can successfully be monitored by measuring impedance spectra in a wide frequency regime.

The obtained results show that GaAs functionalized with (bio)organic molecular systems possess a large potential to sense the change in potentials on the surface in aqueous electrolytes caused by various chemical/biochemical stimuli, e.g. pH changes, absorption of counter ions, and enzymatic reactions. Owing to the excellent electrochemical stability achieved by deposition of organic monolayers, different electrochemical layers can quantitatively be distinguished by covering a wide frequency range by impedance spectroscopy. The fact that the apparent pH sensitivity found on bulk GaAs is comparable to that of 2DEG devices convinces that the quantitative surface functionalization is a key that determines the electrochemical sensitivity.

Contents

Zusammenfassung	i
Summary	iii
1 Introduction and Motivation	1
2 Materials and Methods	5
2.1 Materials	5
2.1.1 Bulk Chemicals	5
2.1.2 GaAs	6
2.2 Sample Preparation	8
2.2.1 Deposition of Monolayers of MBP on Bulk GaAs and 2DEG Devices	8
2.2.2 Ohmic Contacts	9
2.2.3 Buffers	9
2.2.4 Deposition of Lipid Monolayers	11
2.3 Characterization Methods	11
2.3.1 Atomic Force Microscopy (AFM)	11
2.3.2 Ellipsometry	12
2.3.3 Principles of Contact Angle	12
2.3.4 Current-Voltage Characteristics of 2DEG Devices	13
2.3.5 Electrochemical Impedance Spectroscopy	14

3	Physical Background	17
3.1	Surface Electronic Structure of (GaAs) Semiconductors	17
3.1.1	Band Diagram of Semiconductors at Various Bias Potentials	17
3.1.2	The Depletion Layer Capacitance (Mott-Schottky relation)	19
3.1.3	The Influence of Surface States	20
3.2	Electrochemistry of GaAs Semiconductors in Aqueous Electrolytes	21
3.2.1	Electrochemistry at GaAs/Electrolyte Interface	22
3.2.2	Electrochemical Reactions at GaAs/Electrolyte Interface	24
4	Principles of Electrochemical Impedance Spectroscopy	27
4.1	Fundamental Principles	27
4.2	Frequency Dispersion Impedance Spectra	29
4.3	Equivalent Circuit Models	30
4.3.1	Circuit Elements	31
4.4	Analysis of Impedance Spectra with Circuit Model	34
4.5	Requirements for Biosensor Applications	37
4.5.1	Capacitive Sensing of Surface Potentials	37
4.5.2	Identification of Different Electrochemical Layers	39
5	pH Sensitivity of Bulk GaAs coated with CH₃-MBP Monolayers	41
5.1	Impedance Spectroscopy on Bulk GaAs Electrodes	42
5.1.1	Functionalized GaAs Electrodes: Modelling of Impedance Spectra	42
5.1.2	Response to Bias Potential Sweeps	44
5.1.3	Response to Electrolyte pH	47
5.1.4	Mechanism of the pH Sensitivity	51
5.2	pH Sensitivity of Two-Dimensional-Electron-Gas (2DEG) Devices Functionalized with CH ₃ -MBP Monolayers	56
5.2.1	Stability of Functionalized 2DEG Devices	56

<i>CONTENTS</i>	vii
5.2.2 Response of 2DEG Devices to Electrolyte pH	58
5.3 Summary and Conclusions	60
6 Influence of Counter Ions: Hofmeister Series	63
6.1 Influence of Counter Ions on Impedance Spectra	63
6.2 Response to Bias Potential Sweeps	65
6.3 pH Sensitivity in the Presence of I ⁻ and Cl ⁻	67
6.4 Thermodynamics of Ion Adsorption	69
6.5 Conclusions	72
7 Electrochemical Monitoring of Structure and Function of Lipid Membranes on Functionalized GaAs	73
7.1 Electrochemical Characterization of Lipid Monolayers	74
7.2 Kinetics of Membrane Formation	77
7.3 Capacitive Sensing of Surface Charge Density	79
7.4 Electrical Monitoring of Enzyme Functions	82
7.5 Conclusions	84
Conclusions	85
Outlook	89
A Appendix	91
A.1 Physical Characterization X-MBP Monolayers on GaAs	91
A.1.1 AFM	91
A.1.2 Ellipsometry	93
A.1.3 Contact Angle	93
A.2 Electron Transfer between Redox Couples and Semiconductors	95
A.3 Lipid Bilayers on GaAs coated with OH-MBP Monolayers	97
A.4 Salt Concentration Sensitivity on 2DEG Devices coated with CH ₃ -MBP Monolayers	99

Chapter 1

Introduction and Motivation

Functional immobilization of biological systems on solid surfaces is an interdisciplinary challenge, which embraces numerous scientific and technological applications. Scientific applications include understanding of the basic principle of cell adhesion and signal transduction, while the technological applications include the high throughput screening assays and protein/DNA chips. One of the primary steps towards this goal is to "bridge" hard solids and soft biological matters by functionalization of solid surfaces with organic, biocompatible layers.

Semiconductors exhibit advantageous properties over other substrate materials, such as glass, metal and plastics, which allow for opto-electric sensing with no tracer molecules (e.g. fluorescent probes) at very low noise levels. This enables one to remarkably "down-scale" the sensing units, even down to the molecular-level counting. In fact, recent reports using Si-based nano-wires [1] [2] and carbon nanotubes [3] successfully demonstrated the detection of specific binding on a single molecule level. To date, ion-sensitive field effect transistors (ISFETs) setups [4] setups based on Si [5], GaN [6] [7], and diamond [8] [9] are most widely used sensors for liquid-phase sensor applications. Although the approaches using these micro- and nano-devices can realize a high sensitivity to detect trace of the analyte, i.e. "yes-or-no" type tests, the "quantitative" sensing remains to be difficult due to the fact that the surface chemistry (lateral density, conformation, and orientation of functional molecules on the surface) is ill defined. Furthermore, most of the previous studies merely deal with soluble enzymes, antibodies and proteins, and the functionalization of solid-based devices with membrane associated proteins is still missing. Based on so-called "supported membrane concepts" [10], Tanaka et al. proposed several prototypes of membrane-based biosensors on bulk semiconductor electrodes [11] [12] [13]. To achieve a high signal to

noise ratio, they utilized ultrathin polymer supports to fine-tune membrane-substrate contacts [14] [15], which even allows for the orientation selective spreading of native cell membranes [16].

Among various semiconductor materials, GaAs has a high electron mobility ($\mu_e \simeq 9200 \text{ cm}^2\text{V}^{-1}\text{s}^{-1}$) [17] that can be operated at high frequencies ($> 250 \text{ GHz}$) at low noise. In addition, owing to the almost identical lattice constants, GaAs/AlGaAs heterostructure permits flexible band-gap engineering such as two-dimensional electron gas (2DEG) devices. For instance, Cahen and his co-workers functionalized the surface of native oxide of GaAs with various carboxylated organic molecules, and reported the modulation of band structures of GaAs-based 2DEGs in ambient atmosphere [18] [19].

However, the liquid-phase sensor applications of GaAs have been impeded due to the complex, irreversible electrochemistry in physiological electrolytes [20] [21]. As previous studies demonstrated, GaAs terminated with oxide is not stable, and capping of GaAs with different inorganic layers (e.g. SiO_2 or SiN_3) demonstrated that a layer thickness should be more than 10 nm to overcome a large lattice mismatch with GaAs. On the other hand, passivation of stoichiometric GaAs surfaces with inorganic and organic mercapto compounds has been reported by several groups [22] [23] etc. In 2000, Adlkofer et al. firstly achieved the electrochemical stabilization of GaAs in physiological electrolytes for more than 20 h by covalent coupling of octadecylthiol (ODT) monolayers on photochemically etched GaAs. Almost the same functionalization protocol has been adopted to functionalize near-surface InAs quantum dots [24], which demonstrated not only a stability of quantum dot photoluminescence but also an enhancement of photoluminescence in the presence of ODT monolayers. The enhanced photoluminescence can be attributed to the reduction of surface states density by covalent binding of sulfide and arsenide, verified by the x-ray photoelectron spectroscopy.

This strategy was further extended to mercapto-biphenyl (MBP) molecules that possess rigid backbone with a larger cross-sectional area (21 \AA^2) and no conformational degree of freedom. Flexible 4'-substitution permits a variety of functional headgroups (-H, -OH, -CH₃, -F, -CF₃) [25]. In fact, monolayers of H-, HO- and CH₃-MBPs could effectively passivate stoichiometric [100] GaAs surfaces [26] [27]. Preliminary experiments further demonstrated that H-MBP monolayer electrochemically stabilize 2DEG devices in physiological electrolytes [28].

This thesis deals with electrochemical characterization of GaAs surfaces functionalized with MBP derivatives and phospholipid membranes, and exploits their potentials in chemical/biochemical sensor applications. As presented in the main parts, several

unique results have been obtained, such as a distinct pH sensitivity of bulk GaAs electrodes rendered with a "hydrophobic" CH_3 -MBP monolayer (Chapter 5). Interestingly, the pH sensitivity calculated from the bulk electrodes is almost identical to that of 2DEG devices with the same CH_3 -MBP monolayers (Chapter 5.2). The mechanism of such a pH sensitivity is further discussed in Chapter 6. There, the pH sensitivity is shown to be influenced by the type of anion present in the solution (Hofmeister series). In the last section (Chapter 7), a potential biosensor application of supported lipid monolayer on MBP-functionalized GaAs is exploited, such as the measurement of membrane surface potentials and monitoring of enzymatic activities. Details of the obtained results are discussed in the following sections.

Chapter 2

Materials and Methods

This chapter introduces the materials employed in this thesis and describes the techniques used to fabricate, prepare and characterize the samples. The layouts of the samples and the experimental set-ups are also presented.

2.1 Materials

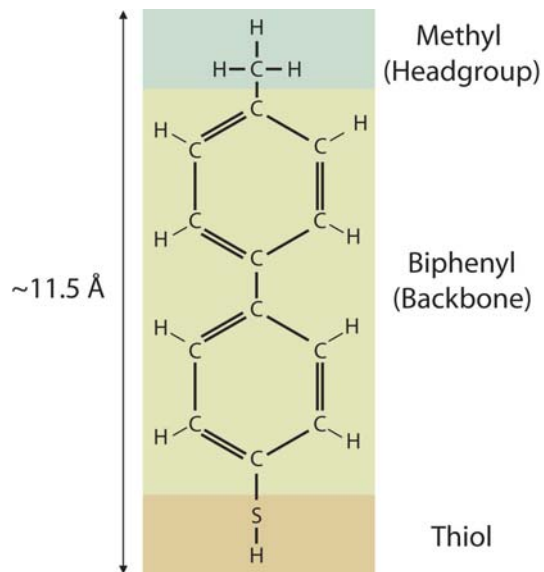
2.1.1 Bulk Chemicals

Mercapto-biphenyl

The 4'-substituted-4-mercaptobiphenyl, $X-(C_6H_4)_2-SH$, is the molecule used in this work to coat GaAs surfaces. The molecules consist of a rigid and bulky backbone with cross sectional area of 21 \AA^2 and a molecular length of $\sim 11.5 \text{ \AA}$ [25]. Their synthesis is reported elsewhere [29] and they were provided by Prof. A. Ulman from the Polytechnic University (New York, USA).

Fig. 2.1 depicts the methyl-mercapto-biphenyl (CH_3 -MBP) molecule, which is extensively employed in this thesis. From the structural and functional viewpoint, the molecule is structured in three parts. The biphenyl forms the main body (backbone), the thiol group is employed to covalently bond to surface As atoms, and the headgroup provides the 'functionality' of the molecule when they form self-assembled monolayers (see Appendix A.1). The family H-, OH-, CH_3 -, F- and CF_3 - of headgroups can also be added to the mercapto-biphenyl molecule. Each headgroup influences the total dipole moment of the entire molecule [30].

Figure 2.1: Methyl-mercapto-biphenyl ($\text{CH}_3\text{-MBP}$) molecule. Three parts can be distinguished. The main body of the molecules is constituted by the biphenyl backbone, the thiol group is employed to covalently react with GaAs surface atoms and the headgroup provides the functionality of the molecule when they form self-assembled monolayers. Different functional groups are available: H-, OH-, CH_3 , F- or CF_3 - headgroups exist. In this work $\text{CH}_3\text{-MBP}$ is extensively employed.



Lipids and Phospholipase A_2

1,2-dimyristoyl-sn-glycero-3-phosphocholine (DMPC), dehexadecyldimethylammoniumbromide (DHDAB), 1,2-dimyristoyl-sn-glycero-3-[phospho-rac-(1-glycerol)] (DMPG) and cholesterol were purchased from Avanti Polar Lipids (Alabaster, Alabama, USA).

Phospholipase A_2 (PLA_2) from honey bee venom was purchased from Sigma Aldrich (Munich, Germany).

2.1.2 GaAs

GaAs Wafers

Single crystalline [100] Si-doped (n-doped) GaAs wafers with a doping ratio of $2.1 - 3.5 \times 10^{18} \text{ cm}^{-3}$ were purchased from Freiberger Compound Materials GmbH (Freiberg, Germany).

To achieve higher space-charge capacitances, which require higher doping ratios, single crystalline [100] Zn-doped (p-doped) GaAs wafers with a doping ratio of $2.2 - 3.5 \times 10^{19} \text{ cm}^{-3}$ (Wafer Technology Ltd (Bucks, UK)) were employed.

Two-Dimensional Electron Gas (2DEG) based on GaAs

A high density of electrons at the conduction band can be confined to a few nanometers by creating an abrupt discontinuity of the Fermi level. This can be achieved by GaAs/AlGaAs heterostructures (band gap engineering).

As depicted in Fig. 2.2 (top part), on an n-doped GaAs [100] substrate, 50 nm of AlGaAs were grown by MBE to form the 2DEG layer at the interface. A Si- δ -doping layer was deposited within the AlGaAs layer at 25 nm from the n-GaAs/AlGaAs interface to obtain a source of electrons for the 2DEG. Finally, on top of the AlGaAs layer, a 10 nm of un-doped GaAs was grown by MBE.

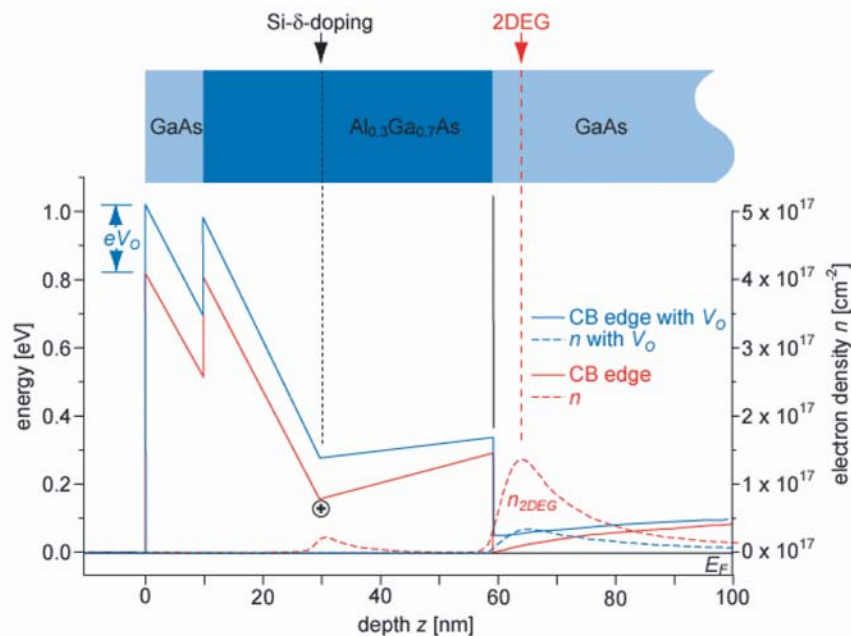


Figure 2.2: Profile of AlGaAs/GaAs 2-Dimensional-Electron-Gas (2DEG) heterostructure. The continuous lines correspond to the calculated conduction band. The 2DEG layer arises at the n-doped GaAs/AlGaAs interface. A source of electron is created by Si- δ -doping in bulk AlGaAs. On top of AlGaAs layer, an undoped GaAs layer is grown. The dashed lines correspond to the density of electrons. As seen, the density of electrons at the 2DEG strongly depends on changes of the surface potentials eV_0 .

In the plot of Figure 2.2, the band structure (continuous lines) and the electron density (dashed lines) are depicted as a function of the depth, as calculated by *nextnano*³ (Walter Schottky Institut, TU München). As seen, upon changes on surface potentials (eV_0), a sensitive change in density of electrons at the 2DEG layer arises. The density of electrons in the 2DEG is measurable by the 'sheet' resistance of the 2DEG layer.

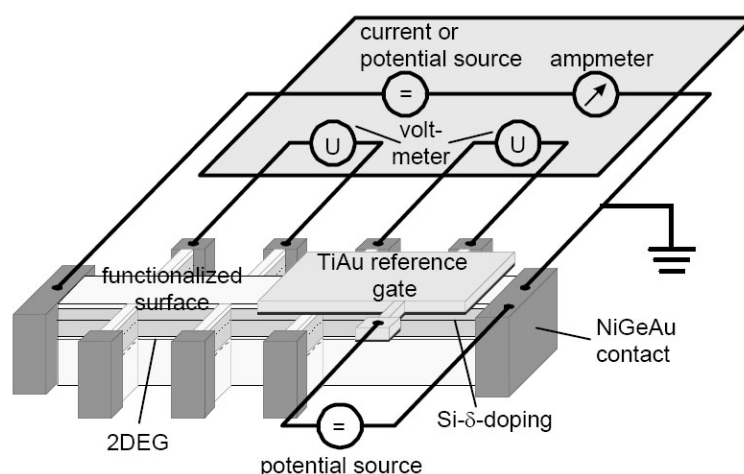


Figure 2.3: Layout of a Hall-Bar structure of 2DEG device. Ohmic contacts of NiGeAu are employed to electrically connect the buried 2DEG structure. MBP molecules are deposited on the surface to prevent the electrochemical degradation of GaAs by electrolytes. Surface potential changes are sensed by changes in sheet resistance R_{sh} of the electron density at the 2DEG layer.

The 2DEG heterostructures were patterned by photolithography to construct different Hall-bar structures in a single chip, as depicted on Fig. 2.3. The ohmic contacts (grey patches) were deposited as described in section 2.2.2, to enable electrical contact with the 2DEG layer. Each chip was designed to have 3 Hall-bar structures.

2.2 Sample Preparation

2.2.1 Deposition of Monolayers of MBP on Bulk GaAs and 2DEG Devices

Coating GaAs with biphenyl-thiol molecules is a self-assembling process that relies on the formation of the covalent bond As-S between the substrate and the molecules.

In a cleaned and dried reactor, 100 μM of X-MBP was dissolved into 99.8% ethanol (Sigma Aldrich, Munich, Germany), so that the presence of oxidizing agents, such as H_2O or O_2 , was minimized.

Before any surface coating, the uncoated GaAs sample was initially sonicated in acetone for 3 min and further rinsed with ethanol, in order to remove all organic material. After evaporating the ethanol with N_2 flow, the sample was soaked in concentrated HCl (35%) for 1 min to strip the native oxide. The resulting surface was a stoichio-

metric [100] GaAs [31]. Once the HCl was removed with a rapid rinsing with Millipore water and ethanol, the sample was placed inside the reactor for 20h-24h at 50°C under a constant and gentle N₂ bubbling and in dark.

Once the grafting process was completed, the samples were removed from the reactor, rinsed with ethanol, dried with N₂ and kept under N₂ atmosphere.

2.2.2 Ohmic Contacts

To perform impedance spectroscopy measurements, an ohmic contact was deposited at the back side of each sample. The 2DEG devices had patterned contacts on the top surface.

Following the procedure initiated by Sebastian Luber [32], a Ni(50 Å) / Ge(250 Å) / Au(500 Å) / Ni(200 Å) / Au(2000 Å) layer was deposited by e-Beam evaporation (Fergutec, Valkenswaard, The Netherlands) on Si-doped (n-doped) GaAs wafers. The ohmic contact was formed after annealing the surface at 430°C for 200 s.

To form ohmic contacts on Zn-doped (p-doped) GaAs, the same deposition protocol was employed. No differences were observed regarding the quality of the ohmic contact.

2.2.3 Buffers

A precise treatment of the buffers is crucial as one is attempting to measure surface potentials.

In this work, double-distilled (dionized) ultra-pure water ($R > 18 \text{ M}\Omega \text{ cm}$) was used (Millipore, Molsheim, France). All salts were purchased by Sigma Aldrich (Munich, Germany).

Buffers for 'pH sensitive' measurements

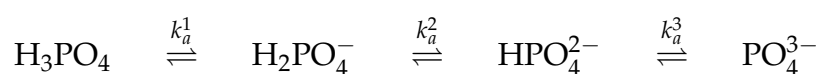
The Henderson-Hasselbach relation

$$pH = pK_a + \log_{10} \frac{[A^-]}{[HA]} \quad (2.1)$$

yields the pH as a function of concentration of ions (i.e. ionic strength) and pK_a of the buffer.

Surface potentials are not only dependent on surface charges, but also on the ion concentration in the solution (see section 3.2.1). The ionic strength is a measure of the ionic nature of the solution, regardless of the ion charge sign. It is defined as $I = \sum_i [A_i] z_i^2$, where $[A_i]$ is the concentration of the i species and z_i their corresponding ionic charge. Experimentally, it can be measured with an osmometer.

Phosphate Buffered Saline (PBS): Phosphate salts have four different ionizable states. In sequence,



where $pK_a^1 = 2.15$, $pK_a^2 = 7.21$ and $pK_a^3 = 12.33$.

From equation 2.1, the total ionic strength can be calculated as a function of the pH of the solution.

To minimize the effect of the ionic strength in our pH sensitive measurements that were carried out within $2 < \text{pH} < 6.75$, a 10 mM PBS and 100 mM of NaCl were dissolved in Milipore water. Under these conditions, the theoretical calculation ensured that the ionic strength varied within 10%. Such results were confirmed with measurements carried out with an Osmometer (Gonotec GmbH, Berlin, Germany), yielding 0.250 ± 0.03 Osm/Kg.

Buffers for Hofmeister series experiments

In chapter 6, NaI and NaCl are used in separate solutions at the same concentrations to perform pH sensitive measurements.

In this experiment, concentrated HI was not used to titrate the buffer to low pH values. The reason is that concentrated HI solution inevitably contained a substantial amount of IO_3^- anions. Therefore, the electrolyte with the lowest pH consisted of 10 mM NaH_2PO_4 and 100 mM NaI or NaCl. The pH was systematically tritrated by adding NaOH.

Buffers for supported lipid layer experiments

For the lipid monolayer experiments, physiological buffers (10 mM PBS and 150 mM NaCl) were prepared and the pH was kept at 6.75. To hydrate lipids and form

vesicles, the same buffer solution was used.

2mM of Ca^{2+} ions was employed to promote the attachment of PLA_2 to the lipid layer by adding 2mM CaCl_2 . To avoid the precipitation of $\text{Ca}_3(\text{PO}_4)_2$ by mixing CaCl_2 with PBS, 10 mM Hepes was used instead of PBS. The use of Hepes buffer did not cause any sensitive changes of the results.

2.2.4 Deposition of Lipid Monolayers

In chapter 7, DMPC, DHDAB^+ , DMPG^- and Cholesterol were mixed to the desired composition in chloroform. After evaporating the chloroform, first drying in a gentle stream of N_2 and subsequently placing overnight in vacuum, the lipids were hydrated in buffer to a concentration of 1 mg/mL to form vesicles.

To facilitate the rupture of the lipid vesicles on the surface, small vesicles were prepared by tip-sonication for 15-25 min. The resulting solution was injected in the flow chamber and was incubated for 2 hours to promote the deposition and spreading of the lipids on the GaAs surface.

The lipid mixture composition was chosen so that it always contained 40% molar of Cholesterol. In the remaining 60% molar was shared among DMPC, DMPG^- and DHDAB^+ to achieve the desired charge density of vesicles.

Phospholipase A_2 (PLA_2) was dissolved to ~ 20 ng/mL in 10 mM Hepes buffer at $\text{pH} = 6.75$. To activate the hydrolysis of PLA_2 on DMPC, 2 mM CaCl_2 was added.

2.3 Characterization Methods

2.3.1 Atomic Force Microscopy (AFM)

The topographic surface roughness of the bare GaAs and MBP functionalized GaAs was determined by Atomic Force Microscopy (AFM). The surfaces were scanned in tapping mode (Nanoscope IIIa Digital Instruments, Mannheim, Germany) with Si cantilevers of spring constant $\simeq 42$ N/m and a tip radius of < 10 nm (NanoAndMore GmbH, Wetzlar, Germany) on surface areas of 200×200 nm², 1×1 μm^2 and 10×10 μm^2 , in order to obtain a reliable roughness quantity.

The surface roughness was calculated by RMS (Root Mean Squared) of the surface topography. It is defined as

$$RMS = \sqrt{\frac{\sum_{i=1}^N (x_i^2 - \bar{x}^2)}{N}} \quad (2.2)$$

x being the height measured by the AFM at a certain point, \bar{x} the height average and N the number of points measured.

2.3.2 Ellipsometry

An air-solid ellipsometer (Multiskop, Optrel, Kleinmachnow, Germany) with a laser of wavelength 632.8 nm and configured to an incidence angle of 70° was used to characterize the X-MBP film thickness on GaAs.

The principle of ellipsometry relies on the multiple reflections of polarized light on a multilayered system with different refractive indexes (n_i, k_i) of each layer i . With the normal component to the surface of the reflected beam R_s and the parallel component R_p , the fundamental equation of ellipsometry

$$\frac{R_p}{R_s} = \tan \Psi e^{-i\Delta}$$

can be derived. Δ and Ψ can be analytically extracted from this equation, taking into account that R_p and R_s are complex variables.

The ellipsometric parameters (Δ and Ψ) can be obtained by the null-ellipsometry technique [33]. They are the result of finding the elliptical polarisation parameters of the incidence beam so that the reflected beam is linearly polarized. In this way, the different thicknesses of the multilayered structure can be calculated [33]. The method is essential as the inversion of the Fresnel reflections' equation to obtain the thicknesses is analytically impossible.

2.3.3 Principles of Contact Angle

A home made contact angle measurement setup (designed and constructed by Thomas Schubert) was used to quantify the Surface Free Energy of the GaAs surfaces coated with X-MBP monolayers. Static contact angles under water (H_2O), diodomethane

(CH₂I₂) and glycerol (C₃H₈O₃) as well as the advancing and receding water contact angles were measured on all molecules.

From the obtained angles, the Fowkes method [34] provides an analytical tool to calculate the polar and dispersive components of the Surface Free Energy. The total free energy is $\gamma = \gamma_d + \gamma_p$, where d and p stand for dispersive and polar components, respectively. Nevertheless, an alternative and simpler method to calculate the surface free energy was developed by Owens and Wendt [35]. From

$$1 + \cos \theta = 2\sqrt{\gamma_s^d} \left(\frac{\sqrt{\gamma_l^d}}{\gamma_{lv}} \right) + 2\sqrt{\gamma_s^p} \left(\frac{\sqrt{\gamma_l^p}}{\gamma_{lv}} \right), \quad (2.3)$$

the dispersion component of the surface free energy of the solid γ_s^d and polar component γ_s^p can be calculated once knowing the free energy of the liquid-vapor γ_{lv} and the liquid dispersive and liquid polar components, γ_l^d and γ_l^p of each liquid, respectively. The liquid dispersive and polar components can be obtained from a database published by Fowkes [36].

2.3.4 Current-Voltage Characteristics of 2DEG Devices

The 2DEG device (see section 2.1.2) was put in contact with electrolytes on a flow chamber which was electrically controlled by means of a three-terminal setup. The setup contained a reference electrode (Ag/AgCl), a counter electrode (Au) and ohmic contacts that enabled (i) a contact to set the bias potential U_{bias} or V_{Sa} between the electrolyte and the 2DEG layer and (ii) additional contacts to control and measure the Source and Drain potential V_{SD} and current I_{SD} . The device was controlled by a Lab-view program (designed and developed by Sebastian Luber) from which the experimental data could be extracted, monitored and processed.

Commonly, in conventional ISFET devices, a Source-Drain Follower (SDF) setup is employed to account for changes of surface potentials. Upon changes of surface potential, SDF readjusts the V_{Sa} (or U_{bias}) so that the source-drain current I_{SD} remains constant. Nevertheless, to prevent from electrochemical degradation, the U_{bias} of our GaAs 2DEG devices was kept constant. To account for changes of surface potentials, the 'Sheet Resistance' R_{sh} was measured. R_{sh} is the result of linearly fitting the

I-V characteristics (Ohmic behaviour) of the 2DEG sheet layer by varying the source-drain potential V_{SD} and measuring source-drain current I_{SD} .

2.3.5 Electrochemical Impedance Spectroscopy

To perform electrochemical impedance spectroscopy, bulk GaAs samples (see section 2.1.2) with an ohmic contact deposited on the back-side were employed. Such samples were placed into a flow cell. The measurement cell was composed of polymethylmethacrylate (PMMA) and had an inlet and outlet that enabled a constant flow of electrolyte which was controlled by an external pulse free pump. The volume of the flow chamber was 1.5 mL and the exposed electrode area was constrained by an O-ring to 0.28 cm^2 .

Despite the variety of techniques and measurement set-ups currently available for impedance spectroscopy, a *three terminal set-up* was constructed in the present thesis. Such three terminal set-up is compounded by a *counter electrode*, i.e. a gold (Au) wire, a *working electrode*, i.e. GaAs, and a *reference electrode*, i.e. Ag/AgCl Reference Electrode

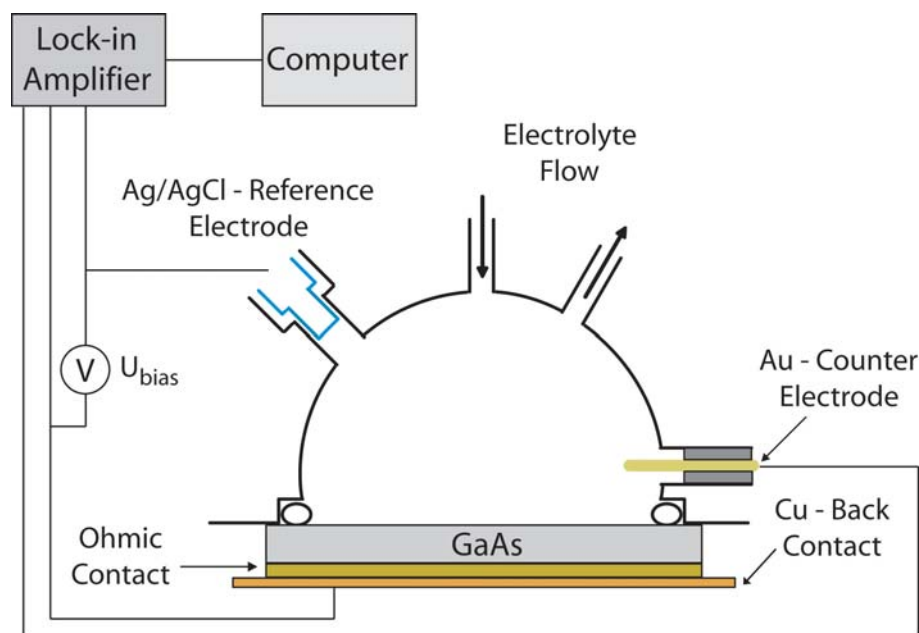


Figure 2.4: Schematic illustration of the measurement setup for impedance spectroscopy. Functionalized GaAs samples with back ohmic contacts rest on a copper plate which defines the bias potential vs Ag/AgCl reference electrode. A constant electrolyte flow is applied in the chamber. The impedance spectrum is obtained after reading out the signals with a lock-in amplifier. The impedance data is further transferred to a computer for numerical processing.

(Metrohm GmbH, Filderstadt, Germany). The reference electrode enables controlled bias potentials (U_{bias}) between the electrolyte and the working electrode. Depending on the electrochemistry of the electrolyte/working electrode interface at a given U_{bias} , interfacial currents may arise. The excess of currents is compensated by the counter electrode.

The impedance spectra were obtained by measuring the interface impedance at a fixed frequency and, subsequently, scanning over the desired frequency window. At each frequency (ω), an additional oscillating potential $U(t)$ of 10 mV of amplitude was superimposed to U_{bias} . The outcomes were read out by a Lock-in amplifier (Voltlab 40, Radiometer-Analytical, Lyon, France) from which the total impedance (real and imaginary parts) of the same frequency could be extracted after integrating over 10 oscillating cycles. In this work, each impedance spectrum was mainly taken between 100 kHz to 50 mHz. To shield the sample from any environmental electromagnetic disturbances and to protect it from light, the flow chamber was placed inside a opaque Faraday box. The resulting impedance data was transferred to a computer, where the data could be conveniently treated and fitted with the desired physical models.

Chapter 3

Physical Background

Bringing in contact a semiconductor and an electrolyte arises particular interfacial physics and chemistry that differ from the ones in the bulk of each phase. This introductory chapter intends to approach the reader to such interfacial phenomenology, making particular emphasis on GaAs. The chapter starts with different relevant aspects of semiconductor interface physics, it is followed by the description of the structure of the electrolyte nearby an interface and finalized with a brief overview of the electrochemical phenomena of GaAs.

3.1 Surface Electronic Structure of (GaAs) Semiconductors

3.1.1 Band Diagram of Semiconductors at Various Bias Potentials

The electron affinity χ is a physical quantity that accounts for the energy required to bring an electron from the surface of the semiconductor into vacuum, immediately outside the surface [37]. In the case of metals, the electron affinity χ_m is equal to its work function ϕ_m and is an intrinsic characteristic of the metal. Nevertheless, in semiconductors, the electron affinity will depend on the band structure at the surface. As depicted in Fig. 3.1, the electron affinity of a semiconductor is

$$\chi = \phi_W - \phi_{BB} - (E_{CB} - E_F). \quad (3.1)$$

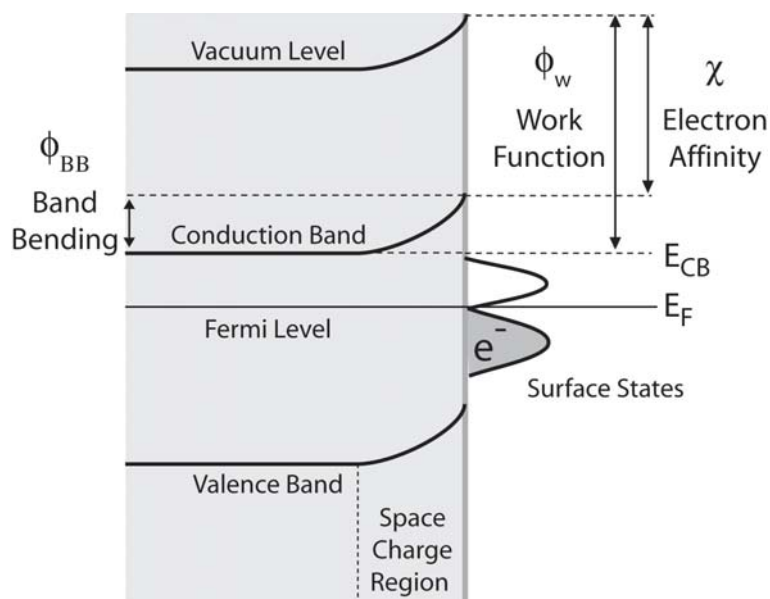


Figure 3.1: Schematic chart depicting the electronic quantities arising on a semiconductor surface.

By bringing in contact a semiconductor with metals or electrolytes, after reaching the thermodynamic equilibrium and assuming no electron-transfer across the interface, the Fermi levels of both components will be equal at the interface. From the intrinsic difference in work function (ϕ_W) between the two materials, a difference in electron affinity arises: the contact potential. For this reason, in the semiconductor, as the dopands are immobile, the majority carriers will redistribute from the surface to the bulk forming the so-called *space charge region*. This redistribution is ultimately reflected by the *band bending*. In the case of electrolytes, an ionic redistribution also arises, as described in section 3.2.1.

The magnitude of the electron affinity can be experimentally obtained by performing Kelvin Probe measurements. For example, on GaAs, Cohen et al. used this technique to measure the impact of different grafted molecules to the electron affinity. They showed the influence of the molecular dipoles and molecule-surface chemical bond [38]. The magnitude of electron affinity is important for interface electronics and surface sensing. If an additional external potential is applied, i.e. bias potential U_{bias} , the potential barrier at the interface is accordingly modified. * If $\Delta U_{bias} > 0$, the Fermi level of the semiconductor bends downwards, which, in other words, means that by keeping the Fermi level constant, the bands bend upwards.

Figure 3.2 depicts the different space-charge regimes of an n-doped semiconductor. The opposite response occurs in a p-doped semiconductor. Under moderate

*Unless the contrary is mentioned in this thesis, the reference potential is set at the bulk electrolyte (vs Ag/AgCl), as agreed in electrochemistry. In semiconductor physics, the reference potential is at the bulk semiconductor, and, thus, the sign convention is swapped.

$\Delta U_{bias} > 0$, the space-charge of an n-doped semiconductor forms the so-called *depletion regime*. The electron density (majority carriers) is depleted nearby the surface. Please, note that for $\Delta U_{bias} > 0$ corresponds to $V < 0$ in the figure, because in the figure the reference of potentials is taken at the semiconductor bulk. In a further increase of U_{bias} , the valence band of the semiconductor may cross the Fermi level. In this case, holes become the majority carriers at the surface while electrons are majority carriers in the bulk. The semiconductor is called to be at the *inversion regime*. Finally, by applying negative $U_{bias} < 0$, the bands bend downwards. Electron density increases at the surface and the semiconductor is at the *accumulation regime*.

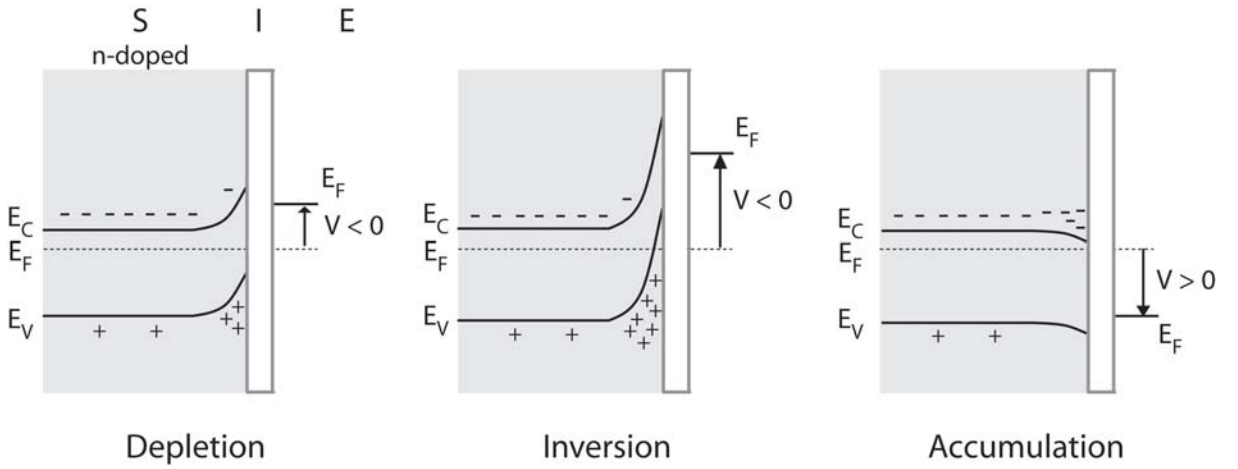


Figure 3.2: Three space-charge regimes for n-doped semiconductor arising from distinct external potential bias, V .

Another important parameter is the *flat band potential* U_{fb} . It corresponds to the external bias potential U_{bias} that needs to be applied so that the semiconductor reaches the flat band conditions ($\phi_{BB} = 0$). Physically, U_{fb} sets an absolute reference of potentials. Therefore, changes of surface potentials other than originated from U_{bias} shift U_{fb} .

3.1.2 The Depletion Layer Capacitance (Mott-Schottky relation)

It is clear that in a general contact involving a semiconductor, at the thermodynamic equilibrium, the conduction and the valence bands are brought into a determined relationship with the Fermi level at the interface. At the *depletion regime*, the distribution of charges of the space charge region can be analytically solved with simple approximations. These analytical relations provide relevant semiconductor parameters that can be extracted by measuring the capacitance of the space charge region [37]. It is found that the space-charge capacitance at the depletion regime follows

$$\frac{1}{C_{SC}^2} = \frac{2}{\epsilon_0 \epsilon_s N_d q} \left(\overbrace{U_{bias} - U_{fb}}^{=\phi_{BB}} - \frac{kT}{q} \right), \quad (3.2)$$

known as the Mott-Schottky relation. Here, C_{SC} is the capacitance of the space charge region, N_d is the doping ratio, ϵ_0 the dielectric constant of the vacuum, ϵ_s the relative dielectric constant of the semiconductor ($\epsilon_s^{GaAs} = 13.1$), U_{fb} the flat band potential, k the Boltzmann constant, T the temperature and q the elementary charge.

Fulfilling the linearity of the *Mott-Schottky* relation $1/C_{SC}^2$ vs U_{bias} is important because (i) it demonstrates that the semiconductor is operated at the depletion regime, (ii) it provides a direct link between the doping ratio N_d of the semiconductor (intrinsic property) and the space charge capacitance, and (iii) it offers an analytical relationship between the surface potential, i.e. ϕ_{BB} or U_{fb} , and its space charge capacitance. When the semiconductor is operated at the *accumulation* or the *inversion* regimes, the Mott-Schottky relation is not fulfilled.

3.1.3 The Influence of Surface States

When the lattice periodicity of the bulk semiconductor is broken, as it occurs at the surface, the electronic states of the atoms facing outside ready to form bonds remain unpaired. New electronic states, named as *surface states*, arise. Surface states of energy levels within the band gap can trap charge and thus influence the semiconductor surface electronic properties. Indeed, one can classify the surface states depending on its physical origin. Two different types can be distinguished. First, the *intrinsic* surface states are originated by the physical properties of the semiconductor, i.e. surface atoms with unpaired electrons or defects of the lattice due to strain gradients. And second, the *extrinsic* surface states stem from the type of external adsorbates (chemical nature) and their degree of contamination.

A surface state can be considered as a donor, if it becomes neutral or positive by donating an electron or an acceptor if it becomes neutral or negative by accepting an electron[†]. When a voltage is applied, the surface states move up or down with respect to the semiconductor Fermi level E_F giving a resulting surface charge. Consequently, the higher the density of surface charges $D_{ss}(E)$ and the closer they are to the mid-gap

[†]Please note the distinction between surface charge generated by surface states and surface charge generated by adsorbates. The latter have a charging mechanism that does not depend on the position of the Fermi level.

(deep-surface states), the less impact will have external (surface) potential changes to changes on the space-charge region. This would make the semiconductor less sensitive to surface potentials. In other words, the higher the surface states density, the more *pinned* is the Fermi level. The pinning of E_F is another source of band bending.

GaAs, after extensive research during the 80's towards its metallization for integrated circuits, revealed a high dependency of the devices' performances upon the density of surface states, the so-called '*pinning level*'. This is critically influenced by the degree of contamination, the chemical composition of the contaminants, i.e. oxides, as well as the exposed surface direction of the cleaved surface [39]. The chemical reactivity of the adsorbates with GaAs [40], the defects they introduce to GaAs [41] and the surface states reconstruction via chemical bonding [42] are understood to be the responsible for the pinning of the Fermi level, too. Despite such great diversity of phenomenology originating surface states on GaAs, nowadays, among the scientific community, the density of surface states in a Metal/GaAs contact is assumed to be of $\sim 10^{13} \text{cm}^{-2}$ [17].

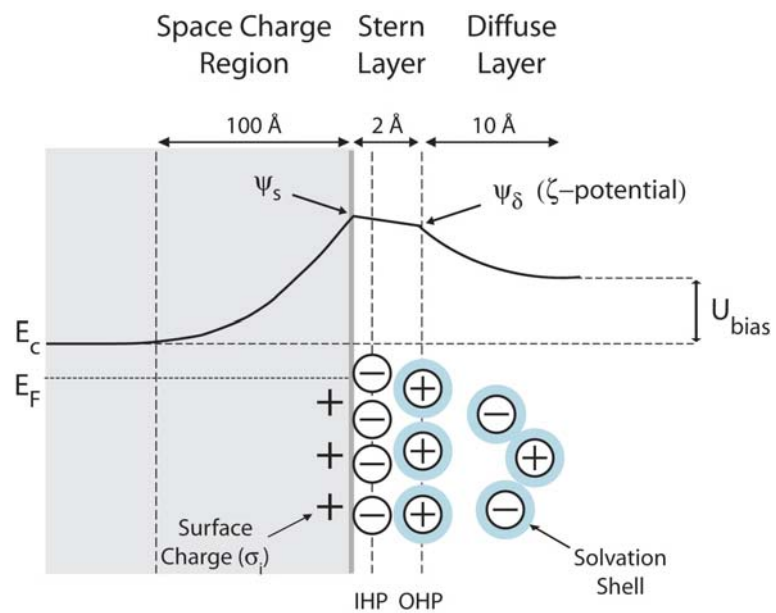
Nevertheless, studies carried out on electrolyte/GaAs interfaces show a sensitive reduction of the *pinning* of the surface states [43], in contrast to the Metal/GaAs contacts.

The existence of the surface states is not only influencing the Fermi level at the surface. As the surface states get charged as a function of the U_{bias} , $Q_{SS}(\psi_s)$, its capacitance, $C_{SS} = -dQ_{SS}/d\psi_s$, where ψ_s is the surface potential, is seen to linearly depend on the density of surface states as well as on the voltage applied [44]. Because the capacitance of the surface states C_{SS} is 'connected' in parallel to the capacitance of the space-charge C_{SC} , the higher C_{SS} becomes, the more dominant in the overall capacitance it is. Gersicher calculated that for a density of surface states of 10^{13}cm^{-2} , C_{SS} can achieve a maximum value of $20 \mu\text{cm}^{-2}$ [44]. In contrast, in an electrolyte/GaAs contact, because of the lower pinning level, the surface states capacitance remains at $C_{SS} < 0.1 \mu\text{Fcm}^{-2}$ [43].

3.2 Electrochemistry of GaAs Semiconductors in Aqueous Electrolytes

At the semiconductor/electrolyte interface, charges (ions) can be accumulated and/or transferred across the interface. In this part, firstly, the ionic structure of the electrolyte is described towards the calculation of the surface potential. And secondly, because GaAs undergoes complex electrochemical reactions in contact with aqueous

Figure 3.3: Sketch of an electrolyte/semiconductor contact. At the bottom, the three main charge distributions are shown, corresponding to the surface charge density (σ_i), the Stern layer (that includes the Inner Helmholtz plane (IHP) and Outer Helmholtz Plane (OHP)) and the Diffuse layer. Charges are arranged to fulfil the charge neutrality. On top, the continuous line depicts the electric potential associated to the charge density profile. ψ_s is the surface potential



electrolytes, a brief overview of GaAs electrochemistry is developed. For completeness, the principles of electron transfer involving semiconductors are presented in Appendix A.2.

3.2.1 Electrochemistry at GaAs/Electrolyte Interface

Regardless of the charging mechanism of a given surface, either chemical or physical, leading to a surface charge density σ_i , electrolyte ions redistribute to preserve the overall *charge neutrality*. Despite the complexity of the system, an approximate model to explain the rise of surface potentials has progressively been developed since the beginning of the XX century. As depicted in figure 3.3, ions forming the so-called *Stern layer* remain adsorbed on the surface. To satisfy the charge neutrality, a 'cloud' of solvated ions arises by interacting via electrostatic forces among each other (*Gouy-Chapman layer*). These ionic charge distributions model the electrical potential profile and its value at the surface corresponds to the surface potential ψ_s .

The Graham Equation

The surface potential originated from the Diffuse layer (or Gouy-Chapman layer) can be solved analytically. Assuming the dilute approximation (< 100 mM of monovalent ions), where ions do not interact with each other and the chemical potential remains constant, the Boltzmann equation can be employed for each ion i . Applying the Poisson

equation to account for the electrical potential and solving in a case for a given surface charge density, σ_i , the Graham equation can be written as [45]

$$\begin{aligned}\sigma_i &= 2\epsilon\epsilon_0KT \left(\sum_i \rho_i(0) - \sum_i \rho_i(\infty) \right) = \\ &= \sqrt{8\epsilon\epsilon_0KT} \sinh \left(\frac{e\psi_0}{2KT} \right) \left([M^+]_\infty + [D^{2+}]_\infty (2 + e^{-\frac{e\psi_0}{KT}}) \right)^{\frac{1}{2}}.\end{aligned}\quad (3.3)$$

Here, ∞ denotes the bulk, ρ_i the concentration of ion i , ϵ the relative dielectric constant of water, ψ_0 the surface potential, and $[M^+]$ and $[D^{2+}]$ the concentrations of monovalent and divalent ions, respectively. K , T , ϵ_0 and e are the Boltzmann constant, the temperature, the dielectric constant of vacuum, and the elementary charge, respectively.

This expression provides an analytical relation between the *salt concentration*, the *surface charge density* and the *surface potential*.

Stern Modification

The previous model suffers from some limitations. An oversimplification arises from considering that ions are treated as point particles, instead of having a finite size.

This led Stern [46] to modify the Graham equation (above model) by assuming the adsorption of finite-sized ions at hypothetical free binding sites of the surface. The ions would adsorb following the Langmuir adsorption kinetics and change the actual value of surface charge, that would now depend on the *concentration of ions* of the electrolyte. Thus, the change in surface potential across the 'Stern layer' (layer of adsorbed ions) can be expressed as

$$zeN_s \cdot \left(\frac{c_{ads,bulk}}{c_{all,bulk}} \cdot e^{(ze\psi_\delta + \Phi)/kT} \right) = \sigma_{ads} = \epsilon'\epsilon_0 \frac{\psi_s - \psi_\delta}{\delta}, \quad (3.4)$$

where N_s is the number density of available sites, $c_{ads,bulk}$ and $c_{all,bulk}$ the concentration of adsorbates in the bulk and ions in the bulk, respectively, and Φ an additional adsorption potential. ψ_δ stands for the so-called ζ -potential, being δ the thickness of the layer, and ψ_s the surface potential. [32]

Fulfilling charge neutrality implies that the Diffuse layer charge must compensate the charge density of the Stern layer σ_{ads} and the intrinsic charge density σ_0 . σ_0 corresponds

to the space charge, the surface states of the semiconductor and/or specific adsorption. Thus, $\sigma_{diff} = \sigma_i = -(\sigma_0 + \sigma_{ads})$. For this reason, the Graham equation solves for the ζ -potential ($\equiv \psi_\delta$), given the salt concentration and surface charge density. The additional potential drop across the Stern layer is defined by the above equation to be $\Delta\psi = \psi_s - \psi_\delta$.

3.2.2 Electrochemical Reactions at GaAs/Electrolyte Interface

All semiconductor materials in contact with electrolytes can undergo a decomposition process under suitable conditions by oxidation or reduction. The zinc-blend crystal structure of the majority of III-V semiconductors, and in particular of GaAs, forces that surface atoms to be bonded to three underlying atoms by means of valence electrons. These bonding states form the valence band of the semiconductor [47]. Additionally, the surface states of GaAs become deep surface states by interacting with appropriated redox species [48]. Therefore, the interplay among the surface states, the state of the conduction and valence band, the type of doping and the redox couples of the electrolyte can develop a myriad of complex electrochemical phenomena which involve electrons and holes from the surface of the GaAs semiconductor [49].

As Gerischer and Mindt summarized [47] the main decomposition process in a semiconductor occurs normally in two steps when

1. the interruption of the surface crystal bonds under presence of electrical forces either provided by the ions in the solution or the semiconductor itself, resulting in a new bond linking a crystal and an ion species,
2. the other radical of the semiconductor atom reacts with another ion species.

In both steps, electrons or holes from GaAs are involved, and therefore, the rate of which either these electrons/holes or electrolyte reaction species are provided and the energy relationship between them determine the decomposition process.

Anodic Dissolution

As seen in Fig 3.4, the anodic dissolution of GaAs involves 6 holes from the semiconductor and 2 reduced species from the electrolyte solution. The mechanism is irreversible and different reaction constants may also be involved. As depicted in Fig. A.2,

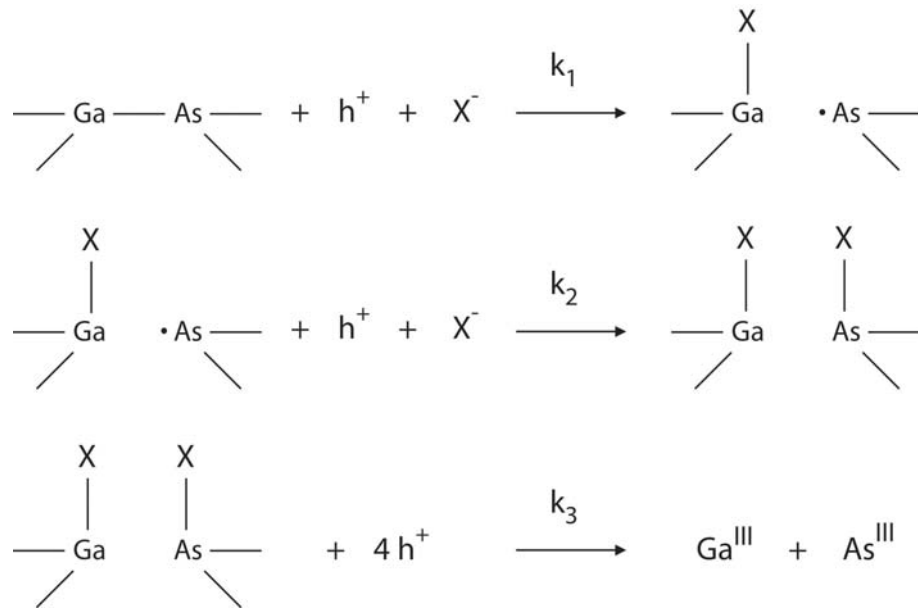


Figure 3.4: Reaction pathway corresponding to the anodic dissolution of GaAs. As the Ga-As bonds form the valence band of the semiconductor, the presence of holes at surface atoms, needed for these electrochemical process, dissolve the semiconductor. In the anodic dissolution, 6 holes and 2 anions (X^-) are required.

the rate of this process can therefore be controlled by the U_{bias} , as well as the concentration of reduced ions.

Notten, van der Meeraker and Kelly [48] remark that particularly when $X^- = OH^-$, i.e. at neutral or high electrolyte pH, this process does not follow the theoretical Nernst response, 60 mV/decade of current. Such deviation is interpreted to be caused by the products of the anodic dissolution reaction which remain adhered on the surface. They change the Helmholtz layer and therefore shift U_{fb} (flat band potential) as the reaction goes on. In an extent, this can be understood as the formation of an oxide film. Impedance spectroscopy measurements on bare GaAs in contact with neutral electrolytes show a constant and irreversible drift of impedance parameters, which is consistent with supposed formation of an oxide film [50].

Hydrogen Formation

H^+ ions do react on the surface of GaAs in a different manner regarding the H_2 formation. In GaAs, the Volmer-Tafel mechanism and/or the Volmer-Heyrovsky mechanism can occur [51]. Uhlendorf et al. [52] demonstrated by impedance spectroscopy of GaAs in contact with low pH electrolytes that the processes involving H^+ were kinetically

controlled (limited by the provision of electrons from the semiconductor), and, therefore, responded at 60 mV/decade (of current). Although they observed a linear shift of U_{fb} with U_{bias} (bias potential) within the potential window, $-1.5 \lesssim U_{bias} \lesssim -0.5$ V, it was attributed to changes in surface polarity, through changes in the surface dipole moments. Within the potential range of $-0.5 \lesssim U_{bias} \lesssim 0$ V, U_{fb} proved to remain constant.

Adsorption of Non-reacting Ions

Although, for some ions, the energetic distance between the valence band of GaAs and the Fermi Energy of their redox couple does not favour charge transfer processes, their adsorption on the surface can occur as a function of U_{bias} . They may be attracted by charges of the surface states, semiconductor surface space-charge or even adhered by specific adsorption. Consequently, the adsorption of such ions shifts the U_{fb} as a function U_{bias} and, thus, the interface current response to U_{bias} deviates from the nernstian response, i.e. 60 mV/decade of current.

Irreversible Electrochemical Processes

When an interface is unstable and responds irreversibly to reversible changes of external control parameters, the electrochemistry is understood to be irreversible. This is the situation of GaAs in contact with neutral (physiological) electrolytes [50]. In these cases, the Gieseler & Marcus model [44] [53] of electron transfer (see Appendix A.2) cannot model the interfacial currents as the interfacial conditions are undefined (density of sites available for electron transfer, Gibbs energy, band bending among others) and the system may not have reached the thermodynamic equilibrium at a certain instant. For these reasons, as soon as irreversible electrochemistry arises, interpreting impedance outcomes in terms of the theory of reversible electrochemistry can be incorrect.

Chapter 4

Principles of Electrochemical Impedance Spectroscopy

4.1 Fundamental Principles

Impedance Spectroscopy (IS) is a well established technique, particularly in interfacial electrochemistry. For example, in our particular GaAs/electrolyte system, the technique has been used to study the dynamics of the electron transfer involving different ions [54], the H₂ formation [52], or even to elucidate different electrical properties of the surface of GaAs, as introduced by Gersicher [44].

Besides these electrochemical issues, impedance spectroscopy has gained growing interest in the field of Biophysics and Biosensing in recent years. In order to explore the potential achievements of this technique in biophysics, substantial efforts have been devoted to design and characterize appropriately the biophysical systems. Most of them involve functional proteins, such as ions channels or specific adsorption on lipid membranes which are deposited on solid supported planar electrodes [10] [55] [56] [57] [58], or on field effect transistors [59].

The procedure to analyze the systems in IS are charted in the flow scheme of figure 4.1, as described by MacDonald [60]. In a IS measurement, the raw data is converted into impedance values $Z(\omega)$ which are later employed to be fitted with theoretical impedance circuit models. Such circuit models are constructed out of *equivalent circuit elements* (figure 4.2), that are associated to specific physical or chemical processes at a general interface, as described in section 4.3.

Technically, the advantage of IS is that the measurement principle, the measuring setup,

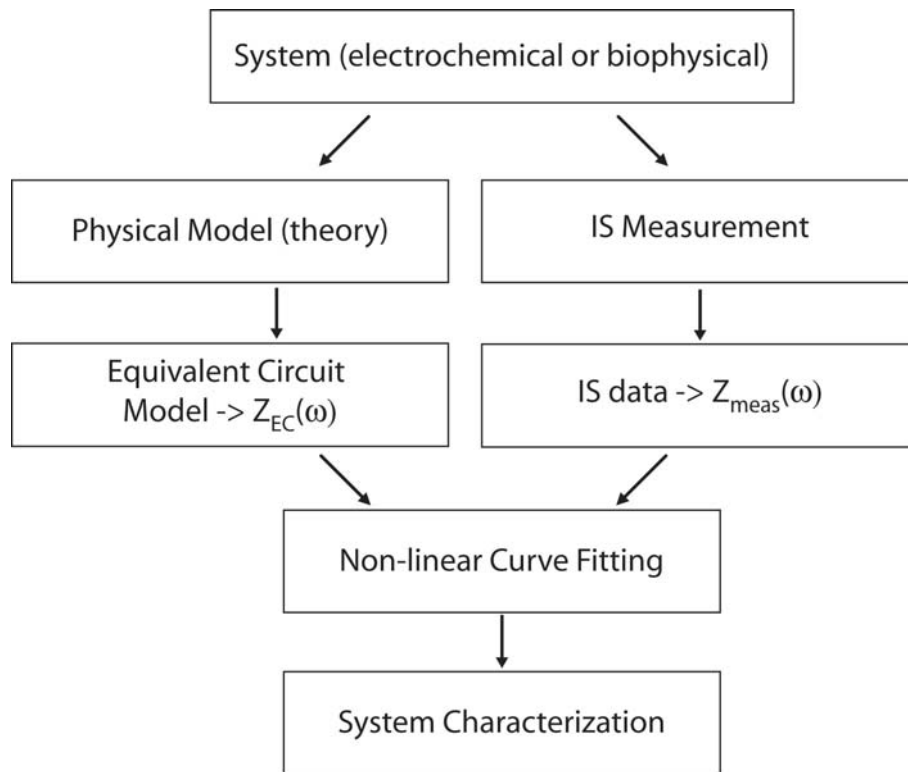


Figure 4.1: Flow chart depicting the procedure to analyze systems by impedance spectroscopy. The extracted spectra is processed to compute the impedance $Z_{meas}(\omega)$. By fitting $Z_{meas}(\omega)$ with an equivalent circuit of impedance $Z_{EC}(\omega)$ allows the characterization of the system in physical and chemical terms.

the electrode preparation and the measurement automation is relatively simple. Additionally, the results after analyzing the IS allow an accurate insight to physical features and processes occurring to the biological system, such as many material parameters (dielectric constants and thicknesses, diffusion constants), as well as detecting mass transport, rate of chemical reactions, microstructure and compositional influences on the conductance of the liquids, ions, membranes or solids. Last but not least, IS is a non-invasive and label-free technique, enabling the biophysical system under investigation to be analyzed on its natural environment.

However, the technique also suffers from substantial disadvantages. Complications on the analysis of the data arise from the inadequate interpretation and use of ideal electrical elements, i.e. resistance and capacitors. Particularly in biomembrane or biological systems, their structural inhomogeneities (space related) and dynamical instabilities (time related) play a decisive role and the use of ideal circuit elements may induce errors in the interpretation. To elucidate such instabilities, not only different non-ideal circuit elements have been developed, but also new experimental setups are suggested.

For example, Wiegand [61], developed a novel impedance spectroscopy technique that by Fast Impedance Spectroscopy (FIS) method, based on Fourier analysis, made possible the characterization of the dynamics of the systems with enhanced time resolution.

4.2 Frequency Dispersion Impedance Spectra

The complex electrical impedance $Z(\omega)$, where ω is the angular frequency, is defined from the ratio between the Fourier-transform $\hat{U}(\omega)$ of the applied ac-voltage $U(t)$, and the Fourier-transform $\hat{I}(\omega)$ of the current response $I(t)$

$$Z(\omega) = \frac{\hat{U}(\omega)}{\hat{I}(\omega)}. \quad (4.1)$$

The complex quantity $Z(\omega)$ can be given in cartesian or in polar coordinates

$$Z(\omega) = \text{Re}[Z(\omega)] + i \cdot \text{Im}[Z(\omega)] = Z_0(\omega)e^{i\phi(\omega)}. \quad (4.2)$$

There are two different major principles to obtain the impedance spectra $Z(\omega)$. The measurements can be performed either in the *time domain* or in the *frequency domain*. The measurement in the time domain can be also called *spectral analysis* as the ac perturbing signal is composed of a multitude of frequencies all applied simultaneously [60] [62] [63]. This measurement technique enables an enhanced time resolution, which is necessary to analyze highly dynamic processes such as the opening of membrane channels [61] [64].

The frequency domain or *harmonic measurement* is the method that consists of applying sinusoidal potentials of determined frequencies $U(\omega) = U_0(\omega) \sin(\omega t) + U_{bias}$ over a certain number of cycles, while simultaneously reading out the current $I(\omega) = I_0(\omega) \sin(\omega t + \phi(\omega))$ at the same frequency with a Lock-in amplifier. The polar coordinates of the impedance at a particular frequency ω are therefore $Z_0(\omega) = U_0(\omega)/I_0(\omega)$ and $\phi(\omega)$. The entire spectrum is obtained after a sequential frequency sweep over the desired frequency range. The perturbation amplitude $U_0(\omega)$ should be small in order to keep the linear response of the system and large enough to overcome the thermodynamic fluctuations. An oscillation amplitude of 10 mV accomplishes these conditions.

Although acquiring the entire spectrum in the harmonic method may take long (normally from 3 to 10 min per spectrum) and it may not be adequate for fast time-resolved experiments, this setup is particularly advantageous due to the use of the Lock-in amplifier technique. The Lock-in amplifier mixes the input signal of known frequency and the outcomes of the measurement. By benefiting from the orthogonality of sinusoidal functions, the amplitude and the phase of the outcomes at the frequency of the input signal can be extracted in low Signal-to-Noise ratio readout signals. In this manner, by exciting the electrode with $U(\omega)$ at a fixed ω , $I(\omega)$ can be obtained.

In this work a typical impedance spectrum was taken with 5, 10 or 20 frequencies per decade over a range between 100 kHz and 50 mHz. The obtained impedance spectra were plotted either in the polar representation, the so-called *Bode Plot*, or by in cartesian coordinates, known as *Nyquist Plot*, as described in 4.5.

4.3 Equivalent Circuit Models

One clear advantage of the IS as a tool to characterize physical and electrochemical properties and processes of the system is the direct connection to an idealized *electric circuit model*, which is compounded of series of elementary and discrete *circuit elements*.

Each circuit element can be demonstrated to be associated to particular electrochemical process. The 'electrical connections' with other circuit elements to an equivalent circuit enables the characterization of the interfacial processes. This is achieved by fitting the experimental impedance spectrum with the function $Z_{EC}(\omega)$ resulting from the designed equivalent circuit model. Unfortunately, as all processes on the surface cannot be modelled and resolved with the impedance methods described, the equivalent circuit becomes a simplification of actual impedance response. In this context, the designed circuit models are not imperatively unique, especially if the amount of circuit elements becomes large. [60]

The connection of different circuit elements can be done in such a way that follows Kirchoff's first and second Law [60]. Thus, considering the impedance $Z(\omega)$, a serial connection of i elements $Z_i(\omega)$ results in an equivalent impedance $Z_{EC}(\omega)$ of

$$Z_{EC}(\omega) = \sum_i Z_i(\omega)$$

and a parallel connection in,

$$\frac{1}{Z_{EC}(\omega)} = \sum_i \frac{1}{Z_i(\omega)}.$$

The different circuit elements used throughout this work are presented in figure 4.2. It is worth mentioning that resistances R and capacitances C are ideal circuit elements because they assume lumped-constant quantities which involve ideal properties.

Nevertheless, biophysical systems may introduce some deviations due to mainly (i) the structural inhomogeneities (ii) the finite permeability and (iii) the size restriction of the biophysical system. That is why *distributed elements* are employed, such as the Warburg element and the Constant Phase Element. Their interpretation is somewhat elusive [60]. There are mainly two types of distributions which we will be concerned. The first is associated to the non-local processes, such as diffusion, and occurs even though the system is ideally homogeneous. And the second type arises because microscopic materials are themselves inhomogeneously distributed.

As the minor processes underplaying the total impedance cannot be discriminated, a careless simplification of the circuit models may lead to misinterpretation. Furthermore, one should notice that the characteristics of a growing complex equivalent circuit, especially when it is composed by a large number of circuit elements, the equivalent circuit is not unique. Only the simplest circuits can be said to be unambiguous in their description of the experimental data. [60]

4.3.1 Circuit Elements

Capacitance C

Ideal capacitors react to external potentials by distributing charges, reaching a current-free stationary charge distribution on DC-voltages. On applied AC-voltages, the current response $i_c(\omega)$ is shifted $\Delta\phi = -90^\circ$ with respect to the applied voltage $U(\omega)$. Analytically, a capacitor is defined by

$$C = \frac{\partial\sigma}{\partial V} = A \frac{\epsilon_0\epsilon}{d}$$

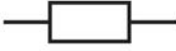
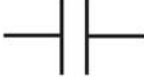


Symbol	Element	Impedance Contribution, $Z_i(\Omega)$
	Resistance (R)	$Z_R(\omega) = R$
	Capacitance (C)	$Z_C(\omega) = \frac{1}{i\omega C}$
	Warburg Element (σ)	$Z_W(\omega) \equiv W(\sigma) = \left(\sigma + \frac{1}{\sigma}\right)\omega^{-\frac{1}{2}}$
	Constant Phase Element (α)	$Z_{CPE}(\omega) = K\omega^{-\alpha}$

Figure 4.2: Summary of the different equivalent circuits elements used in this work.

where the second equality is the result for a planar capacitor. Here, ϵ_0 is the dielectric constant in vacuum, ϵ the relative dielectric constant ($\epsilon(\text{water}) = 80$, $\epsilon(\text{organic molecules}) = 2.1 - 2.3$ [65]), A the area of the capacitor and d the interplate distance. The planar two-plate capacitor approximation is useful to account for the Helmholtz layer or organic layers, where a clear boundary between the two 'plates' exists. However, the last equality does not hold for the space-charge of a semiconductor or the diffuse layer of the electrolytes, as distributed charge density affects the potential profile. In these cases, $C = \partial\sigma/\partial V$ needs to be computed. On section 4.5.1, the analytical result for the depletion regime is shown.

In AC-voltages of frequency ω , the resulting impedance element will be

$$Z_C(\omega) = \frac{1}{i\omega C} \quad (4.3)$$

where $i = \sqrt{-1}$ and ω , the angular frequency.

Resistance R

Resistance R reflects the ohmic behaviour of the interface. It includes all those 'impedance' events that occur in phase ($\Delta\phi = 0$) with the applied voltage perturbation $U(\omega)$ and that are not dependent on frequency. Thus, as part of the overall charge transfer mechanisms, ohmic currents include those processes that are kinetically controlled (see section 4.4). Its AC-impedance response is

$$Z_R(\omega) = R \quad (4.4)$$

Warburg Element $W(\sigma, \omega)$

On diffusively controlled charge transfer, the real and imaginary part of the total impedance Z relate as $-Im(Z(\omega)) = Re(Z(\omega))$. Here, the phase becomes $\Delta\phi = -45^\circ$ and frequency dependency of the total impedance grows with the power of -0.5 [60].

Although the Warburg element was originally introduced to account for the electron transfer from bulk electrolyte to a semiconductor [66], subsequently it was used to describe the diffusion of metals into electrodes [67]. These works motivated Finklea et al. [68] to demonstrate that the Warburg element could also be applied to quantify the diffusion of ions across thin layers. The Warburg impedance

$$Z_W(\omega) \equiv W(\sigma) = \left(\sigma + \frac{1}{\sigma} \right) \omega^{-\frac{1}{2}}$$

enables to extract the diffusion constant of the ions across the layer D , by

$$\sigma = \frac{4RT}{\sqrt{2}n^2F^2A\rho} \cdot \frac{1}{\sqrt{D}} \quad (4.5)$$

which has the units of $V/As^{1/2}$. In Eq. 4.5, A is the active electrode area, D the diffusion constant, ρ the density of ions on the surface. The constants R , T , n , and F are gas constant, absolute temperature, the charge of ions in the electrolyte, and Faraday constant, respectively.

The Warburg element has a gradual dominant contribution to the total impedance as the frequency is diminished. The higher the frequency is, the lower influence diffusion forces have.

Constant Phase Element

The *Constant Phase Element* (*CPE*) is an empirical impedance element that has proven of considerable value in fitting experimental data. It takes into account the non-linear and frequency dependencies induced by inhomogeneities appearing in real systems, regardless of their physical origin [60] [69].

The Debye theory of dielectric constants is derived considering the existence of a single relaxation time. However, at interfaces involving biophysical systems, such conditions may not be sustained. The first to observe and accept the existence of distributed material properties were Cole & Cole [70]. In their experiments with polar liquids and organic solids they found deviations from the theoretical predictions of Debye [60], originally developed for gases and diluted solutions. In order to explain their results, they introduced a distribution of relaxation times τ given by $(i\omega\tau)^\alpha$, and claimed that the Debye theory had to be modified for condensed and concentrated system in such a way. Other examples are the distribution of conductivity in polycrystalline materials [60] or studies to account for the roughness of interfaces. Some later works on rough surfaces proof that the contribution of *CPE* can be related to the fractal dimension of the surface [71] [72] [73].

Analytically, the *CPE* impedance element has the following frequency response

$$Z_{CPE} = K\omega^{-\alpha}. \quad (4.6)$$

For ideal systems, the frequency exponent $\alpha = 0$ and $K = R$ corresponds to the ideal resistor, $\alpha = 1$ and $K = 1/C$ for the ideal capacitance and $\alpha = 0.5$ for the ideal Warburg impedance. Therefore, the deviations from the ideal values are attributed to inhomogeneities of the system, like defects or roughness. Since the *CPE* is just an empirical element that improves significantly the quality of the fit, only a qualitative analysis can be gained by using this approach.

4.4 Analysis of Impedance Spectra with Circuit Model

As an electrochemical electrode, the electrolyte-(insulator)-semiconductor system can also be modelled by an *equivalent circuit*. However, caution must be taken, regarding the interpretation of the each element to the actual system.

From the discussion in sections 3.2.1 and A.2, the *ac impedance* phenomena of the interface must be compounded of the sum of a faradaic currents i_f (currents across the interface) and capacitive (charging) currents i_c . Supposing that the system is in thermodynamic equilibrium, i.e. with small enough ac amplitudes slightly above $k_B T$, i_f and i_c currents are understood to be occurring in parallel. That is why the associated impedances, Z_f and C_p , representing the impedance elements corresponding to currents i_f and i_c , respectively, are connected in parallel as shown in figure 4.2. In this case, R_s is the ohmic resistance associated to the bulk electrolyte.

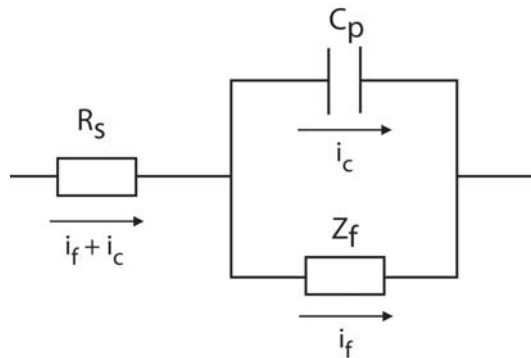


Figure 4.3: Simplified equivalent circuit model that represents electrolyte/electrode interface. R_s refers to the electrolyte ohmic resistance, C_p is the total interface capacitance responsible for capacitive currents (i_c) and Z_f is resistive element accounting for faradaic currents (i_f).

As the faradaic currents may stem from very complex physical phenomena, they are, in general, frequency dependent. Thus, the attributed impedance element is generally assigned as Z_f . Faradaic currents are the result of processes that must involve charge transfer across the interface between ion species of the electrolyte and the solid. Therefore, processes such as ion diffusion, multistep charge transfer or adsorption of reactants can also contribute to the final impedance Z_f .

To achieve electron (charge) transfer across a semiconductor/electrolyte interface, (i) carriers (electrons or holes) should be available at the solid surface and (ii) the electrolyte ions should be at a sufficient distance from the surface (adsorption). Once a charge transfer reaction occurs, which may involve single or multiple ions, the product ions may or may not desorb.

Charge transfer on semiconductor interfaces (see Appendix A.2) is more complex than on metal interfaces. The density of electrons and holes on the bands or the density of surface states depends on the external potential, and can therefore affect the rate of electron transfer [74]. Henz and Gomes [75] demonstrated analytically that, despite

the material differences with metals, the equivalent circuit of figure 4.3 can also be applied to account for the electrochemical impedance at the semiconductor/electrolyte interface.

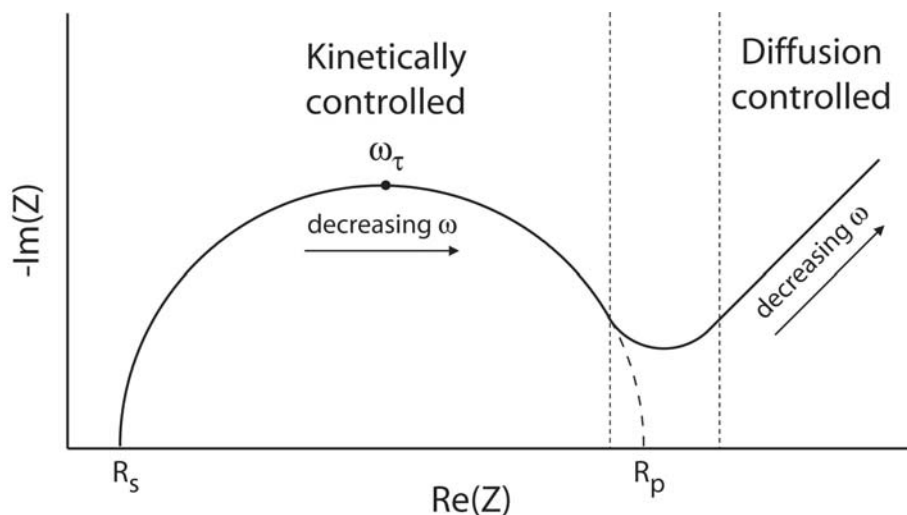


Figure 4.4: Scheme of an impedance spectrum plotted in Nyquist representation. Two different interfacial faradaic processes are clearly distinguished. The kinetically controlled processes can be modelled with an ohmic resistance, while the diffusion controlled faradaic processes with a Warburg resistance. Here, R_s is electrolyte resistance, R_p total interface resistance and $\omega_\tau = \frac{2\pi}{\tau} = \frac{2\pi}{R \cdot C}$. The angular frequency ω_τ represents the frequency above which the capacitance of the equivalent circuit dominates over the ohmic resistance, and below which ohmic resistance dominates over the capacitance.

Because the interfacial electron transfer involves different steps, two limiting situations can be distinguished: the kinetically controlled and the diffusion controlled processes. Two classical examples carried out by Sluyters and Oomen [76] show the difference and their influence to the impedance spectrum. In brief, in a *diffusively controlled* process, the rate of ion adsorption is slower than the rate of electron transfer and, therefore, it limits the speed of the overall charge transfer. The other limiting case, *kinetically controlled* processes are limited by the rate of electron transfer.

To each of such processes an equivalent electrical circuit element can be attributed. For the kinetically controlled processes an ohmic resistance accounts for the impedance response, while for diffusively controlled process, the Warburg element. Figure 4.4 depicts the impedance spectrum (Nyquist plot) of a realistic system where kinetic and diffusive controlled processes coexist. In this case, Z_f is composed of a serial connection of an Ohmic resistance and a Warburg resistance.

4.5 Requirements for Biosensor Applications

4.5.1 Capacitive Sensing of Surface Potentials

The surface electronic structure of semiconductor materials (i.e. majority carriers distribution) can be modified by the surface potential, ψ_s . Depending on the strength of ψ_s , different space-charge regimes arise (see section 3.1.1). That is why, the associated space-charge capacitance depends on the voltage applied, giving rise to different C_{SC} vs ψ_s relations, so-called differential capacitance. For the depletion regime, the differential capacitance can be analytically calculated and results in [37]

$$C_{SC}(\psi_s) = \frac{\partial \sigma_s}{\partial \psi_s} = \frac{\epsilon \epsilon_0}{\sqrt{2} d_n} \frac{\frac{p_0}{n_0} (1 - e^{-\beta \psi_s}) + e^{\beta \psi_s}}{\sqrt{\frac{p_0}{n_0} (e^{-\beta \psi_s} + \beta \psi_s - 1) + e^{\beta \psi_s} - \beta \psi_s - 1}}. \quad (4.7)$$

Here $d_n = \sqrt{\epsilon \epsilon_0 / e \beta n_0}$ is the Debye length and $\beta = e/kT$, ϵ the permittivity of the semiconductor ($\epsilon^{GaAs} = 13.1$), ϵ_0 the permittivity of vacuum, e the elementary charge, k the Boltzmann constant and T the temperature. n_0 refers to the electron carrier density and p_0 the hole carrier density in bulk semiconductor.

In an electrolyte-semiconductor contact, the electrolyte Helmholtz capacitance (C_H), double-layer capacitance (C_{DL}), the insulator capacitance (C_i) and the space charge capacitance (C_{SC}) are connected in series. Therefore, the dominant capacitances of interface are the smaller ones of the series.

Figure 4.5 * is the result of a simulation of an electrolyte/insulator/semiconductor system, in which the differential capacitance normalized to an insulator capacitance C_i is plotted against the surface potential ψ_s . The three space-charge regimes are depicted. Clearly, the sensitivity of the space-charge capacitance to changes of surface potentials is optimal when the semiconductor is at the inversion regime. However, in the inversion regime the potential window is narrow and the relation between C_{SC} and ψ_0 is approximate. It is because, in the inversion regime, the minority carriers of the bulk semiconductor become majority on the surface. In this case, the Boltzmann approximation accounting for the density of carriers provided by the dopands may fail. These difficulties do not arise at the depletion regime. There, the Mott-Schottky relation ($1/C_{SC}^2$ vs ψ_0) is linear and a direct correlation between the surface potential and

*The figure is extracted from Heiko Hillebrandt's doctoral thesis [77], who kindly offered it to be shown here for better argumentation.

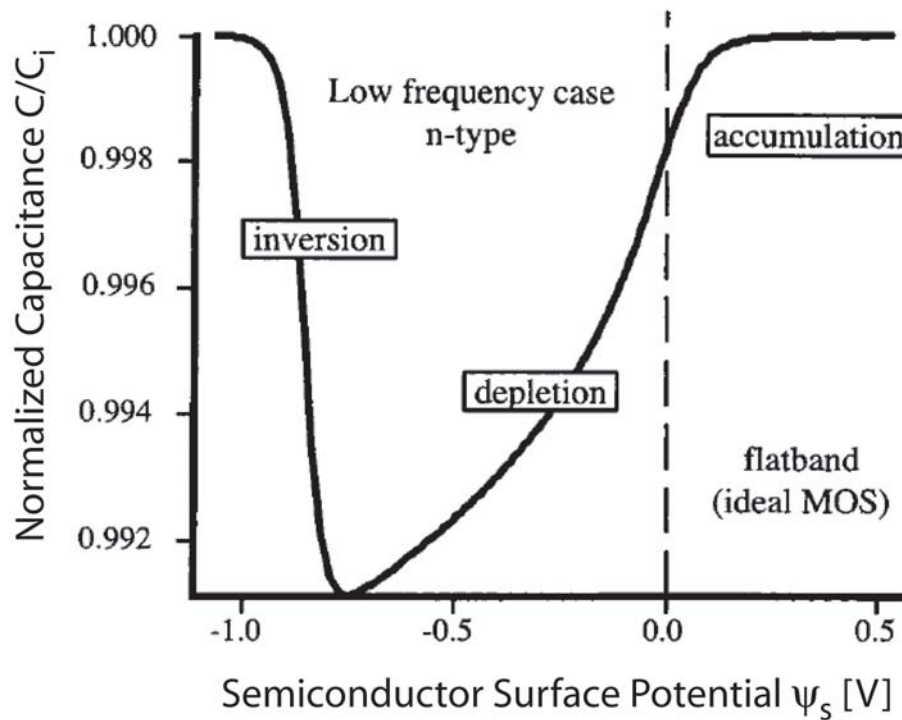


Figure 4.5: Normalized capacitance of a EIS system plotted as a function of semiconductor surface potential (ψ_s). C_i is the insulator capacitance. The three different space-charge regimes show different capacitive sensitivities to changes of surface potentials.

the flat band potential of the semiconductor is possible.

In an electrolyte-(several layers)-semiconductor contact, the space-charge capacitance may not be detectable in general. To experimentally confirm that C_{SC} is traced, it is convenient to perform a Mott-Schottky analysis ($1/C_p^2$ vs U_{bias}), where C_p is the total interface capacitance. Note that, the relation between C_p and C_{SC} depends on the design of the equivalent circuit. If $1/C_{SC}^2$ vs U_{bias} is linear and the extracted doping ratio (equation 3.2 of page 20) matches with the doping ratio of the semiconductor measured by independent methods, like Hall Measurements, the calculated C_{SC} corresponds to the actual space-charge capacitance. Additionally, the semiconductor is ensured to be operated at the depletion regime. This is a key issue because under these conditions, as surface charges and dipoles induce changes in surface potential, the measurement of the space-charge capacitance enables to sense electrical changes occurring at the electrolyte-(several layers)-semiconductor contacts.

4.5.2 Identification of Different Electrochemical Layers

The presence of additional layers on the surface aggregates to the total interface impedance. The circuit elements presented above (section 4.4) and new ones (if an association to a particular physical phenomenon is possible) can be combined to an equivalent circuit representative of distinct interfacial processes.

To show the importance of performing impedance spectroscopy in a wide frequency range, figure 4.6 is elaborated. It models three different cases and it depicts the absolute impedance (above plots) and the phase (bottom plots) of the total impedance in the Bode representation. The black curves correspond to a simple electrolyte/insulator/semiconductor interface of total capacitance $C_p = 2 \mu\text{F}$ and total ohmic resistance $R_p = 10^6 \Omega$ of a sample of 1 cm^2 of surface area (Model A). Subsequently, an additional layer is deposited on top of this surface. Two cases are differentiated. The first case (red dashed curve) corresponds to a layer with capacitance $C_m = 1 \mu\text{F}$ and high ohmic resistance, $R_p = 10^5 \Omega$ (Model B). The second case (blue dash-dotted curve) corresponds to a layer with diffusive barrier properties (Warburg resistance) $\sigma = 10^4 \text{ V/As}^{1/2}$ and a capacitance of $C_m = 1 \mu\text{F}$ (Model C).

Clearly, the different layers can be distinguished when the entire frequency spectrum is obtained. In fact, if the impedance spectrum were taken between 10 Hz and 100 Hz, the distinction between the cases of Model B and Model C would be difficult. Besides, in this narrow frequency window, the quantification of the circuit elements by applying equivalent circuits can be erratic, as different equivalent circuits could also fit the observations. Consequently, broadening the frequency range enables not only the distinction of different electrochemical layers, but also quantification of the (bio)physical processes once fitting the experimental data with the appropriately designed equivalent circuit models.

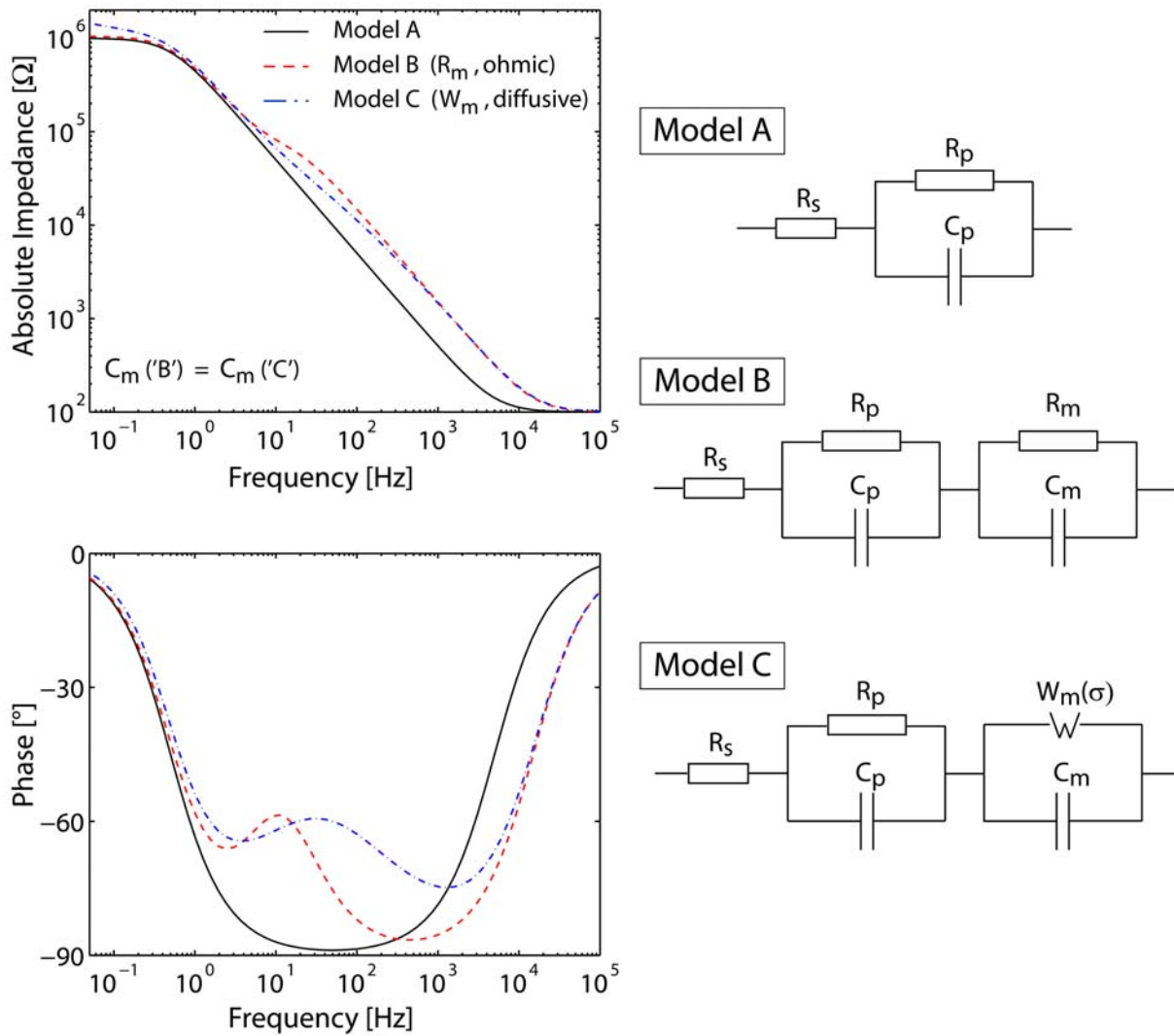


Figure 4.6: Simulated impedance spectra (Bode plots) based on circuit models. Model A represents an electrolyte/insulator/semiconductor (EIS) interface of 1 cm^2 of surface area and $R_p = 10^6 \text{ } \Omega$ and $C_p = 2 \text{ } \mu\text{F}$ (black continuous line). Model B adds an additional layer of resistance $R_m = 10^5 \text{ } \Omega$ and capacitance $C_m = 1 \text{ } \mu\text{F}$ (red dashed curve). Model C adds a diffusive layer of $\sigma = 10^5 \text{ V/As}^{1/2}$ and capacitance $C_m = 1 \text{ } \mu\text{F}$ on the EIS system (blue dashed-dotted curve). It is necessary to perform impedance spectroscopy over a wide frequency window to distinguish the different electrochemical layers.

Chapter 5

pH Sensitivity of Bulk GaAs coated with CH₃-MBP Monolayers

There are several physical and chemical processes that can lead a surface to be electrically charged as a consequence of aqueous ions. A common charging mechanism on surfaces in contact with aqueous electrolytes is the protonation or deprotonation of surface atoms or molecules, usually involving -OH radical groups [78]. In this context, the protonation-deprotonation equilibrium is controlled by the pH of the electrolyte [79].

In this chapter, the response of GaAs surfaces coated with CH₃-MBP monolayers to electrolyte pH is investigated. CH₃-MBP molecules cannot undergo the protonation-deprotonation reaction as CH₃- group and the phenyl rings of the molecule are stable over a wide pH range. In the first part, impedance spectroscopy on bulk GaAs electrodes is exploited towards quantifying the pH sensitivity and elucidating the charging mechanism. Impedance spectroscopy (see chapter 4) is a valuable tool to analyze interfacial processes in physical and chemical terms. In the second part, AlGaAs/GaAs 2-Dimensional-Electron-Gas (2DEG) devices functionalized with CH₃-MBP monolayers, which are designed to be sensitive to changes of surface potentials, are also exploited in order to provide independent observations of the pH sensitivity and supporting arguments for the charging mechanism.

5.1 Impedance Spectroscopy on Bulk GaAs Electrodes

5.1.1 Functionalized GaAs Electrodes: Modelling of Impedance Spectra

Prior to the potential/pH scans, the electrochemical stability of the GaAs sample coated with CH₃-MBP monolayers was firstly confirmed by monitoring the impedance spectra at the current minimum potential $U_{bias,j=0} = -350$ mV (vs. Ag/AgCl) over a period longer than 30 min. A typical spectrum is depicted on figure 5.2 in the Bode representation. From the experience we gained with the same system, such stability can be sustained up to 20 hours, as demonstrated by Adlkofer et al. [26]. To obtain the frequency dispersion of the electrochemical response, the impedance spectra are taken over a wide frequency window, from 100 kHz to 50 mHz. Throughout this study, the interface was exposed from neutral to acidic pH conditions, as irreversible degradation of the GaAs surface can readily occur at the local defects under basic pH conditions [48]. After the completion of the experiments, the sample was again investigated at the initial condition in order to ensure the electrochemical stability of the sample as well as the reproducibility of the experimental data.

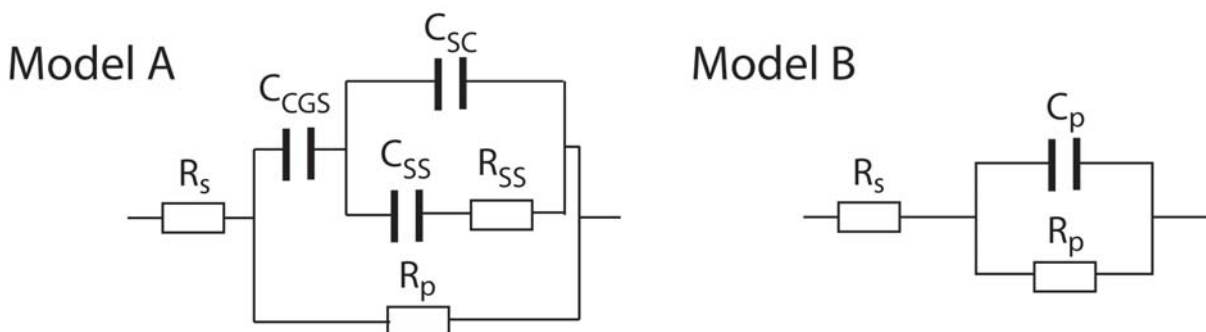


Figure 5.1: The elementary equivalent circuits employed to fit the impedance spectroscopy results. Model A includes all different contributions to the Electrolyte-(Insulator)-Semiconductor interface impedance. C_{CGS} represents the Chapman-Gouy-Stern (CGS) capacitance, C_{SS} the capacitance and R_{SS} the resistance of the surface states (SS), C_{SC} the capacitance of the space-Charge (SC), R_s the electrolyte resistance and R_p the total interface resistance. Model B is justified to be the resulting approximated circuit for Model A of the Electrolyte/CH₃-MBP/GaAs interface. Here, R_p accounts for the total interface resistance and C_p the total interface capacitance.

In general, the GaAs/electrolyte interface can be represented by the equivalent circuit model proposed by Allongue et al. (Model A in Chart 5.1) [43] [80]. The serial resistance R_s corresponds to the Ohmic behaviour of the electrolytes and/or electrical contacts,

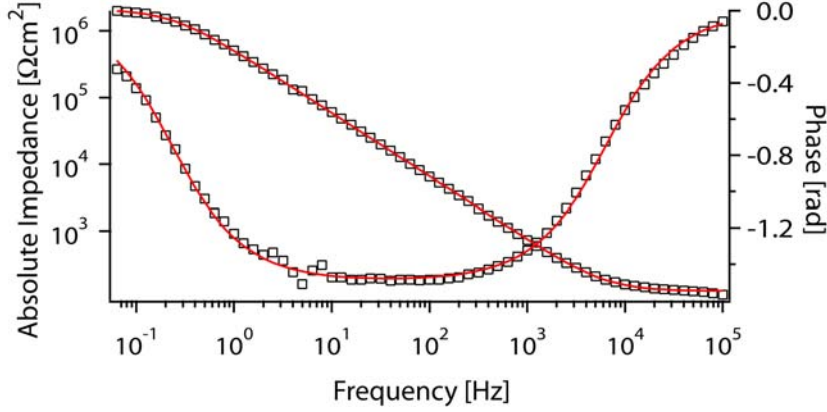


Figure 5.2: Impedance spectrum (Bode Plot) of GaAs electrode coated with $\text{CH}_3\text{-MBP}$ monolayer in contact with electrolyte. The experimental data (\square) could be fitted with Model B (red continuous curve) of figure 5.1 yielding the interface resistance and capacitance. Model B fits the entire spectrum within 1% of error.

and the parallel resistance R_p is attributed to the Ohmic behaviour of the interface. C_{SS} and R_{SS} denote the capacitance and resistance, respectively, of the surface states. C_{SC} is the capacitance of the semiconductor space charge region, and C_{CGS} is the capacitance of the Chapmann-Gouy-Stern (CGS) layer.

For our experimental system, we can simplify the model step by step as following. As discussed in detail on section 3.1.3 and also by Adlkofer et al. [81], the contributions of the *surface states* to the interface capacitance, C_{SS} , are not detectable if $C_{SS}/C_{SC} < 0.1$ [43]. Such argument is further supported by the fact that Adlkofer et al [24] attributed the enhancement of photoluminescence of X-terminated mercapto-biphenyls on GaAs to the sensible reduction of density of surface states, as the capacitance of the surface states scales almost linearly with density of surface states, see 3.1.3 and [44]. As R_{SS} cannot be separated from the measurements, it is included into R_p .

The capacitance of the Chapman-Gouy-Stern C_{CGS} can be described as a serial connection of the Helmholtz layer capacitance C_H and the capacitance of the diffuse layer C_{diff} ,

$$C_{CGS} = \frac{C_H C_{diff}}{C_H + C_{diff}}.$$

Typically, $C_H \simeq 140 \mu\text{Fcm}^{-2}$ and $C_{diff} \simeq 0.9 \text{Fcm}^{-2}$.

Consequently, the impedance spectra can be analyzed according to the simplified equivalent circuit Model B in Chart 5.1, instead of Model A. Here C_p stands for the combined capacitance of the interface, and it is the serial connection of the capacitance

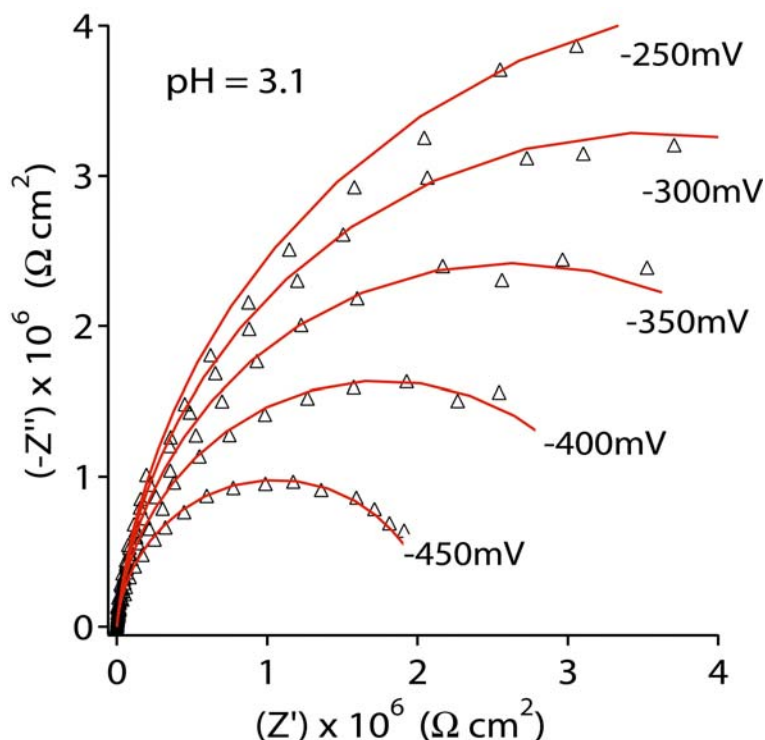


Figure 5.3: Impedance spectra of GaAs coated with a CH₃-MBP monolayer in contact with 10mM phosphate buffered saline (PBS, pH = 3.1), measured at around the current minimum potential $U_{bias,j=0} = -350\text{mV}$ (vs. Ag/AgCl). The symbols correspond to the measured data points, while the line to the fit with Model B (see Chart 5.1). No clear sign of diffusion of ions across the CH₃-MBP monolayer could be observed within the measured frequency range (from $f = 100\text{ kHz}$ to 50 mHz), suggesting that the CH₃-MBP monolayer can be treated as an insulator. In fact, the constant phase element (Model C, in Chart 5.4) at $f = 1\text{ kHz} \sim 5\text{ Hz}$ was found to be $\alpha = 0.96$, which is close to that of an ideal capacitor $\alpha = 1.0$.

of the Space Charge, C_{SC} of about $1 - 2\ \mu\text{Fcm}^{-2}$ and the capacitance of a monolayer $C_{SAM} \simeq 0.5\ \mu\text{Fcm}^{-2}$. In fact, the interface capacitance of the freshly etched GaAs, $C_p = 2.0\ \mu\text{Fcm}^{-2}$, agrees reasonably well with the space charge capacitance of GaAs with a comparable carrier density ($2 \times 10^{18}\ \text{cm}^{-3}$), $C_{SC} \simeq 1.7\ \mu\text{Fcm}^{-2}$ [52]. The result of fitting with Model B on a typical impedance spectrum is depicted in Bode representation on figure 5.2 by the red continuous lines.

5.1.2 Response to Bias Potential Sweeps

In Figure 5.3, impedance spectra of GaAs coated with CH₃-MBP monolayer in contact with 10 mM PBS at pH = 3.1 are presented in the form of Nyquist represen-

tation. Here, $-Z''$ is plotted against Z' , where Z' and Z'' are the real and complex part of the complex impedance, $Z(\omega)$. The symbols correspond to the data points measured at their particular frequency (not explicitly marked) and bias potentials of $U_{bias} = -450 \sim -250$ mV. The continuous lines are the fitting curves with the Model B of Chart 5.1.

As can be seen from the figure, all the spectra show excellent agreements with the ideal circuit model, Model B, within the measured frequency windows with fitting errors $< \pm 2\%$. To further understand the nonlinear frequency dispersion of the measured impedance, the total interface capacitance C_p can be replaced to a Constant Phase Element, CPE, which is parameterized by a frequency exponent α ($0 < \alpha < 1$), see section 4.4. The CPE element represents information about inhomogeneities at the interface of any kind, regardless of its exact physical origin [60]. In brief: $\alpha = 1$ represents a pure capacitor, $\alpha = 0.5$ a Warburg element and $\alpha = 0$ a pure resistor.

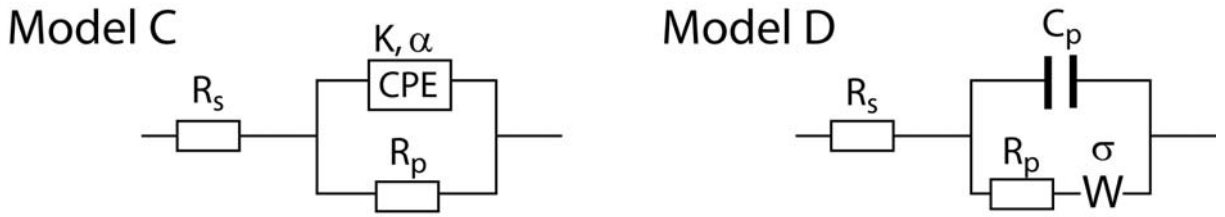


Figure 5.4: Advanced circuit models employed to analyze the electrolyte/CH₃-MBP/GaAs interface. Model C includes the constant phase element (CPE) usually employed to account for inhomogeneities of the surface. Model C adds Warburg resistance $W(\sigma)$ to track the diffusion of ions species across the self-assembled monolayer.

The impedance data are dominated by the interface capacitance from 200 to 1 Hz, which can be determined by the measured phase shift. Within this frequency regime, the CPE exponent values calculated for all the measured spectra are $\alpha = 0.95 \pm 0.01$. On the other hand, the impedance data below 200 mHz exhibit no deviation from the ideal resistor. The frequency exponent obtained by replacing R_p to CPE remains $\alpha = 0$, Fig 5.4. Thus, the obtained results clearly indicate that it is reasonable to treat the CH₃-MBP monolayer as an ideal RC element, i.e. Model B.

In Fig. 5.5, the calculated $1/C_p^2$ is plotted versus the bias potential, U_{bias} (Mott-Schottky plot). Here, it should still be noted that the combined interface capacitance C_p is taken, since the frequency range at which the impedance spectra are dominated by C_{SC} overlaps to the range dominated by the monolayer capacitance C_m .

The linear fit $1/C_p^2$ vs U_{bias} yields the doping ratio of $n = 3.0 \times 10^{18} \text{ cm}^{-3}$, which agrees well with that of a bare GaAs sample obtained from an independent Hall mea-

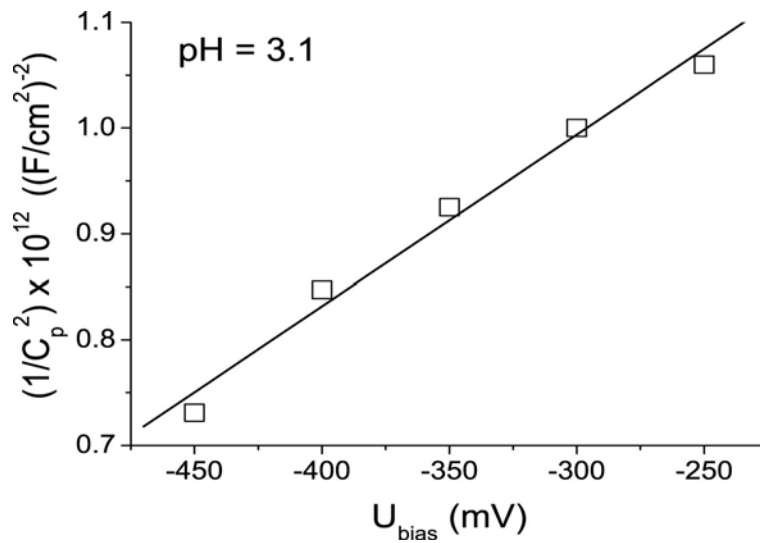


Figure 5.5: Mott-Schottky plot ($1/C_p^2$ vs. U_{bias}) extracted from the results presented in Fig. 5.3. The plot is almost linear within the measured potential range, and the doping ratio obtained from the slope, $n(Mott) = -3 \times 10^{18} \text{ cm}^{-3}$, agrees well with that obtained by Hall measurements, $n(Hall) = -2.23 \times 10^{18} \text{ cm}^{-3}$. The linear extrapolation to $1/C_p^2 = 0$ yields the flat band potential of $U_{fb} = -910 \text{ mV}$. Although electrochemical measurements at a wider potential range are not possible due to the intrinsic instability of GaAs in aqueous electrolytes, the obtained value is comparable to that of GaAs with an alkanethiol monolayer.

surement, $n(Hall) = 2.2 \times 10^{18} \text{ cm}^{-3}$ (see 3.1.2). The intercept with the x-axis by the extrapolation of the plot to $1/C_p^2 = 0$ yields the corresponding flat-band potential, $U_{fb} = -910 \text{ mV}$. Despite of the difficulty to carry out electrochemical measurements at a wider potential range due to the intrinsic instability of GaAs in aqueous electrolytes, the obtained value is comparable to that of GaAs with an alkanethiol monolayer, $U_{fb} = -850 \text{ mV}$ [81], obtained by the same extrapolation. In fact, although the calculated C_p consists of both C_{SC} and C_m , a systematic dependence of the C_p on the bias potential could also be observed at pH = 6.8. The obtained results clearly indicate that GaAs functionalized with a CH₃-MBP monolayer is operated at the depletion regime at the current minimum potential ($U_{bias,j=0} = -350 \text{ mV}$), which can further be used for capacitive sensing of the change in surface potentials.

Figure 5.6 represents the interface resistance R_p calculated from the measured impedance spectra at bias potentials $U_{bias} = -450 \sim -250 \text{ mV}$, plotted as a function of time and at two extreme pH conditions (3.1 and 6.8).

In contact with acidic electrolyte (pH = 3.1), R_p exhibited a stepwise increase of $\Delta R_p = 0.64 \text{ M}\Omega \text{ cm}^2$ with each voltage step of $\Delta U_{bias} = 50 \text{ mV}$, which remains constant

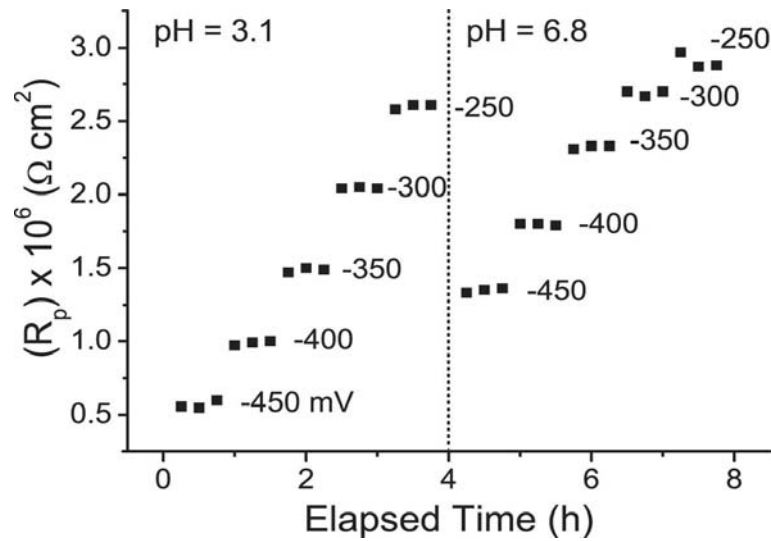


Figure 5.6: Interface resistance R_p obtained from Model B (Chart 5.1) plotted as a function of time. The impedance spectra are reproducible at each potential during successive three impedance measurements, confirming the electrochemical stability of GaAs with a $\text{CH}_3\text{-MBP}$ monolayer in both acidic ($\text{pH} = 3.1$) and neutral ($\text{pH} = 6.8$) electrolytes.

during three successive impedance measurements (~ 30 min). At $\text{pH} = 6.8$, the absolute R_p values clearly differ from the corresponding values at $\text{pH} = 3.1$, however, the width of the stepwise increase in the resistance at each voltage step of $\Delta U_{bias} = 50$ mV remains constant, $\Delta R_p = 0.64 \text{ M}\Omega \text{ cm}^2$. At $\text{pH} = 6.8$, the interface resistance shows a drift at $U_{bias} = -250$ mV, suggesting the anodic oxidation of the GaAs surface. From the latter Figure, not only is R_p demonstrated to be sensitive to changes of U_{bias} , but also over a period of 8 hours of the experiment, R_p showed no symptoms of degradation.

5.1.3 Response to Electrolyte pH

As shown in Figure 5.6, at a fixed U_{bias} , R_p exhibit two different values at the different pH. For example, at $U_{bias} = -450$ mV, the resistance at $\text{pH} = 6.8$ ($R_p = 1.3 \text{ M}\Omega \text{ cm}^2$) is about as twice as large as that at $\text{pH} = 3.1$ ($R_p = 0.6 \text{ M}\Omega \text{ cm}^2$). This finding suggests a possibility that the GaAs functionalized with a $\text{CH}_3\text{-MBP}$ monolayer might be sensitive to the change in the electrolyte pH.

To verify this hypothesis, the impedance spectra under various pH conditions were measured, while fixing the bias potential constant at $U_{bias,j=0} = -350$ mV. To be sure that the electrolyte passed the flow chamber was unchanged, the pH value of the electrolyte

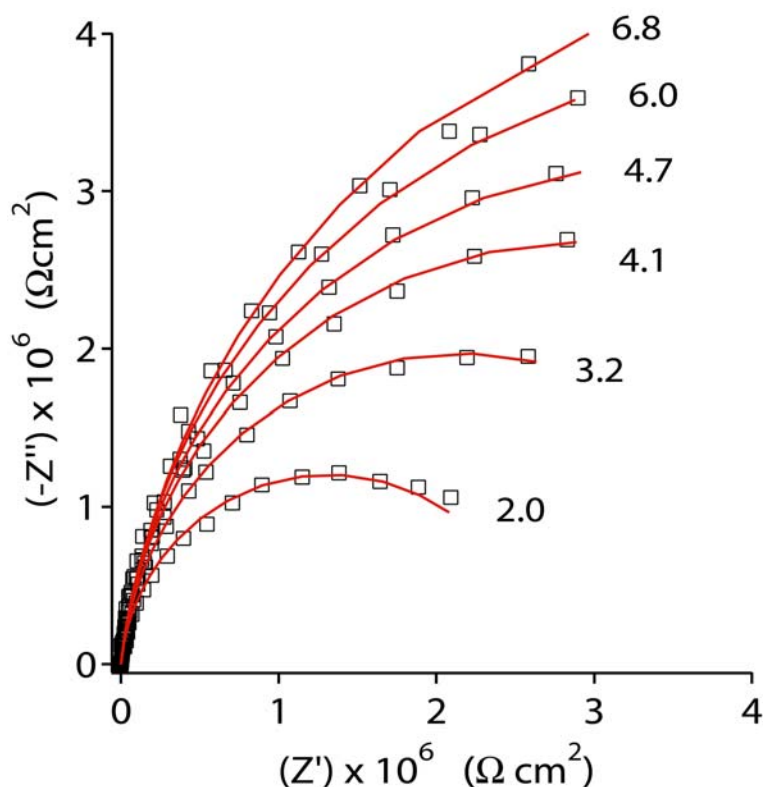


Figure 5.7: Impedance spectra of GaAs coated with a CH₃-MBP monolayer measured under pH titration from 2.0 to 6.8 in the Nyquist form. Here, the bias potential was set constant, $U_{bias,j=0} = -350$ mV. The impedance spectrum at pH = 2.00 was reproducible after the titration. All the impedance data can be well fitted with Model B (Chart 5.1)

at the outlet from the electrochemical cell was checked, showing a deviation from the pH at the inlet of less than ± 0.1 . As presented in Figure 5.7, the impedance spectra show also a clear dependence on the pH conditions. The fitting with Model B of Chart 5.1 (continuous lines of Fig. 5.7) indicate that interface resistance R_p systematically increases with increasing pH.

Figure 5.8 shows the relationship between the absolute interface resistance R_p and the bias potential, U_{bias} , measured in acidic (pH = 3.1, squares) and neutral (pH = 6.8, circles) electrolytes. As given by solid lines in the figure, despite of the difference in absolute R_p values, both sets of data exhibit an identical linear dependence with a slope of $12.8 \pm 0.5 \text{ } \Omega\text{cm}^2\text{V}^{-1}$. Although it is not plotted, the same slope can be obtained from the other experiments at pH = 2.0, 3.8, 4.5 and 6.0. This proves the systematic increase in the absolute R_p value with increasing pH.

The observed 'parallel' shift in the linear relationship between R_p and U_{bias} suggests that there is a certain relationship between R_p and pH. Certainly, if one chooses one

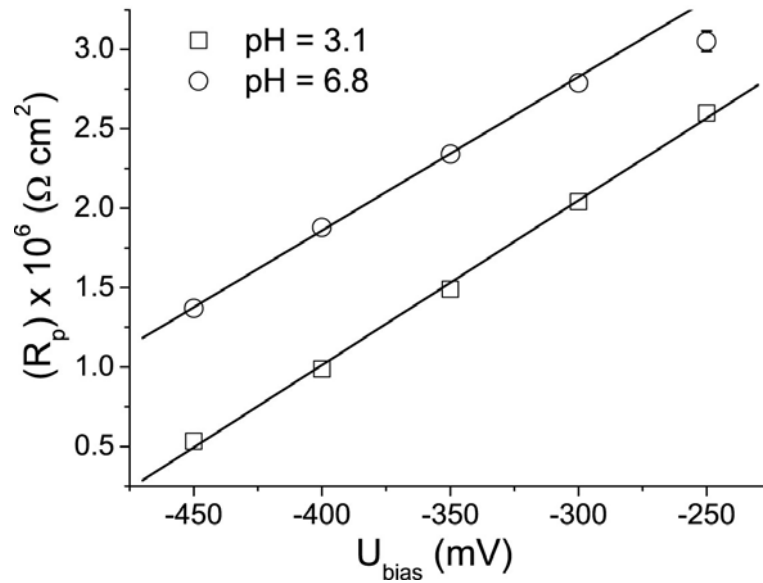


Figure 5.8: The interface resistance R_p plotted as a function of the bias potential. R_p scales linearly with the bias potential in both acidic (pH = 3.1) and neutral (pH = 6.8) electrolytes. The slopes at other pH conditions were found to be almost identical between pH = 2.0 and 6.8 (some data not show in the figure), $1.28 \times 10^4 \Omega \text{ cm}^2 \text{ mV}^{-1}$, suggesting the linear relationship between R_p and U_{bias} .

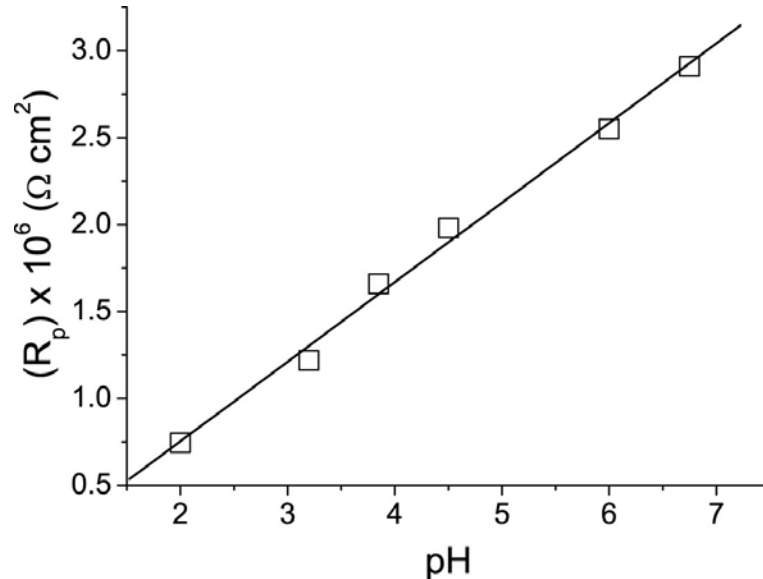


Figure 5.9: The linear relationship between R_p and pH at $U_{bias,j=0} = -350 \text{ mV}$, obtained from the same series of experiments presented in Fig. 5.7. From the slope of the plot, $4.55 \times 10^5 \Omega \text{ cm}^2 \text{ pH}^{-1}$, the 'pH sensitivity' of GaAs coated with a $\text{CH}_3\text{-MBP}$ monolayer can be estimated to be 35 mVpH^{-1} .

bias potential ($U_{bias} = -350$ mV) and plots R_p as a function of pH, a linear relationship between R_p and pH can be observed, Figure 5.9. The slope of this plot (the solid line) yields $4.55 \times 10^5 \Omega\text{cm}^2\text{pH}^{-1}$, which is identical for the other bias conditions (data not shown).

From the relationships found for R_p vs U_{bias} , Fig. 5.8, and R_p vs pH, Fig. 5.9, one can obtain a linear relationship between the bias potential U_{bias} and pH. Its slope is 35 ± 3 mVpH⁻¹. It should be noted that the experimental results can be reproduced by several pH and potential cycles (time scale of > 12 h).

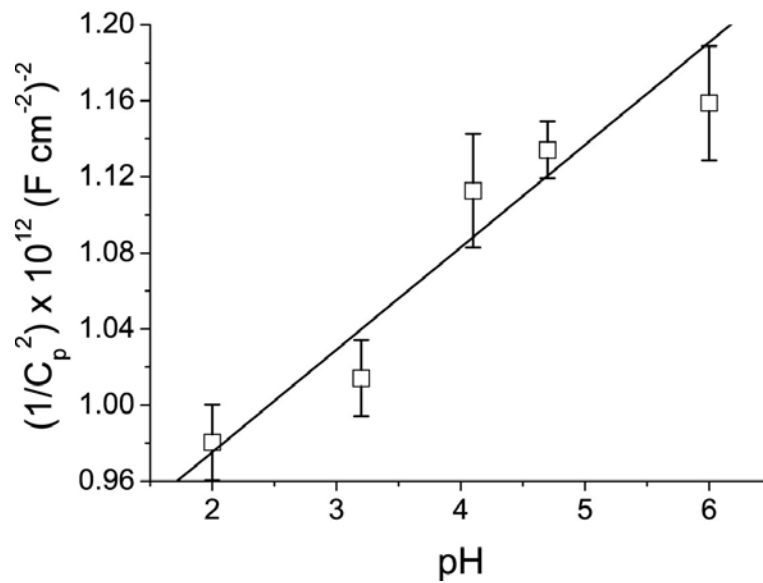


Figure 5.10: The linear relationship between $1/C_p^2$ vs pH. Together with the linear relationship found between $1/C_p^2$ vs. U_{bias} (Fig. 5.5), one can extrapolate the pH sensitivity from capacitance measurements to be 32 ± 3 mVpH⁻¹.

Furthermore, a linear relationship $1/C_p^2$ vs U_{bias} can be found at various pH conditions between 3.1 and 6.8. In Figure 5.10 shows the linear relationship found $1/C_p^2$ vs pH at $U_{bias} = -350$ mV. The linearity of the relationship, suggests, once more, that changes on pH alters the surface potential of the interface. A linear fit on this data yields a slope of $5.25 \times 10^{10} (\text{Fcm}^{-2})^{-2}\text{pH}^{-1}$. From the slopes of $1/C_p^2$ vs U_{bias} (Fig. 5.5) and $1/C_p^2$ vs pH (Fig. 5.10), a sensitivity of 32 ± 3 mVpH⁻¹ is derived.

The slightly lower sensitivity and larger errors of the capacitive sensing in comparison to the resistive is attributed to the fact that C_p includes the contribution of both the semiconductor space charge capacitance C_{SC} and the insulating biphenylthiol monolayers capacitance C_m , which lie in the same order of magnitude.

5.1.4 Mechanism of the pH Sensitivity

The previous observations provided with evidences that the pH of the electrolyte influences the surface potential of the surface of GaAs coated with CH₃-MBP monolayer. To understand the mechanism of the pH sensing several possible scenarios are discussed in the following subsections.

(i) Influence of the Ionic Strength

A possibility to the origin of such changes of surface potentials is the influence of the supporting salts, in particular the buffering ones. The Henderson-Hasselbach equation, eq 2.1, shows the influence of the pH to ionic strength of the electrolyte. In prevention to this effect, the supporting electrolyte was designed in such a way to minimize the changes of ionic strength due to pH changes by dissolving 10 mM PBS and 100 mM NaCl.

The change in the osmolarity by pH titration was checked by an osmometer. Within the pH range of 2-7, the osmolarity of the electrolyte remained to 0.25 ± 0.03 Osm/kg. Such changes were negligible to explain the pH sensitivity observations. Furthermore, in contrast to its linear dependence to pH, the dependence of the interface resistance R_p on the ionic strength, i.e. concentration of NaCl, was found to be negligible between 1 and 500mM of NaCl (data not shown). This result seems plausible since the space charge in the electrolyte becomes a delta function distribution near the surface at high salt concentrations. [82]

(ii) Diffusion of Ions across the CH₃-MBP Monolayer

Another possible reason to account for such changes in the interface resistance is the change in the permeability of the monolayer against H⁺ or OH⁻ ions under pH changes. For example, the permeation coefficients of H⁺ or OH⁻ ions across hydrocarbon chains, such as the permeation across a lipid bilayer membrane, is in the order of 10^{-8} ms⁻¹ that is about six orders of magnitudes larger than the corresponding values of other inorganic ions, such as Na⁺, Ca²⁺, etc. [65]

To verify this possibility, another equivalent circuit model was taken, Model D in Chart 5.4, that takes the diffusion of the ions across the monolayer into account. This model includes the so called Warburg impedance which was originally used to describe the electron transfer from a bulk electrolyte to an electrode. [66] Although the application

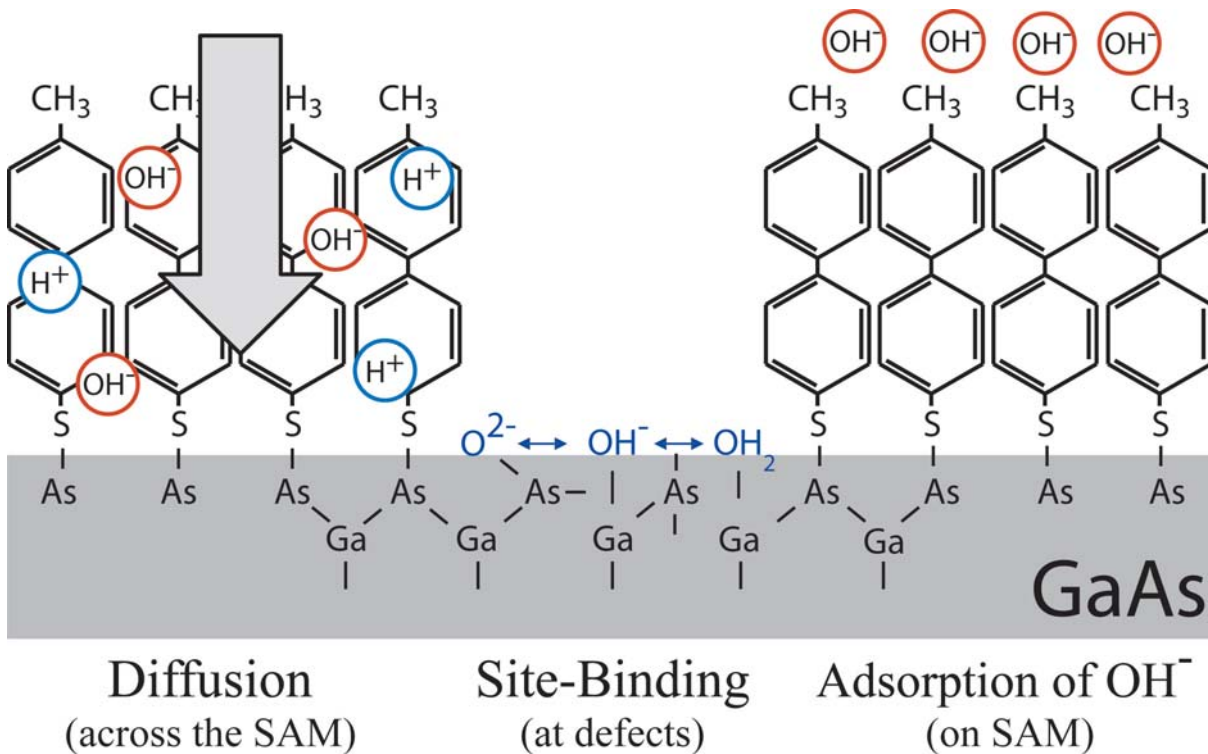


Figure 5.11: Schematic representation of the different charging scenarios discussed in this chapter.

of Warburg impedance for the diffusion across a layer with a finite thickness is based on an approximation that the distance between the diffusion pathways is small enough for an overlap of their spherical diffusion layers, this model has served well to describe the diffusion of ions across other organic monolayers on metal [68] and semiconductor electrodes [83]. The Warburg impedance $W(\omega)$ is represented by

$$W(\omega) = \left(\sigma + \frac{1}{\sigma} \right) \omega^{-\frac{1}{2}} \quad (5.1)$$

where ω is the angular frequency and σ the Warburg parameter *

$$\sigma = \frac{4RT}{\sqrt{2}n^2F^2A\rho} \frac{1}{\sqrt{D}} \quad (5.2)$$

A is the active electrode area, D is the diffusion constant of the ions, and ρ is their concentration at the interface. The constants R, T, n , and F are gas constant, absolute temperature, the charge of ions in the electrolyte, and Faraday constant, respectively.

*Please note not to confuse between σ (Warburg parameter) and σ_i , which employed to designate the surface charge density.

All σ values calculated from the impedance data presented in Figure 5.7 are $>10^6 \Omega\text{s}^{1/2}$. Assuming that ρ equals to the concentration in bulk, $D < 10^{-3} - 10^{-4} \mu\text{m}^2\text{s}^{-1}$ which is much smaller than the values reported for organic monolayers with defects, $D > 10^{-2} \mu\text{m}^2\text{s}^{-1}$.

Besides, such a small diffusion term shows no influence on the quality of the fit. It suggests that the influence of the change in permeation or diffusion H^+ or OH^- according to the pH change is negligible. In fact, when we replace the circuit model to Model C including a CPE, the frequency exponent α at the window between $f = 200$ and 1 Hz is always above 0.95 ± 0.01 . This is clearly different from the exponent corresponding to the diffusion barrier described by the Warburg element, $\alpha = 0.5$, and, as previously argued, suggests that the monolayer can be represented as a parallel connection of an ideal resistor and an ideal capacitor. This argument is further supported by the very high electric resistance of the GaAs coated with an organic monolayer of about 1 nm thick, $R_p = 10^5 - 10^6 \Omega\text{cm}^2$. Thus, we conclude that the change in the absolute R_p values upon pH titration *cannot* be explained in terms of the difference in permeation of H^+ or OH^- ions across the CH_3 -MBP monolayer.

(iii) Site-Binding Model

The third possible scenario is the reaction of oxide corresponding to local defects with H^+ or OH^- ions, which can be treated with the "site binding" theory [78]. The oxide locally expressed on the surface acts as the binding sites for H^+ or OH^- ions. The equilibrium between the "occupied" and "free" sites by the protonation and deprotonation of the oxide determines the surface potential (ψ_0). As expressed within the framework of the theory for highly reacting sites ($q\psi_0/kT \ll \beta$), the sensitivity equation is given by

$$\psi_0 = 2.303 \frac{k_B T}{q} \frac{\beta}{\beta + 1} (pH_{pzc} - pH) \quad (5.3)$$

$$\beta = \frac{2q^2 N_S \sqrt{K_a K_b}}{k_B T C_{CGS}} \quad (5.4)$$

where pH_{pzc} is the pH at the point of zero charge, N_S the number density of binding sites (in this case, $-\text{OH}$ groups), q the electron charge, and C_{CGS} the double-layer capacitance. K_a and K_b are the equilibrium constants of $A - \text{OH} \rightleftharpoons A - \text{O}^- + \text{H}^+$ and $A - \text{OH} + \text{H}^+ \rightleftharpoons A - \text{OH}_2^+$ for a given surface A . Qualitatively, the larger β value

means that the surface is highly reactive. To obtain β of GaAs experimentally, the pH sensitivity measurement on bare (freshly etched) GaAs was carried out. Initially, impedance spectra showed irreversible drifts. After some hours, the response to pH changes came closer to 60 mV/pH. As reported for GaAs with an inorganic oxide layer [48], as soon as the adsorption rate dominates the entire adsorption-desorption process of charging, the sensitivity should result in 60 mV/pH [79]. Thus, considering that the reactivity of the defects is the same as that of bulk electrodes, the observed sensitivity of 35 mV/pH could not be explained with the Model. It should be noted that neither K_a , K_b , nor N_s values are known for bare GaAs in aqueous electrolytes due to the complex electrochemistry of GaAs/Electrolyte interfaces.

Although this scenario cannot be completely excluded to account for our experimental results, the reproducibility of the measurements ensured that the process is reversible within our experimental conditions, in contrast to irreversible drifts observed for bare GaAs.

(iv) Hydroxide Ions Adsorption on the Hydrophobic CH₃-MBP Monolayer

The last scenario is the adsorption of OH⁻ ions on the CH₃-MBP self-assembled monolayer (hydrophobic headgroup). Previously, Marinova et al. [84] measured the electrophoretic mobility of oil droplets, and suggested, after considering diverse possible charging mechanisms, that the charging mechanism was caused by the adsorption of OH⁻ ions at the oil/water interface. More recently, Schweiss et al. [85] and Chan et al. [86] used a micro-slit electrokinetic setup to measure simultaneously the streaming potential and streaming current to determine the ζ -potentials of gold substrates coated with methoxytri(ethylene-glycol)(EG₃OMe)-terminated alkanethiols. From their observations, the suggested mechanism responsible for their negative ζ -potential was also the adsorption of OH⁻ ions at the interface. Furthermore, numerical simulations by Density Functional Theory (DFT) on self-assembled monolayers of PEG-terminated alkanes (hydrophobic) show the preferential adsorption of OH⁻ ions at the PEG/electrolyte interface [87]. Although the quantitative separation of the surface resistance and the bulk resistance is impossible for our system, the measurement of the isoelectric point seems to agree well with the one reported for Au with alkanthiol monolayers (pI \sim 4) [85].

More recently, the spontaneous adsorption of OH⁻ ions on a 'hydrophobic surface' /water interface was demonstrated by Molecular Dynamics simulations. The phenomenology relies on the following. On a hydrophobic/water interface, the impossibility of inter-

facial water molecules to form hydrogen bonds with the hydrophobic surface forces them to acquire a preferential orientation towards their neighbouring water molecules. Owing to the high polarity of the water molecule, this interfacial water structure generates an electrical potential profile within the first layers that favourably attracts and, therefore, enhances the adsorption of OH^- ions [88].

5.2 pH Sensitivity of Two-Dimensional-Electron-Gas (2DEG) Devices Functionalized with CH₃-MBP Monolayers

2DEG (2-Dimensional-Electron-Gas) devices based on AlGaAs/GaAs heterostructures were fabricated at the laboratory of Prof. G. Abstreiter (Walter Schottky Institute, Technische Universität München). The experimental results presented in this section have been obtained under collaboration with S. Luber of WSI.

The aim of the experiment was to provide an independent evidence for the pH sensitivity observed by impedance spectroscopy. To achieve this goal, the 2DEG devices needed to (i) be functionalized with CH₃-MBP monolayers, (ii) be stable in contact with aqueous electrolytes and (iii) offer enough sensitivity to measure changes of pH/surface potentials. This section begins with the study of the stability of 2DEG devices of different coatings and follows with the pH sensitive measurements of 2DEG devices functionalized with CH₃-MBP monolayers. Further results concerning the measurements on sensing salt concentration on 2DEG devices coated with CH₃-MBP monolayers are presented in Appendix A.4.

5.2.1 Stability of Functionalized 2DEG Devices

Before any pH sensitive and stability measurements, the experimental conditions that minimized the electrochemical dissolution of GaAs at the surface of the device were found. A relevant parameter to account for the interfacial current transport is the leakage current (= counter electrode current). For 2DEG devices coated with CH₃-MBP monolayers in contact with electrolytes at pH = 7 (the most electrochemically degradable conditions in our experiment), the external bias potential that minimized the leakage currents was $U_{bias} = -400$ mV. This result is consistent with the current minimum potential observed in bulk GaAs electrodes coated with CH₃-MBP monolayers, which resulted in $U_{bias} = -350$ mV (see section 5.1.1). The difference in 50 mV is attributed to the difference in band bending between both devices. The cap layer of the 2DEG devices was compounded of an undoped GaAs layer whereas bulk GaAs electrodes used for impedance spectroscopy were highly doped.

The stability of the 2DEG device was checked by recording the sheet resistance R_{sh} as a function of time at the (leakage) current minimum potential. R_{sh} is the resistance of the 2DEG layer, which, in our configuration, is sensitive to changes of surface potentials and U_{bias} (see section 2.1.2 for operational details).

Figure 5.12 shows the time evolution of R_{sh} when 2DEG devices of different surface coatings were put in contact with electrolytes at pH = 7. For freshly etched surfaces (green data), the 2DEG device did not stabilize from the moment it was put in contact with the electrolyte. The result is consistent with the fact that bare GaAs undergoes an irreversible electrochemical decomposition in contact with aqueous electrolytes of neutral pH. In contrast, the functionalization of the surface of the 2DEG device with either OH-MBP or CH₃-MBP monolayers managed to stabilize (passivate) them against electrochemical decomposition. As depicted in the figure, in both cases, R_{sh} persisted at its initial value within an error of 10% for at least 10 hours. The lower stability obtained with OH-MBP monolayers (red data) is attributed to the poorer surface coverage with respect to CH₃-MBP monolayers (black data).

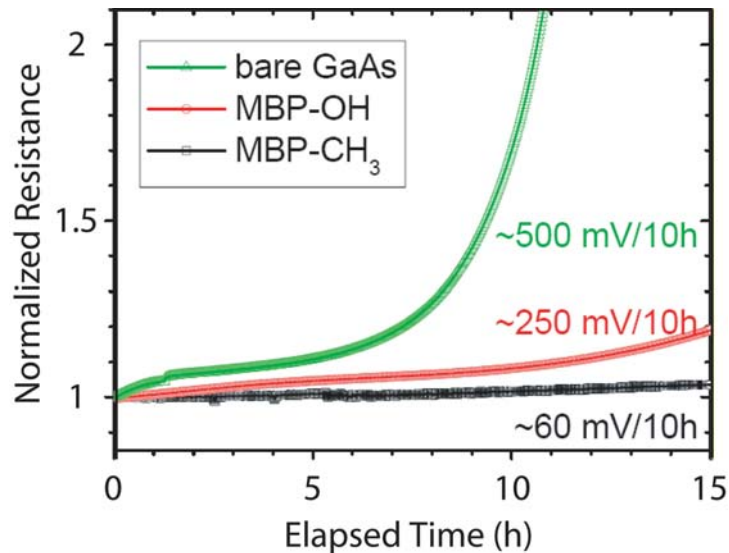
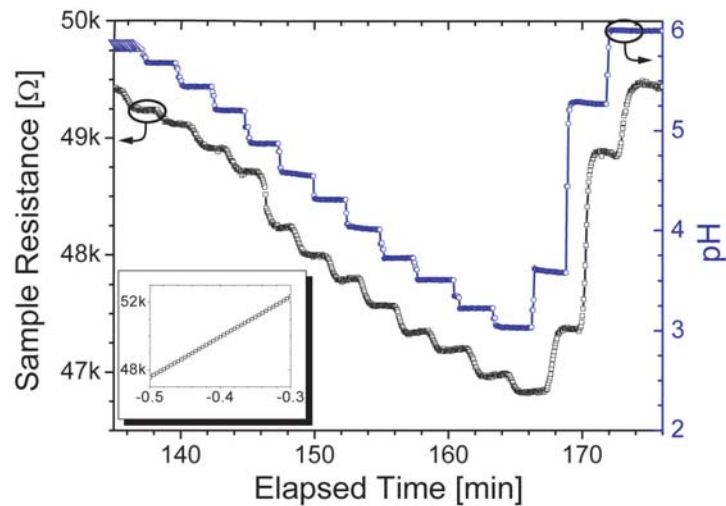


Figure 5.12: Time evolution of the sheet resistance (R_{sh}) of 2DEG devices with different surface coatings in contact with electrolytes. The green curve (Δ) corresponds to freshly etched devices, the red curve (\circ) to devices coated with OH-MBP and the black (\square) to the devices coated with CH₃-MBP monolayer. At pH = 7, freshly etched 2DEG devices were unstable as irreversible electrochemistry arose at the interface. The electrochemical stability was achieved for over 6-8 hours when the devices were coated with OH-MBP or CH₃-MBP monolayers. The higher stability provided by CH₃-MBP monolayers was attributed to the higher surface coverage with respect to OH-MBP monolayers.

The sensitivity limit to surface potentials of the device in contact with neutral electrolytes was also examined. The experiment consisted of measuring the smallest detectable changes of R_{sh} as a function of U_{bias} . For uncoated 2DEG devices the sensitivity limit could not be obtained given the rapid drift of R_{sh} . Nevertheless, for 2DEG devices coated with CH₃-MBP monolayers, the sensitivity limit was 100 μ V.

Figure 5.13: Main set: Sheet resistance (R_{Sh}) (black) of CH₃-MBP coated 2DEG devices and electrolyte pH (blue) as a function of time. In set: R_{sh} is plotted against U_{bias} (mV) vs Ag/AgCl. A direct correlation of between R_{sh} and pH and between R_{sh} and U_{bias} is evident and suggests that changes of pH correspond to changes of surface potentials.



5.2.2 Response of 2DEG Devices to Electrolyte pH

pH sensitive measurements were carried out on 2DEG devices functionalized with CH₃-MBP monolayers. The electrolyte pH was set and continuously measured at an external reservoir, from where it was constantly pumped through the flow chamber.

The pH sensitive measurements consisted in measuring changes in R_{sh} as a function of the electrolyte pH when the bias potential was kept constant at $U_{bias} = -400$ mV (vs. Ag/AgCl). The main set of figure 5.13 plots the results of an experiment. It depicts the raw data of R_{sh} (black, \square) and the pH value of the electrolyte at the reservoir (blue, \circ) as a function of time. The time delay between R_{sh} and pH curves is the time the electrolyte took to reach the flow chamber from the external reservoir. The results not only demonstrate an evident correlation between R_{sh} and pH but also that R_{sh} was reproducible upon reversible pH variations.

A potential sweep (-500 mV $< U_{bias} < -300$ mV vs. Ag/AgCl) at different pH values was carried out to correlate changes of surface potentials with R_{sh} . In the inset of figure 5.13, R_{sh} vs U_{bias} is plotted only for pH = 6. The accumulated results show that, regardless of the pH value, the slope of R_{sh} vs U_{bias} was the same within $\pm 1\%$ (data not shown).

Leakage currents across the interface could influence R_{sh} . In these measurements, R_{sh} is calculated from a linear (ohmic) fit of the source-drain I-V curves (see section 2.3.4). To account for such influence, leakage currents (= counter electrode currents) were also measured at all U_{bias} and pH values. Within U_{bias} and pH range of these experiments, the leakage currents varied about $i_{leak} < 5$ nA, and were negligible compared to the source-drain currents of the 2DEG $i_{SD} \simeq 500$ nA.

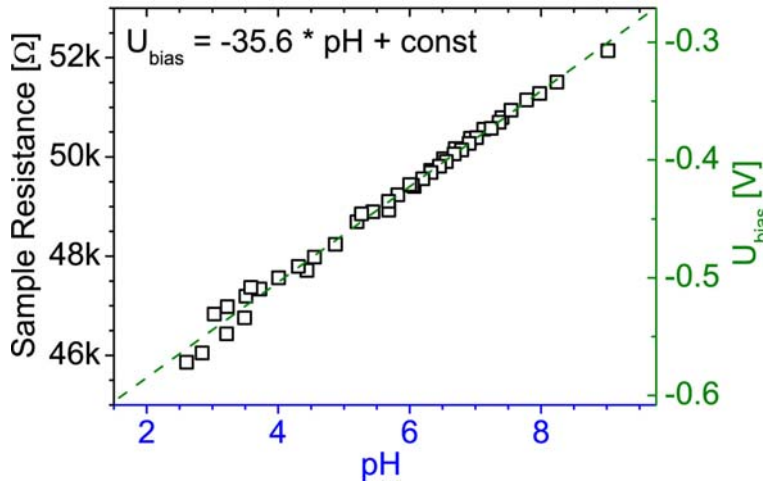


Figure 5.14: Correlation between sample resistance (R_{sh}) and bias potential (U_{bias}) with electrolyte pH. Upon reversible pH scans, the sample could reproduce the R_{sh} , indicating that the charging process is reversible. From the slope of the relationship of pH sensitivity of 36 mV/pH is extracted.

The fact that (i) leakage currents negligibly contributed to R_{sh} , and (ii) it existed a direct correlation between R_{sh} with the electrolyte pH and U_{bias} convinced that changes in electrolyte pH corresponded to changes in surface potentials ψ_s . This important conclusion is consistent with the electrochemical stability of the device (achieved by coating the 2DEG device with CH₃-MBP) and proves that the device is operative as a field effect device in contact with aqueous electrolytes (capacitive sensing).

Figure 5.14 shows the relation R_{sh} vs pH (left axis) after applying the calibration R_p vs U_{bias} (right axis). Here, the data-points correspond to the values extracted from different pH scans, a part of which is represented on the previous figure 5.13. Each data-point is an average over 2 min of the raw data just before the new pH value was inserted in the chamber. As seen, all data-points follow a linear relationship between pH and U_{bias} , regardless of the sense of the pH sweep. This fact indicates that variations of electrolyte pH correspondingly modified the surface potential and, therefore, the surface chemistry was not altered (to our sensitivity limit). In fact, the irreversible electrochemistry of bare GaAs in aqueous electrolytes would change the surface chemistry leading to an irreversible response (instability). From the linear relationship between R_{sh} vs pH and R_{sh} vs U_{bias} (the slope of the plot), the pH sensitivity could be calculated and resulted in 36 ± 6 mV/pH (average over different samples).

Remarkably, the pH sensitivity obtained in 2DEG devices coated with CH₃-MBP coincided with the pH sensitivity of bulk GaAs electrodes coated with CH₃-MBP monolayers observed by impedance spectroscopy (see section 5.1.3 on page 47). This excellent agreement suggests that the charging mechanism responsible for the pH sensitivity is fundamentally the same.

5.3 Summary and Conclusions

GaAs surfaces coated with hydrophobic CH₃-MBP monolayers exhibited a clear sensitivity to changes of electrolyte pH. Two different experimental methods have been exploited hereby, in order to sense and explain the phenomenology.

Firstly, owing to the electrochemical stability of functionalized bulk GaAs samples, impedance spectroscopy on a wide frequency range enabled the study of the interfacial processes behind the pH sensitivity. To quantify and elucidate such processes, (i) the samples were exposed to systematic variations of potential bias U_{bias} and electrolyte pH, and (ii) distinct impedance equivalent circuit models were employed to reproduce the impedance spectra. The best fit of the impedance spectra for all U_{bias} and pH conditions was achieved by the equivalent circuit Model B of figure 5.1 from which the total interface resistance (R_p) and total interface capacitance (C_p) could be extracted. This result demonstrated that changes of electrolyte pH corresponded to changes of surface potentials. From the relationships R_p vs U_{bias} and R_p vs pH, the pH sensitivity yielded **35 mV/pH** which also agreed with the sensitivity obtained by tracing the total interface capacitance (C_p).

Three distinct charging mechanisms have been proposed as the responsible for the pH response. First, diffusion of aqueous ions (H_3O^+ , OH^-) across the CH₃-MBP monolayer was discarded because the diffusion constant of the sample (obtained from Model D of figure 5.4) was two orders of magnitude lower than the diffusion constant of defected self-assembled monolayers. Second, the protination and deprotination reactions on defects (GaAs/electrolyte interface) were also discarded as it would introduce irreversible response of R_p and C_p to U_{bias} and pH variations, which was not observed. Thus, third, the charging mechanism was attributed to the adsorption of OH^- ions on the CH₃-MBP monolayer as a consequence of the structure of water nearby the hydrophobic CH₃-MBP monolayer/water interface.

Secondly, the pH sensitivity of 2-Dimensional-Electron-Gas (2DEG) devices functionalized with CH₃-MBP monolayers was also studied. To this aim, the samples were also examined at different U_{bias} and electrolyte pH. 2DEG devices measure changes of surface potentials via changes of the sheet resistance R_{sh} . As the devices were electrochemically stable, demonstrated a linear relation between R_{sh} vs pH and R_{sh} vs U_{bias} , and at these various conditions leakage currents had negligible effects to R_{sh} , changes of electrolyte pH were also associated to changes of surface potentials. The pH sensitivity of the 2DEG devices was **36mV/pH**.

Section 5.2: pH Sensitivity of 2DEG devices coated with CH₃-MBP monolayers

The excellent agreement between the pH sensitivities obtained for bulk GaAs and 2DEG devices convinces that the fundamental charging mechanism is identical.

Chapter 6

Influence of Counter Ions: Hofmeister Series

In chapter 5, impedance spectroscopy provided with valuable arguments suggesting the adsorption of OH^- ions on the $\text{CH}_3\text{-MBP}$ self-assembled monolayer coating GaAs surfaces as the charging mechanism responsible for the observed pH response. The adsorption of OH^- ions was argued to rely on the structure of water that arises at 'hydrophobic surface'/water interfaces. This conclusion was mainly based on the exclusion of different hypothetical charging mechanisms and on independent observations of analogous systems carried out by other research groups (see section 5.1.4).

In this chapter, to gain a deeper insight into such charging mechanism, the effect of different counter ions to the pH sensitivity is studied. The experiment consists in quantifying by impedance spectroscopy the pH sensitivity of GaAs planar electrodes coated with $\text{CH}_3\text{-MBP}$ monolayers in contact with two distinct electrolytes: one containing iodide anions and another chloride anions. The particular feature of these two anions is that they are placed at different positions at the Hofmeister series. The effects derived from the Hofmeister series have demonstrated to play an important role in biophysics. They give rise to an enormous variety of phenomena on solid/aqueous electrolyte interfaces and on molecules, as reviewed by Cacace et al. [89].

6.1 Influence of Counter Ions on Impedance Spectra

To finely compare the influence of iodide (I^-) and chloride (Cl^-) anions along the entire work, two solutions that only differed in the anion type were prepared, as it is

described in detail in section 2.2.3. The GaAs samples were p-doped and were coated with CH₃-MBP monolayers.*

Prior to any pH sensitivity measurements, the impact of the iodide and chloride-based electrolytes to the interfacial electrochemistry was studied by cyclic voltammetry and impedance spectroscopy.

Firstly, cyclic voltammetry experiments were carried out at pH = 6.75, in a potential range of $-1000 \text{ mV} < U_{bias} < +500 \text{ mV}$ and scan rate of 25 mV/s for both electrolytes. The results show that the I-V characteristics were apparently undistinguishable between both electrolytes (to our sensitivity limit) and the current minimum potential was $U_{bias,j=0} \simeq -350 \text{ mV}$ (vs Ag/AgCl) (data not shown).†

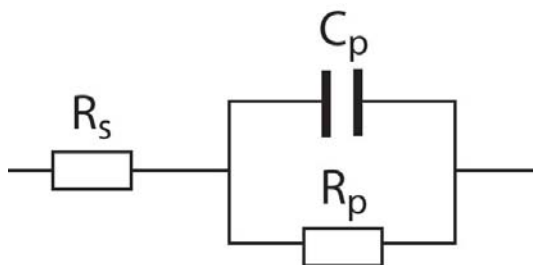


Figure 6.1: Equivalent circuit used to fit impedance spectra of GaAs coated with CH₃-MBP monolayers in contact with electrolytes containing I⁻ or Cl⁻ anions. R_s is the electrolyte ohmic resistance, R_p corresponds to the total interface resistance and C_p the total interface capacitance.

Secondly, the samples were also examined by impedance spectroscopy on both electrolytes, at the current minimum potential, pH = 6 and in a frequency range of $10^{-2} < \nu < 10^5 \text{ Hz}$. The impedance spectra were analogous to the one depicted in figure 5.2 of page 43 and did not differ for both electrolytes, either. The equivalent circuit of figure 6.1 was used to fit the data and accounts for the total interface resistance (R_p) and the total interface capacitance (C_p). The equivalent circuit could fit the entire spectrum for both systems. From the fitting results, the same total interface resistance of $R_p \simeq 10^6 \Omega\text{cm}^2$ and total interface capacitance of $C_p \simeq 1.8 \times 10^{-6} \text{ Fcm}^2$ could be extracted for both electrolytes. Besides, under this conditions, the samples were electrochemically stable regardless of the type of electrolyte, as R_p and C_p remained constant for more than 10 hours ($< \pm 5\%$).

*Note that, in contrast to the experiments carried out in the previous chapter, where n-doped GaAs samples were employed, here we use p-doped GaAs. Distinct electrochemistry may arise as, in p-doped GaAs, holes are the majority carriers.

†The I-V characteristics and the current minimum potential were comparable to the ones obtained in n-doped GaAs coated with CH₃-MBP monolayers [26].

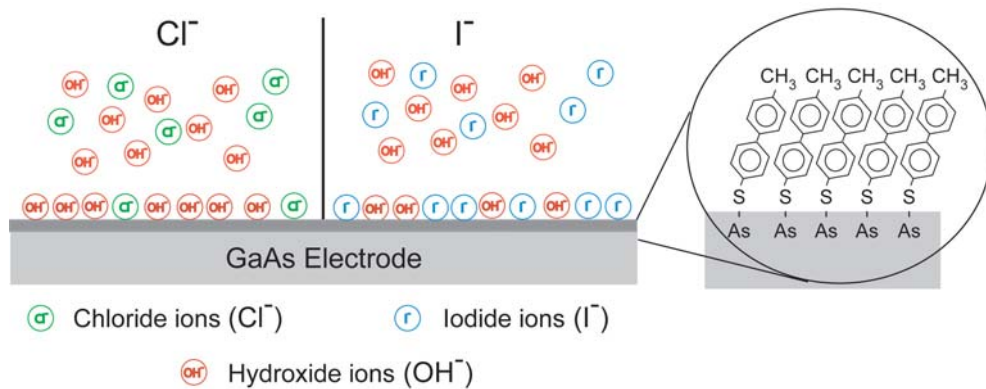


Figure 6.2: Schematic illustration of the experiment. Two different electrolytes with identical ionic concentrations were prepared, which only differed in the type of counter-ion: chloride and iodide. The plot depicts the difference in competition between the counter-ions (iodide and chloride) and hydroxide ions (OH^-) against the adsorption at the interface.

From the fact that the I-V characteristics and the impedance spectra were undistinguishable between samples in contact with either iodide or chloride-based electrolytes, the presence of any of both ions was interpreted to negligibly affect the interfacial electrochemistry.

The drawback of using only Ag/AgCl reference electrode in these experiments is (i) the possible migration of chloride ions from the reference electrode to the electrolyte solution (especially in the iodide electrolytes) and (ii) the reference potential shift between iodide and chloride solutions. Nevertheless, the potential difference between chloride and iodide solutions resulted in $\simeq 10$ mV, the I-V characteristics and the impedance spectra were undistinguishable when either ion was present and no drifts were observed. In conclusion, the reference electrode negligibly affected the outcomes of the present experiment.

6.2 Response to Bias Potential Sweeps

Figure 6.3 depicts the impedance spectra (triangles) at different external bias potentials (U_{bias}) of the samples in contact with Cl^- - (left plot) and I^- - (right plot) based electrolytes at $\text{pH} = 6$ (Nyquist plot). A clear relationship between the impedance spectra and U_{bias} is evident. The equivalent circuit of chart 6.1 was used to fit the data. For all cases, the equivalent circuit could fit the entire spectrum (red continuous lines) with an error of $< 1\%$. Equivalent circuits Model C and Model D of chart 5.4 on page 45 in

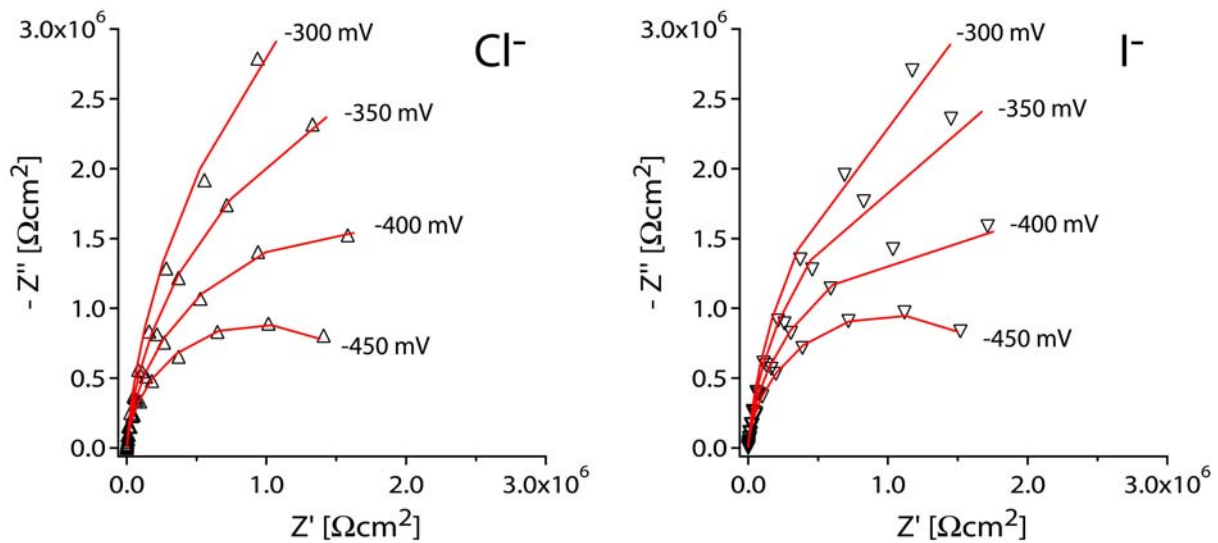


Figure 6.3: Impedance spectra (Nyquist plot) of GaAs electrodes coated with $\text{CH}_3\text{-MBP}$ monolayer in contact with chloride-based (left) and iodide-based (right) electrolytes measured at different potential bias conditions and at $\text{pH} = 6$. The experimental data (triangles) were fitted with equivalent circuit 6.1 resulting in fitting errors $< 1\%$ (red continuous curves). The impedance spectra are not altered by the presence of different anions.

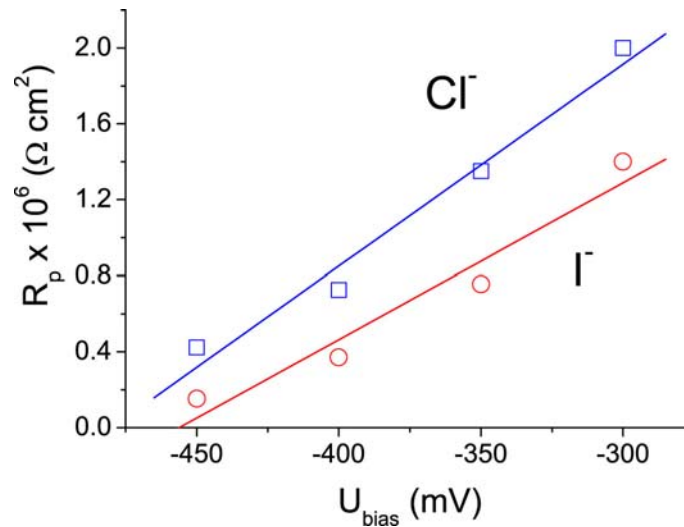


Figure 6.4: Total interface resistance (R_p) as a function of the U_{bias} for chloride-based (\square) and iodide-based (\circ) electrolytes at $\text{pH} = 6$. R_p was extracted from fitting the impedance spectra of Figure 6.3 with the equivalent circuit of chart 6.1. R_p vs U_{bias} is empirically fitted with a linear function yielding the slopes of $1.21 \times 10^4 \text{ } \Omega\text{mV}^{-1}$ (iodide) and $1.25 \times 10^4 \text{ } \Omega\text{mV}^{-1}$ (chloride). The high quality of the fit from figure 6.3 and the difference between the slopes $\simeq 2\%$ demonstrates that the interfacial electrochemistry was irrespective to the anion type.

chapter 5, which include circuit elements that account for deviations from the electrolyte/insulator/semiconductor system (see chapter 4), could not improve the quality of the fit.

Figure 6.4 depicts relationship between the total interface resistance (R_p) and U_{bias} resulting from the fits shown on figure 6.3. The relation R_p vs U_{bias} was further fitted empirically with a linear function, whose slope yielded $1.21 \times 10^4 \Omega mV^{-1}$ for iodide-based and $1.25 \times 10^4 \Omega mV^{-1}$ for chloride-based electrolytes. The fact that both slopes fall within 2% of error from each other is consistent with the previous observations by cyclic voltammetry. In fact, as R_p ultimately reflects the charge transfer across the interface, the similarity of both slopes demonstrates the *inertness* of each anion to the charge transfer mechanism. Indeed, although Cl^-/Cl_2 and I^-/I_2 have different redox potentials, this is the expected behaviour as both redox couples have their redox potentials at a distance $\gtrsim 900$ mV below the valence band of GaAs (at $U_{bias} = -350$ mV). For this reason, they have a negligible probability for a charge transfer reaction with the semiconductor bands or surface states, see figure A.2 on page 95.

6.3 pH Sensitivity in the Presence of I^- and Cl^-

To study the pH sensitivity, the electrolyte pH was systematically changed. Figure 6.5 shows the response of the impedance spectra of the decorated sample to the electrolyte pH at $U_{bias} = -350$ mV when the samples were in contact with chloride (\square , left) and iodide (\triangle , right) electrolytes. The plot makes clear the dependency of the interface impedance to electrolyte pH, in both electrolytes. For clarity of the plot, just selected results are shown. The impedance spectra could be reproduced after different pH scans cycles (data not shown). In all conditions, the equivalent circuit of figure 6.1 best fitted the data within an error of 1%, as well.

Figure 6.6 plots the relationship between R_p and pH for both electrolytes. The results were empirically fitted with a linear function, too. Respectively, for iodide and chloride electrolytes, the slopes yielded $1.82 \times 10^5 \Omega/pH$ and $4.31 \times 10^5 \Omega/pH$.

The fact that the same equivalent circuit model fits the entire spectrum at all pH values, U_{bias} and ion type, and that the spectra could be reproduced after different pH/ U_{bias} scan cycles convinces that the interfacial electrochemistry remains unaltered. This justifies that changes of electrolyte pH modify the surface potential. In conclusion, we can state that (i) iodide and chloride are inert to the interfacial electrochemistry and (ii) the charging mechanism responsible for the pH sensitivity relies on the adsorption of

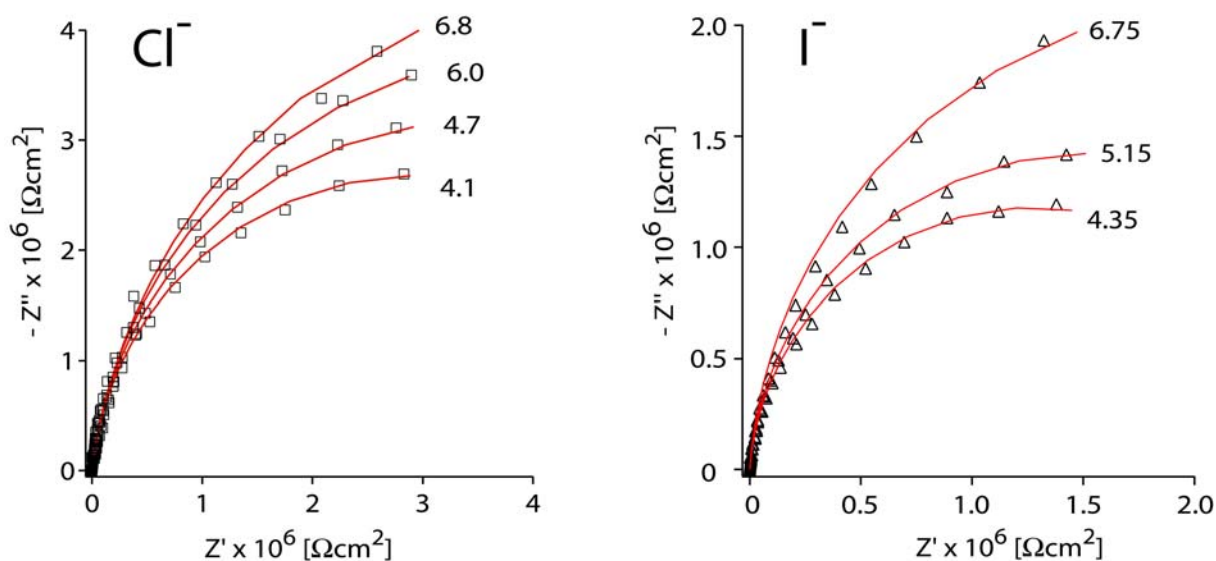


Figure 6.5: Impedance spectra of the sample in contact with chloride and iodide-based electrolytes (Nyquist plot) as a function of the electrolyte pH (values on the curves) at $U_{bias} = -350$ mV. The interfacial impedance showed a clear dependence to pH and ion type (note different scale-bar). Nevertheless, equivalent circuit of chart 6.1 alone fitted the entire spectra at all pH values and for both electrolytes (red continuous curves) with an error $\simeq 1\%$. The fact that the same equivalent circuit fitted also the impedance results of figure 6.3 demonstrates that changes in pH correspond to changes of surface potentials at the interface.

OH^- ions on the hydrophobic CH_3 -MBP monolayers. The latter conclusion is derived from the main conclusion of chapter 5.

The pH sensitivity of the sample could be calculated from the linear relations R_p vs U_{bias} and R_p vs pH for each electrolyte. Iodide-based electrolytes yielded a pH sensitivity of 15 ± 3 mV/pH while chloride electrolytes, 33 ± 6 mV/pH.

Remarkably, the pH sensitivity for iodide electrolytes was half of the one for chloride electrolytes. The difference is argued as following. As a consequence of the adsorption of counter-ions on the hydrophobic CH_3 -MBP monolayer, the structure of water at the hydrophobic/water interface is altered. This structure of the water favours the adsorption of OH^- , which is the charging mechanism responsible for the pH sensitivity (see chapter 5 and [88]). Thus, the competition between counter-ion and OH^- adsorption at the interface determines the pH sensitivity. For this reason, the lower pH sensitivity in iodide electrolytes is interpreted as the higher adsorption strength of iodide anions with respect to chloride anions on the hydrophobic CH_3 -MBP surface.

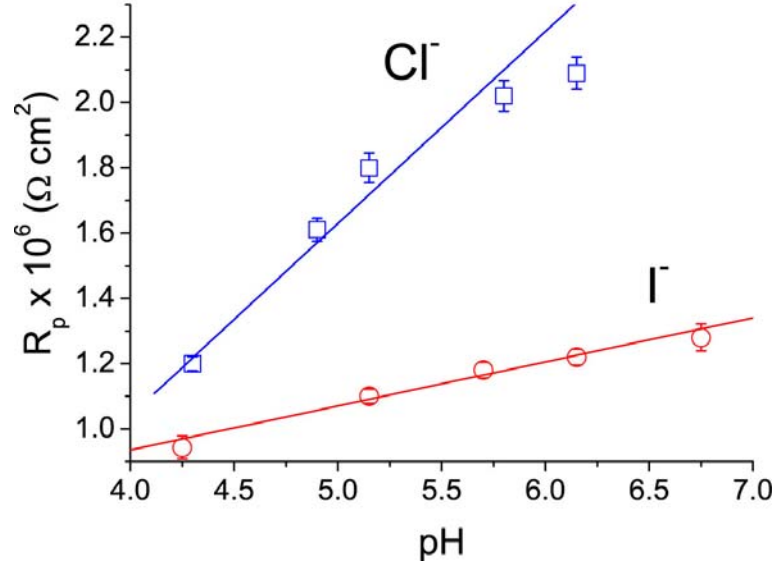


Figure 6.6: Total interface resistance (R_p) as a function of the pH for electrolytes based on iodide (○) and chloride (□) at $U_{bias} = -350$ mV. The extracted data is empirically fitted with linear function, yielding the slopes of 1.82×10^5 (iodide) and 4.31×10^5 $\Omega \text{ cm}^2 / \text{pH}$ (chloride). A higher response of the samples to pH in chloride electrolytes with respect to iodide electrolytes is evident. Employing R_p vs U_{bias} relationship (figure 6.4) enabled to calculate the pH sensitivity, resulting in 15 mV/pH (iodide) and 33 mV/pH (chloride). The lower pH sensitivity of iodide electrolytes is attributed to the higher adsorption strength of iodide ions on the surface

6.4 Thermodynamics of Ion Adsorption

The adsorption of ions on a surface can be treated thermodynamically by defining the subsystem \mathcal{S} (adsorbed ions on the surface) submerged in a reservoir \mathcal{R} (bulk electrolyte). It can thus be described by the Grand Canonical ensemble, where partition function is accounting for the microstates that not only depend on the energy but also on the number of particles of the subsystem \mathcal{S} . In this way, at the thermodynamic equilibrium, the concentration of adsorbed ions (θ_{ads}) can be described analytically by

$$\theta_{ads} = \theta_0 \exp\left(-\frac{\Delta G}{k_B T}\right) \quad (6.1)$$

where θ_0 is a reference concentration constant and the Gibbs potential

$$G = U - TS + PV = \sum_i \mu_i N_i. \quad (6.2)$$

Here, U is the energetic contribution of the subsystem, T the temperature, S the entropy, P the pressure, V the volume, μ the chemical potential and N the number of particles in the subsystem. ' i ' refers to type of particle.

As shown by equation 6.1, processes that evolve to a higher negative ΔG favours the adsorption of ions. Here, $\Delta X = X_{adsorbed} - X_{solvated}$, being X the extensive potential.

As the volume of the entire system does not change on an adsorption process ($\Delta V = 0$), ΔG only includes the energetic and the entropic contribution. Different ions have different solvation energies and entropies once interacting with water molecules, leading to the categorization of such ions in the so-called Hofmeister series. The Hofmeister series originally ranked ions according to their ability to precipitate egg white proteins [90] [91]. This effect is mediated by direct ion-surface and by the influence of ions on bulk water. Marcus [92] provides the thermodynamic potentials upon solvating of different ions, the most relevant of them for this work are summarized in the following table.

Cation	$\Delta^s G$	$T\Delta^s S$	Anion	$\Delta^s G$	$T\Delta^s S$
Mg^{2+}	-1838	132	$(PO_4)^{2-}$	-473	na
Ca^{2+}	-1515	132	F^-	-472	70
H^+	-1056	na	Cl^-	-347	-6
Na^+	-375	5	Br^-	-321	-28
K^+	-304	-34	I^-	-283	-55

where ΔG and $T\Delta S$ are given in $[kJmol^{-1}]$ at $T = 298$ K and are the *solvation* energies defined as $\Delta^s X = X_{solvated} - X_{vacuum}$.

The adsorption process on the surface depends thermodynamically on the Gibbs solvation energy. A first look at table above indicates that the internal energy of solvation of anions (U) is sensibly larger than the entropic contribution ($T\Delta S$). In values at $T = 298$ K, $\Delta^s U(Cl^-) = 341$ $kJmol^{-1}$ and $\Delta^s U(I^-) = 228$ $kJmol^{-1}$. This may imply that

the energetic contribution (U) plays an important role in the thermodynamics of adsorption. Nevertheless, the final state of the adsorbed ions is undefined and cannot be postulated a priori. The solvation shell can be disturbed to a certain degree, influencing the magnitude of the contributing interactions. That is why, it is not possible to analyze the adsorption process in terms of either ΔU or $T\Delta S$, independently.

Therefore, the problem must be treated by considering Gibbs free energy of the subsystem 'adsorbed ions' including water molecules interacting with the adsorbed ions, ion-ion interactions, ion-surface and water-surface interactions as well as the intrinsic properties of the ions such as their polarizability, α_{ion} , and volume, V_{ion} . In this approach, the Gibbs energy can be analytically be decomposed to

$$G_{adsorbed} = G_{vdW} + G_e + G_{im} + G_{pol} + G_{rest}. \quad (6.3)$$

Here, G_{vdW} is the contribution of the van der Waals interaction between ion-ion and ion-surface, G_e the ion potential interaction (electrostatic), G_{im} the image forces arising from abrupt changes in the dielectric constant at the interface ($\epsilon_{water} = 80$, $\epsilon_{solid} \simeq 1-3$) [93], G_{pol} the polarizability of the ions [94] and G_{rest} the rest of contributions important at the particular surface employed. As an example, in hydrophilic surfaces, G_{rest} is dominated by Hydrogen-bonds between water molecules and the surface. For hydrophobic surfaces, direct Hydrogen bonds are absent and the interfacial structure of the water determines G_{rest} .

As such functions are analytically complex and there exists a complex interplay among numerous amount of particles contributing to the total Gibbs free energy, Monte Carlo or Molecular Dynamics simulations, similar to the ones performed by Zangi et al. [88], may provide arguments to explain the observed pH sensitive difference between I^- - and Cl^- -based electrolytes. They can account for the difference in adsorption strength of iodide and chloride ions as well as the influence of other ions. In fact, our experimental results suggest that there is a correlation between the solvation entropy and the strength ion of adsorption which seems to follow the Hofmeister series (see previous table on page 70). Despite the new physics and the strong supporting arguments that these computational tools can provide, performing these simulations falls outside the scope of the present work.

6.5 Conclusions

GaAs electrodes coated with CH₃-MBP monolayers demonstrated an excellent electrochemical stability irrespective of being in contact with either iodide- or chloride-based electrolytes. Impedance spectroscopy in a wide frequency range was exploited to study the phenomenology of electrolyte/sample interface. The entire impedance spectra could be reproduced by the equivalent circuit of figure 6.1 when either U_{bias} , pH or anion type were varied systematically. Besides, when the external conditions were reversed, the impedance spectra could also be reproduced. These important results confirmed that (i) the presence of different electrolyte anions did not alter the electrochemistry of the interface (up to our sensitivity limit), (ii) changes in electrolyte pH correspondingly modified the surface potential, and (iii) the charging mechanism responsible for the pH sensitivity stemmed from the adsorption of OH⁻ ions on the hydrophobic CH₃-MBP monolayer (main conclusion of the previous chapter 5). The stability of the samples made possible a systematic study of the impact of each counter ion to the pH sensitivity of the surface.

The total interface resistance (R_p), that is extracted from fitting the impedance spectra with the equivalent circuit of figure 6.1, enabled to correlate quantitatively the changes of electrolyte pH to changes of surface potentials. For electrolytes containing iodide anions, the pH sensitivity resulted in $15 \pm 3 \text{ mV/pH}$ which was about a factor of two smaller than for chloride-based electrolytes, $33 \pm 6 \text{ mV/pH}$. The lower pH sensitivity of iodide electrolytes is interpreted to be caused by the higher adsorption strength of iodide ions on the hydrophobically functionalized surface with respect to chloride ions. The ion specific adsorption on the surface seems to follow the Hofmeister series, which reflects the solvation entropy of different ion species. Nevertheless, given the complex interplay of different interactions among 'adsorbed ions', water and surface, the calculation of the total Gibbs free energy of the 'ion adsorbed state' would be necessary for a quantitative discussion.

Chapter 7

Electrochemical Monitoring of Structure and Function of Lipid Membranes on Functionalized GaAs

A crucial step to engineer GaAs towards biological applications is the biofunctionalization of its surface with supported lipid membranes. Being lipid membranes the physical support of many biological processes at (and between) the inner cell and the outer environment, its electrochemical processes are of special relevance. The functionalization and electrochemical stability of GaAs surface coated with CH₃-MBP monolayers provide a biologically-friendly interfacial environment for the deposition of lipid layers. Benefiting from impedance spectroscopy, in this chapter, different electrical properties of the lipid membranes are traced by an equivalent circuit especially designed for the present system. The different circuit elements of the equivalent circuit not only demonstrate to independently characterize distinct physical features of the lipid membrane and the GaAs substrate, but also to be able to sense the membrane formation, membrane electrical potential and enzymatic reactions. On appendix A.3, further results on lipid bilayers deposited on GaAs coated with OH-MBP monolayers are also presented.

7.1 Electrochemical Characterization of Lipid Monolayers

Prior to the lipid membrane deposition, the electrochemical stability of each GaAs sample coated with a methyl-mercaptopbiphenyl (CH₃-MBP) monolayer was checked by measuring the impedance spectroscopy [26]. To quantitatively identify various electrochemical layers, measurements are carried out in a wide frequency range (10⁵ - 10⁻¹ Hz) at the current minimum potential $U_{bias,j=0} = -400$ mV (vs. Ag/AgCl), determined by cyclic voltammetry [50] [27] *. Only the samples that show negligibly small deviations (within ± 1 %) in interface resistance and capacitance over several scans are subjected for the further functionalization steps.

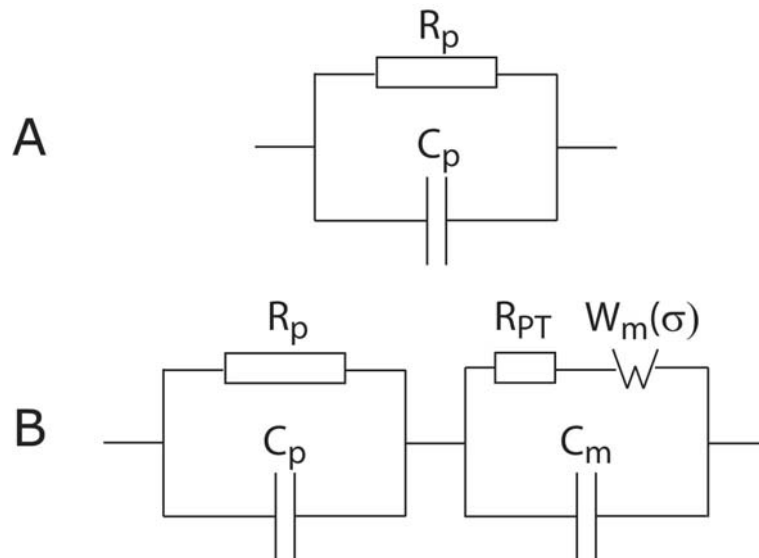


Figure 7.1: Equivalent circuit models used to fit the impedance spectra. Model A consists of resistance of electrolyte and Ohmic contact R_s , interface capacitance C_p , and interface resistance R_p . For analyzing impedance spectra in the presence of a lipid monolayer, Model B is employed that additionally includes Warburg element $W_m(\sigma)$, the phase transition resistance at the electrolyte/membrane interface R_{pT} , and the membrane capacitance C_m .

Figure 7.2 represents the absolute impedance and the phase shift plotted as a function of frequency (Bode plot) of the GaAs coated with CH₃-MBP before (+) and after (●) the deposition of a lipid monolayer. To analyze the measured impedance spec-

*Different from our previous studies dealing with n-GaAs, we use p-GaAs as an electrode in this study. Thus, the current minimum potential of the p-GaAs sample, i.e., the bias potential at which the sum of the oxidative and reductive currents is minimum, is determined by cyclic voltammetry to be $U_{bias,j=0} = -400$ mV (vs. Ag/AgCl).

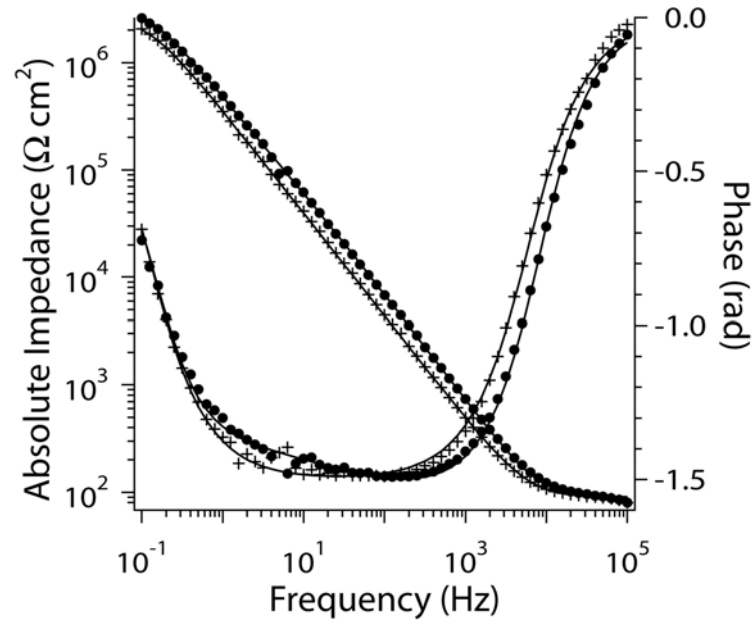


Figure 7.2: Impedance spectra (Bode plot) before (+) and after (●) the deposition of a lipid monolayer on a GaAs electrode coated with a CH₃-MBP monolayer, recorded at the current minimum potential ($U_{bias,j=0} = -400$ mV). The solid lines correspond to the fitting results using Model A (+) and Model B (●) in Scheme 7.1.

tra, two different circuit models are taken, as presented in scheme 7.1. The best fit of the impedance spectra before the membrane deposition (+) can be achieved with Model A (solid lines). R_s reflects the Ohmic resistance of the electrolyte and/or electronic contacts in the high frequency regime ($f > 10^5$ Hz), while C_p and R_p characterize the capacitance and resistance of the solid/electrolyte interface, respectively. The fitting yields the interface capacitance and resistance of interface to be $R_p = 1.2$ M Ω cm² and $C_p = 1.9$ μ Fcm⁻², respectively.

As discussed in our previous accounts in detail [81], the interface capacitance C_p can be simplified to a serial connection of capacitance of the electrolyte (Gouy-Chapman-Stern capacitance) C_{GCS} , capacitance of the self-assembled monolayer (SAM) C_{sam} , and space charge capacitance of the semiconductor C_{SC} . Here, C_{GCS} is a serial connection of the Helmholtz layer capacitance $C_H \geq 140$ μ Fcm⁻², and the diffusion layer capacitance $C_{diff} \geq 0.9$ Fcm⁻². Moreover, our preliminary simulation with the detailed model [43] implied that the capacitive contribution from the surface states C_{SS} is negligible in our experimental system. Thus, C_p of the freshly etched, bare GaAs (which has the doping ratio of $n_A^p \simeq 3 \times 10^{19}$ cm⁻³) is concluded to be governed by C_{SC} , which is in the range of 2 - 3 μ Fcm⁻².

The impedance spectra of the sample with a lipid monolayer (containing 60 mol%

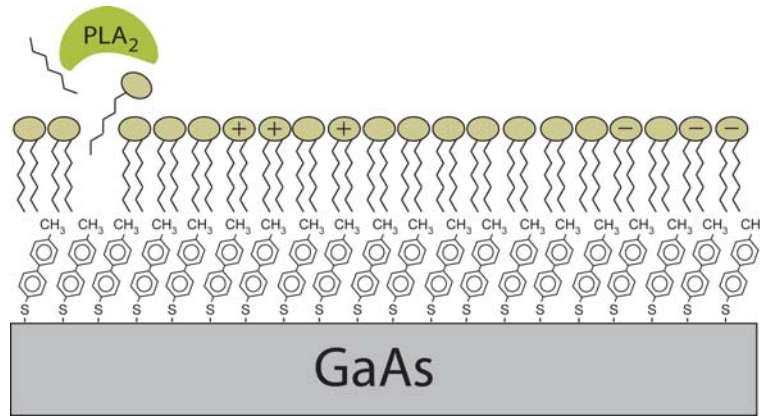


Figure 7.3: Schematic illustration of the system. Over the self-assembled monolayer of methyl-mercaptopiphenyl ($\text{CH}_3\text{-MBP}$) grafted on freshly etched GaAs, lipid monolayers are spread by vesicle fusion. On one part of the experiment, the influence of the charge concentration of the lipid layer is systematically changed, while on the other, neutrally charged lipid monolayers were exposed to the action of enzymatic degradation of PLA_2 .

DMPC and 40 mol% cholesterol) reach to the saturation level (\bullet) about 2 h after the injection of vesicle suspensions (see Fig. 7.5 for more details). Here, the best fit can be achieved with the Model B of scheme 7.1, which includes a new set of circuit elements representing the phase transition resistance at the electrolyte/membrane interface (R_{PT}), membrane capacitance (C_m), and so-called Warburg resistance (W_m). Here, Warburg resistance W_m is introduced to account for the diffusion of ions to the electrode surface [67] [68]. In fact, the fitting of the membrane without Warburg resistance, i.e. with a parallel pair of Ohmic resistance and capacitance, results in a large fitting error ($\pm 15\%$).

Analytically, the Warburg resistance can be expressed as

$$W_m(\sigma, \omega) = \left(\sigma + \frac{1}{\sigma} \right) \omega^{-\frac{1}{2}} \quad (7.1)$$

where σ is the Warburg parameter,

$$\sigma = \frac{4RT}{\sqrt{2}F^2n^2\rho A} \cdot \frac{1}{\sqrt{D}} \quad (7.2)$$

A is the active electrode area, D the diffusion constant of the ions across the interface,

ρ their concentration at the surface and ω the angular frequency of the read-out signal. The constants R, T, n and F have their usual meanings.

Taking this model (Model B), the electrochemical parameters of a lipid monolayer can be calculated to be $R_{PT} = 9 \times 10^2 \Omega\text{cm}^2$, $C_m = 1.5 \mu\text{Fcm}^{-2}$, and $W_m = 4.2 \times 10^5 \Omega\text{cm}^2$. Note that R_{PT} merely represents the resistance of the electrolyte/membrane interface, which does not include the diffusion barrier characteristics of the hydrophobic core region of the membrane. Here, the barrier capability of the membrane against the diffusion of ions can be represented mainly by W_m . If one assumes that the concentration of ions on the surface is the same as in the bulk electrolyte, a diffusion constant of $D_m = 5 \times 10^{-5} \mu\text{m}^2\text{s}^{-1}$ can be calculated from the Warburg constant, $\sigma_m = (5 \pm 0.5) \times 10^5 \Omega\text{s}^{1/2}$. This diffusion coefficient is about 7 orders of magnitude smaller than the diffusion of ions in aqueous electrolyte, $D = 1 \times 10^3 \mu\text{m}^2\text{s}^{-1}$ (calculated from the Stokes-Einstein equation of the ion with the radius of 3.5 Å) and about 3 - 4 orders of magnitude smaller than those across alkylsiloxane monolayers, $D = 0.01 - 0.1 \mu\text{m}^2\text{s}^{-1}$ [83]. Such a significantly high Warburg resistance well explains the excellent electrochemical stability the membrane-coated GaAs, where we observe no sign of electrochemical instability for more than 3 days within the experimental limit.

The capacitance of the lipid monolayer, $C_m = 1.5 \mu\text{Fcm}^{-2}$, is almost double of the capacitance value reported for free-standing [95] [96] and supported lipid bilayers [13], $C_{bilayer} = 0.7 \mu\text{Fcm}^{-2}$, which provides a proof of the formation of a lipid monolayer on GaAs electrode coated with a CH_3 -MBP monolayer. As the membrane capacitance can be represented by

$$C_m = \frac{\epsilon_m \epsilon_0}{d_m}, \quad (7.3)$$

the thickness of the hydrocarbon region can be calculated to be $d_m = 12 \text{ \AA}$ by assuming the dielectric constant of the hydrocarbon core region of lipid membranes to be $\epsilon_m = 2.2$ [95] [96] [97]. This value agrees with the corresponding values reported previously [98] [58] [12].

7.2 Kinetics of Membrane Formation

Figure 7.4 represents the plots of $W_m(\sigma)$ and C_m as a function of time, corresponding to the time evolution of the membrane formation. Each of the data-points is calculated

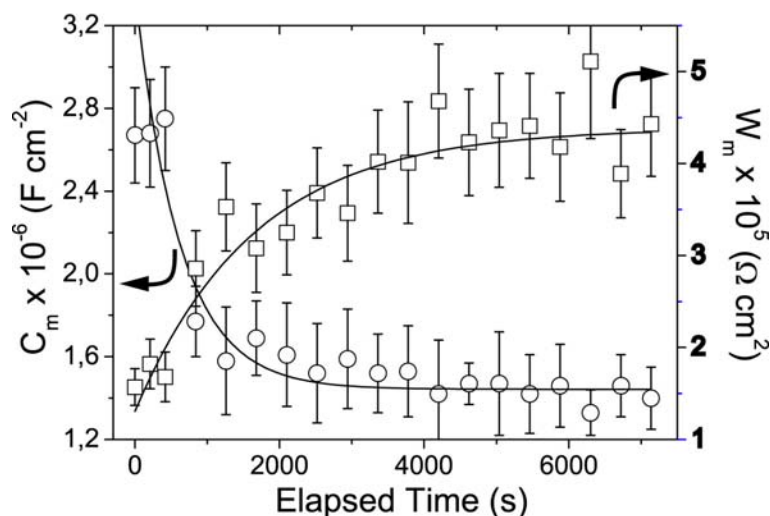


Figure 7.4: Growth kinetics of a lipid monolayer on a GaAs electrode coated with a $\text{CH}_3\text{-MBP}$ monolayer. At $t = 0$, vesicle suspension was injected to the electrochemical cell, and changes in the Warburg element W_m (\square) and the membrane capacitance C_m (\circ) are recorded as a function of time. Both W_m and C_m reached to the saturation level at $t \sim 7000$ s. Such time evolutions can be fitted empirically with a first order exponential function, yielding the characteristic time constants of $\tau_{W_m} = 1350 \pm 200$ s for W_m and $\tau_{C_m} = 310 \pm 30$ s for C_m , respectively.

from individual impedance spectra collected every 7.5 min. After 7000 s of the injection of lipid vesicles at $t = 0$, both W_m and C_p reach to the saturation levels, i.e. the prolonged incubation time and the increase of the sample temperature do not lead to any change. Flushing of remaining vesicles from the flow chamber does not result in any change in both parameters, suggesting that vesicles adsorbed on the surface, even if they exist, do not influence the electrochemical characteristics of the supported membrane. Using the surface plasmon resonance and quartz crystal microbalance, Keller et al. reported that the kinetics of supported membrane formation on a hydrophilic silica surface includes two steps: (i) adsorption of vesicles and (ii) spreading on the surface [99]. It should be noted that the kinetics observed here should mainly reflect the kinetics of the decrease of the active membrane area by spreading of the membrane on a hydrophobic surface, because the adhered vesicles cannot form the shielded 'barrier' that significantly slows down the diffusion of ions. Thus, we performed empirical fitting of the observed kinetics with a first-order exponential function, yielding the characteristic time constants, $\tau_{W_m} = 1350 \pm 200$ s and $\tau_{C_m} = 310 \pm 30$ s, respectively. The apparent difference between the characteristic time constants obtained from changes in resistance and capacitance seems consistent with the qualitative tendency observed for the formation bilayer lipid

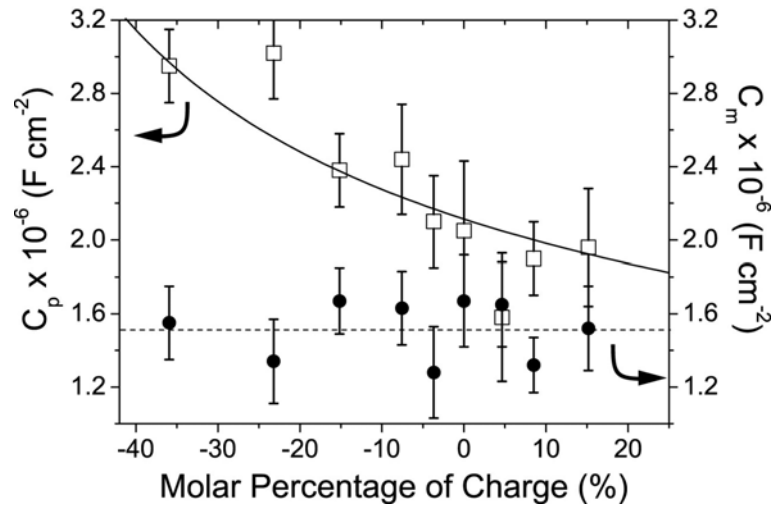


Figure 7.5: Dependence of C_m (●) and C_p (□) on the doping ratios of charged lipids. Here, the signs in x -axis coincide with the signs of charges. It should be noted that C_m remains almost independent from the charge density on the membrane surface, $C_m = (1.5 \pm 0.2) \times \mu\text{Fcm}^{-2}$ (broken line). In contrast, C_p shows a clear dependence on the surface charge density, which seems to scale with $[\text{charged lipid}]^{-0.5}$ (solid line).

membranes on Si/SiO₂ electrodes, where the capacitance reaches to its saturation level much faster than the resistance [13].

7.3 Capacitive Sensing of Surface Charge Density

The effect of the charge density Q on C_p and C_m can be studied by changing the composition of lipids in a systematic manner. Here, the molar concentration of cholesterol is kept to be 40 mol%, and positively charged lipids (DHDAB) or negatively charged lipids (DMPG) are mixed with zwitterionic DMPC matrix to achieve the total lipid fraction to be 60 mol%. Figure 7.5 represents the C_p and C_m values plotted as a function of molar percentage of charged lipids. Note that the sign in x -axis coincides with the sign of net surface charges, and the experimental errors out of several experiments fall within $\pm 10\%$.

As presented in the figure, the capacitance of a lipid monolayer C_m is almost independent from the mole fraction of charged lipids, $C_m = 1.5 \pm 0.2 \mu\text{Fcm}^{-2}$ (the broken line in Fig. 7.5). In contrast, C_p , which is dominated by the semiconductor space charge capacitance, shows a systematic dependence on the charge density on the membrane Q . As indicated by the solid line in Fig. 7.5, the dependence of C_p on the lateral charge density and thus on the mole fraction of charged lipids can be fitted with

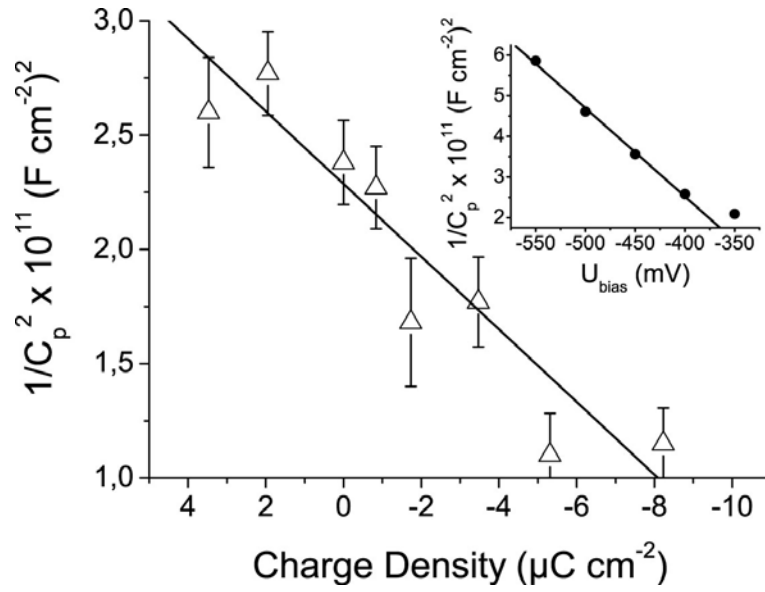


Figure 7.6: Plot of $1/C_p^2$ vs. lateral charge density Q . Lateral charge density (note the sign of x -axis is inverted for the correspondence to 'bias' potentials (U_{bias} vs. a reference electrode, Ag/AgCl) can be calculated from the molar fraction of charged lipids using the known mean molecular area of a phospholipid ($\approx 70 \text{ \AA}^2$). [65] $1/C_p^2$ vs U_{bias} plot of a neutral lipid monolayer ($Q = 0 \text{ } \mu\text{Ccm}^{-2}$) is presented as the inset, from which the carrier concentration $n_p = 1.1 \pm 0.3 \times 10^{19} \text{ cm}^{-3}$ and the flat band potential $U_{fb} = -230 \pm 30 \text{ mV}$ can be calculated. This enables one to estimate the sensitivity of a membrane charge sensor to be $8 \text{ mVcm}^2/\mu\text{C}$, corresponding to 1 charge/ 18 nm^2 .

$$C_p \propto \frac{1}{\sqrt{[\text{Lipid}_{charged}]}} \quad (7.4)$$

It is also noteworthy that both Warburg resistance W_m and characteristic time constants for the membrane formation (τ_{W_m} and τ_{C_m}) remain constant irrespective of the presence of charged lipids, confirming that the electric resistance of the membrane (i.e. surface coverage) and kinetics of membrane formation are not influenced by the lipid compositions.

Since C_m can be quantitatively separated from C_p , this capacitance reflects the serial connection of the capacitance of a CH_3 -MBP monolayer, C_{SAM} , and the semiconductor space charge capacitance, C_{SC} . In Figure 7.6, the influence of surface charge density on C_p is presented by plotting $1/C_p^2$ vs. lateral charge density, Q . Here, the mole fractions of charged lipids are converted to the charge density taking the mean area occupied by one phospholipids molecule in fluid phase ($\approx 70 \text{ \AA}^2$ per molecule) [65] [100]. Therefore,

this is an analogue of Mott-Shottky plots that predict a linear relationship between $1/C_p^2$ vs. U_{bias} when the semiconductor is operated at the depletion regime. The slope of such a plot coincides with the density of the majority carrier in semiconductor n_p since:

$$\frac{1}{C_{SC}^2} \propto \frac{1}{n_p} \left[(U_{ext} - U_{fb}) - \frac{kT}{2} \right] \quad (7.5)$$

U_{ext} is the external potential, and U_{fb} the flat band potential [37] (see also section 3.1.2). The linear relationship observed here qualitatively indicates that C_p is sensitive to the change in the surface charge density Q . In our experimental system, applications of various U_{ext} mean changes in the surface potential ψ_s due to changes in the surface charge density Q according to the Poisson's equation.

To determine the sensitivity of GaAs coated with the supported lipid monolayer, a lipid monolayer consisting of 40 mol% cholesterol and 60 mol% DMPC is deposited. The impedance spectra are collected between $U_{bias} = -550$ mV and -350 mV, where the electrochemical stability of the system is guaranteed for more than a day. Here, U_{ext} is quantitatively represented by U_{bias} . The plot of $1/C_p^2$ vs. U_{bias} (figure 7.6, inset) verifies the linear relationship, and the slope corresponds to the carrier density of $n_p(\text{lipid monolayer}) = (1.1 \pm 0.3) \times 10^{19} \text{ cm}^{-3}$. Despite of the model circuit including many fitting parameters, this value agrees very well with the values obtained from two reference experiments on GaAs coated with $\text{CH}_3\text{-MBP SAM}$: (i) the carrier density of a GaAs electrode determined by impedance spectroscopy in electrolytes, $n_p(\text{SAM-GaAs/imp}) = (3.2 \pm 0.3) \times 10^{19} \text{ cm}^{-3}$, and (ii) the carrier density measured by a Hall measurements in air, $n_p(\text{Hall}) = (3.7 \times 0.2) \times 10^{19} \text{ cm}^{-3}$. From the intercept of the extrapolated linear part with the x -axis, the flat band potential of GaAs coated with a lipid monolayer can be calculated to be $U_{fb}(\text{lipid monolayer}) = -230$ mV. This is slightly shifted from the corresponding value of GaAs with the $\text{CH}_3\text{-MBP SAM}$, $U_{fb}(\text{SAM-GaAs}) = -280$ mV, which can be attributed to a potential drop across the hydrocarbon chain region.

From two linear relationships obtained from our experiments, $1/C_p^2$ vs. Q (figure 7.6, main panel) and $1/C_p^2$ vs. U_{bias} (figure 7.6, insets), the charge sensitivity of the membrane-functionalized GaAs can be calculated to be $8 \text{ mVcm}^2/\mu\text{C}$. Taking the area per lipid molecules of 70 \AA^2 into account, the charge sensitivity can also be given as 1 charge per 18 nm^2 . In fact, the sensitivity achieved here is slightly better than the one of ITO

coated with polymer-supported lipid monolayer, 1 charge per 8 nm^2 [12].

7.4 Electrical Monitoring of Enzyme Functions

As the first step to electrochemically monitor the biochemical reaction on the supported lipid monolayer on semiconductors, the enzymatic activity of phospholipase A₂ (PLA₂) that cleaves the ester linkage of the sn-2 position of glycerophospholipids and transfer them into lysophospholipids and fatty acids [101] is studied. In figure 7.7, the impedance of GaAs electrode with a DMPC monolayer (with 40 mol% of cholesterol) measured before the injection of PLA₂ (solid lines) and the impedance of the same sample measured after incubation with PLA₂ for 2 h at $T = 25 \text{ }^\circ\text{C}$ (dashed lines) are presented. For these series of experiments, the buffer from 10 mM Na₂HPO₄/NaH₂PO₄ is replaced to 10 mM Hepes to avoid undesired interference to the enzymatic activity as well as the precipitation of salts caused by the presence of Ca⁺², employed to activate the enzymatic reaction of PLA₂. The exchange of buffer salts does not cause any detectable change in the electrochemical parameters of the experimental system.

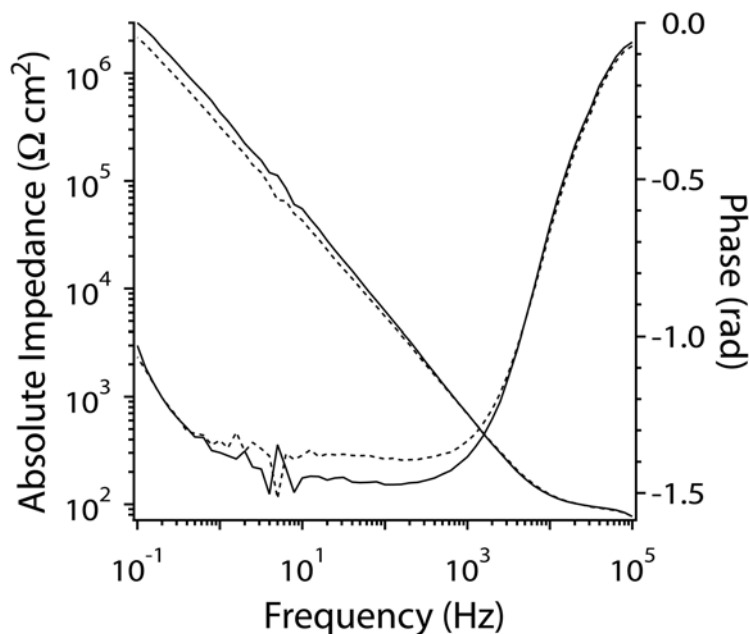


Figure 7.7: Enzymatic degradation of a phospholipids (DMPC) monolayer with phospholipase A₂ (PLA₂). The global shape of impedance spectra significantly changes upon the addition of PLA₂ to a DMPC lipid layer (solid lines). After 2 h, we found that the Warburg resistance of the membrane $W_m(\sigma)$ decreased almost two orders of magnitude (dashed lines).

As can be seen in the figure, the absolute impedance in the low frequency region ($f < 10$ Hz), which is dominated by the Warburg resistance W_m shows a clear decrease after 2 h. This tendency can be interpreted as the decrease in the barrier capability of the membranes against the diffusion of ions, caused by the degradation of lipids by PLA₂.

In fact, the W_m value drops by two orders of magnitude from the initial value, resulting in a significant increase in the diffusion coefficient of ions, $D \simeq 8 \times 10^{-1} \mu\text{m}^2\text{s}^{-1}$. The change in the diffusion barrier capability (i.e. leakiness) of the membrane agrees well with the previous reports using ellipsometry [58] and AFM [102] [103]. Nevertheless, such a significant increase in the diffusion coefficient across the lipid monolayer (almost by four orders of magnitude) does not cause any electrochemical instability, suggesting that the underlying CH₃-MBP layer still prevent the surface from irreversible electrochemistry on GaAs.

7.5 Conclusions

Excellent electrochemical stability of GaAs achieved by covalent coupling of methyl-mercapto-biphenyl (CH₃-MBP) allows for the deposition of a lipid monolayer by fusion of small vesicles on the hydrophobic surface. Electrochemical impedance spectroscopy measurements over a wide frequency region (10⁵ - 10⁻¹ Hz) at the current minimum potential $U_{bias,j=0} = -400$ mV (vs. Ag/AgCl) enables one to quantitatively identify electrochemical parameters of a supported lipid monolayer and those of the GaAs/CH₃-MBP interface with an aid of equivalent circuit models. The best fit results suggest that the presence of a lipid monolayer remarkably slows down the diffusion of ions, so that the electrochemical parameters of the membrane-functionalized GaAs remain stable for more than 3 days. The kinetics of membrane formation can be traced by monitoring the Warburg resistance W_m and capacitance C_m of the membrane, which can empirically be analyzed to gain the characteristic time constant of membrane formation.

Owing to the quantitative identification of the resistance R_p and capacitance C_p of the GaAs/CH₃-MBP interface even in the presence of a lipid monolayer, the change of the interface capacitance C_p that contains the contribution of the capacitance of semiconductor space charge region C_{SC} can be measured as functions of the fraction of charged lipids (i.e. surface charge density Q) and bias potentials U_{bias} . The linear relationships obtained for $1/C_p^2$ vs. Q and $1/C_p^2$ vs. U_{bias} suggests that C_p can be used as a sensitive measure to detect the surface charges, and the charge sensitivity of the system can be calculated to be 1 charge per 18 nm². Moreover, preliminary experiments successfully demonstrate the potential application of membrane-functionalized semiconductor electrodes in the electrochemical monitoring of enzymatic reactions (degradation of phospholipids by phospholipase A₂). The composite membranes established here open a large potential towards the design of new hybrid sensors by functionalization of various GaAs-based semiconductor devices with biological membranes.

Conclusions

Owing to the excellent electrochemical stability achieved by the deposition of monomolecular films of mercaptobiphenyl (MBP) derivatives, potential applications of functionalized bulk GaAs electrodes as well as two-dimensional electron gas (2DEG) devices for various types of liquid-phase sensors are examined, and the possible molecular mechanisms of the observed sensitivity have been discussed. Impedance spectroscopy over a wide frequency range enables to distinguish different electrochemical layers quantitatively by modelling the experimental results with equivalent circuit models.

In Chapter 5.1, the impedance spectra of GaAs electrodes coated with CH₃-MBP monolayers have been measured at various external bias potentials ($-450 \text{ mV} < U_{bias} < -250 \text{ mV}$) and pH conditions ($2 < \text{pH} < 7$). The obtained spectra can be well represented by a serial connection of a resistance R_s (electrolyte and Ohmic contact) and a pair of resistance R_p and capacitance C_p , reflecting the electrochemical properties of the semiconductor space charge region and the CH₃-MBP monolayer. Interestingly, the interface resistance R_p is proportional not only to the bias potential U_{bias} , but also clearly shows a linear dependence on the electrolyte pH. These two linear relationships suggest that the change in electrolyte pH can be translated to the change in external (i.e. surface) potential. The relationship between pH and the bias potential can empirically be deduced: 35 mVpH^{-1} , which agrees well with the pH sensitivity obtained from capacitance measurements (Mott-Schottky analysis). To gain the physical origin of the observed pH sensitivity, different hypothetical mechanisms are proposed and discussed. First, the diffusion of H⁺ and OH⁻ ions across the CH₃-MBP monolayer is discarded, as the diffusion constant obtained by the circuit models with the Warburg element, $D \lesssim 10^{-4} \text{ } \mu\text{ms}^{-1}$, is more than six orders of magnitude smaller than the diffusion of ions in bulk electrolyte. Second, the protonation and deprotonation (site-binding model) on GaAs defects is also discarded, since it should cause irreversible electrochemical reactions at the GaAs/electrolyte interface.

Conclusions

Furthermore, the obtained pH sensitivity does not agree well with that of GaAs coated with a thick oxide layer [48]. In fact, the impedance spectra are fully reproducible upon several pH/U_{bias} cycles. Thus, it has been concluded that the observed pH sensitivity is caused by the charging of the hydrophobic $\text{CH}_3\text{-MBP}$ monolayer surface due to the adsorption of OH^- ions.

In Chapter 5.2, 2DEG devices are functionalized with $\text{CH}_3\text{-MBP}$ monolayers taking the same functionalization protocol, and pH sensitivity of the functionalized device is evaluated by measuring the sheet resistance in 2DEG layer, R_{sh} . As the first step, the stability of the performance of the functionalized 2DEG device in aqueous electrolytes ($\text{pH} = 7$) was confirmed, where R_{sh} varied within $<10\%$ after a period of 10 h near the current minimum potential $U_{bias} = -400$ mV. When subjected to changes of the electrolyte pH and U_{bias} , ($2 < \text{pH} < 7$) and ($-500 \text{ mV} < U_{bias} < -300 \text{ mV}$), R_{sh} responded linearly versus both pH and U_{bias} . It should also be noted that the leakage current remains constant (≈ 10 nA) irrespective to pH and U_{bias} changes. From these relationships, the sensitivity of 2DEG was extracted to be **36 mVpH^{-1}** . Remarkably, the pH sensitivity observed by 2DEG devices is almost identical to the pH sensitivity of bulk GaAs electrodes in the previous chapter. As changes in R_{sh} (i.e. carrier concentration) in a 2DEG layer reflect the energy shift caused by surface potentials, the mechanism of the observed pH sensitivity can also be explained as the adsorption of OH^- on $\text{CH}_3\text{-MBP}$ monolayer.

In Chapter 6, the influence of counter ions was investigated to gain deeper insight into the mechanism of the pH sensitivity of GaAs rendered with hydrophobic $\text{CH}_3\text{-MBP}$ monolayers. Here, the impedance spectroscopy in the presence of I^- ions, instead of Cl^- ions in the previous series. All the impedance spectra can be well modelled with the same circuit model for both Cl^- and I^- ions. Bulk GaAs electrodes with $\text{CH}_3\text{-MBP}$ monolayers show excellent electrochemical stability irrespective of the counter anions, and the current responses of the functionalized GaAs qualitatively follow the same tendency. However, the absolute pH sensitivity in the presence of I^- ions, **15 mVpH^{-1}** , is about by a factor of two lower than that in the presence of Cl^- ions, **33 mVpH^{-1}** . The poorer pH sensitivity found in the presence of I^- ions with respect to Cl^- ions suggests that I^- ions interact 'more strongly' to the $\text{CH}_3\text{-MBP}$ monolayer surface than Cl^- ions. Ion specific adsorption on the surface seems to follow the Hofmeister series, which reflects the solvation entropy of different ion species. Nevertheless, the calculation of the total Gibbs free energy at the molecular (microscopic) level involving ions, water molecules and surface type would be necessary for a quantitative discussion.

In Chapter 7, lipid monolayers were deposited on bulk GaAs electrodes pre-coated

with CH₃-MBP monolayers by fusion of small unilamellar vesicles, and the electrochemical properties of supported membranes were studied with impedance spectroscopy. Here, a new circuit model that takes the diffusion of ions across the lipid membrane into account is employed to model the experimental results. A successful deposition of lipid monolayers can be monitored as changes in membrane resistance (W_m) and capacitance (C_m) as a function of time. After reaching to the equilibrium, the impedance spectra of CH₃-MBP-coated GaAs in the presence of a lipid monolayer show no sign of drift for more than 3 days, which suggests that the formation of a defect-free lipid membrane (characterized by a high resistance $W_m \simeq 0.5 \text{ M}\Omega\text{cm}^2$) further stabilizes GaAs in physiological electrolytes. The possibility for the capacitive sensing of surface charge densities Q was explored by doping positively or negatively charged lipids in zwitterionic matrix lipids. Taking this circuit model, the capacitance of the membrane (C_m) and the interface capacitance governed by the semiconductor space charge capacitance (C_p) can quantitatively identified. In fact, C_m as well as W_m is almost independent from Q , $C_m = (1.5 \pm 0.2) \mu\text{Fcm}^{-2}$ suggesting that changes in the membrane surface potential do not alter the dielectric constant and the thickness of the membrane. In contrast, C_p shows a systematic dependence on Q , and the plot of $1/C_p^2$ vs. Q , indicates a linear relationship. This result suggests that a supported lipid monolayer on GaAs can be treated as the electrolyte-insulator-semiconductor (EIS) system, so that changes in the membrane surface potential can be detected as shifts of the semiconductor flat band potential, U_{fb} . Indeed, $1/C_p^2$ is proportional to U_{bias} , from which the carrier concentration $n_p = 1.1 \pm 0.3 \times 10^{19} \text{ cm}^{-3}$ can be calculated. Hence, from these two linear relationships, $1/C_p^2$ vs Q and $1/C_p^2$ vs U_{bias} , the charge sensitivity of the biomimetic EIS system can be calculated to be $1 \text{ e}^- / 18 \text{ nm}^2$. As the first attempt to utilize such a setup to monitor protein functions, phospholipase A₂ (PLA₂) was injected into a electrochemical cell. After 2 h of incubation, the diffusion constant of ions across the lipid membrane, derived from W_m , increased by 4 orders of magnitude as a result of enzymatic degradation of phospholipids.

The present work demonstrates that GaAs functionalized with bio-organic molecular systems opens a large potential in liquid-phase sensor applications, including biosensors. In fact, as demonstrated in Chapter 5, the pH sensitivity of bulk GaAs is almost identical to that of 2DEG devices. The results obtained in this thesis indicate that the well defined surface functionalization is the key to achieve an excellent electrochemical stability and a high sensitivity to electrically detect changes in surface potentials caused by chemical and biochemical reactions.

Conclusions

Outlook

The electrochemical stability achieved by functionalizing GaAs with CH₃-MBP monolayers and, particularly, with lipid monolayers demonstrates the feasibility of GaAs as a biosensor. Although the sensing of surface potentials and the characterization of different electrochemical layers is possible by means of impedance spectroscopy, an assessment of the current status of the 'sensor' performance would be necessary to justify further investments. Regardless of this fact, there are still various technical aspects and fundamental issues on surface physics and chemistry that remain to be exploited.

From the materials side, the high electron mobility of GaAs enables to operate GaAs devices at low noise and low power. The Fast Impedance Spectroscopy method, developed by Wiegand [64] on ITO electrodes, can be implemented for time-resolved impedance spectroscopy with expectedly higher sensitivity. The method would provide advantageous sensing performance of biophysical systems as it would enable to resolve events at different electrochemical layers down to the millisecond range.

The advantage of AlGaAs/GaAs Band Gap engineering opens a door to a myriad of nanoscaled devices. Unfortunately, on nanoscaled surface areas, high resistive electrochemical layers, like lipid membranes or MBP on GaAs, limits the electrochemical sensing principle to surface potential sensing (capacitive sensing). In this context, Field-effect devices are the most suitable rather than bulk GaAs used for impedance spectroscopy. The optimization of planar 2-Dimensional Electron Gas, embedded nanowires, quantum dots or nanorings devices can benefit from the electrochemical stability granted by MBP and lipid monolayers. If these nanoscaled devices would be integrated in a specifically functionalized single chip, it would favour the detection of small volume, low concentration of analyte, high variety of specificity and high measurement robustness required for label-free High-throughput screening devices, important for medical and biological research. On free-standing (not-embedded, dissolved in a medium) nanoscaled semiconductor devices (nanowires, quantum dots), the surface functionalization may provide enhanced biosensing features, as these de-

vices are smaller than the space-charge region ($l_{SC} \sim 10\text{nm}$).

Self-assembled monolayers can also be engineered. For example, crosslinking of MBP SAM by soft electron beam exposure could enhance the electrochemical stability [104]. Peptides of different lengths, high (even switching) dipole moments and containing specific receptors may be employed for gas or heavy metal sensing on field effect devices. More complex molecules such as proteins or enzymes may be investigated.

The increase of complexity of the self-assembled (organic) molecules for quantitative biosensing suggests a precise characterization of the molecular layer. Synchrotron-based methods can provide valuable information. For example, Grazing Incidence X-ray Off-Specular diffraction (GIXOS) provides the film thickness, roughness and electron density profile in short X-rays exposures (in comparison to reflectivity measurements) minimizing a possible damage of X-Rays to the molecular layers. Additionally, Grazing Incidence Diffraction (GID) makes possible to gain insight of the 2-dimensional crystallographic structure of the molecular layers and therefore quantifying the density of molecules and defected regions. High Resolution X-Ray Photoelectron Spectroscopy (HRXPS) may also be employed to investigate the chemical nature of the surface and Near Edge X-Ray Absorption Fine Structure Spectroscopy (NEXAFS) to account for the ordering and density of the monolayer.

The biological phase of the interface can also be prolifically designed, once demonstrated that lipid monolayers remain stable for more than three days. Lipid monolayers containing different incorporated glycolipids and/or specific receptors adequate to specifically bind to enzymes, proteins or even particular cells would be the first step to demonstrate the use of GaAs as a biosensor of biologically relevant systems.

Appendix A

Appendix

A.1 Physical Characterization X-MBP Monolayers on GaAs

The family of mercapto-biphenyl molecules with different headgroups was grafted on GaAs [100] surfaces. For a quantitative characterization of the surfaces, AFM, Ellipsometry and Contact Angle techniques were exploited. As an addition to former works where different X-terminated biphenyl-thiols monolayers on GaAs were characterized [27], hereby the effect F- and CF₃- headgroups on the formation of the self-assembled monolayers is investigated. Halogen groups are thought to affect the electron density of the thiol group due to their high electronegativity, thereby influencing the S-As covalent binding on the GaAs surface.

A.1.1 AFM

To quantify the surface roughness of freshly etched (oxide free) and X-MBP coated GaAs surfaces (X- stands for any headgroup), AFM topographic scans in tapping mode were carried out on all samples. The maps for 1 $\mu\text{m} \times 1 \mu\text{m}$ surface area for freshly etched, F-MBP and CF₃-MBP coated GaAs are presented in figure A.1.

To quantify the surface roughness, the root-mean-square (RMS) of the outcomes, equation 2.2 on page 12, is computed for all surfaces. The results are summarized in the following table.

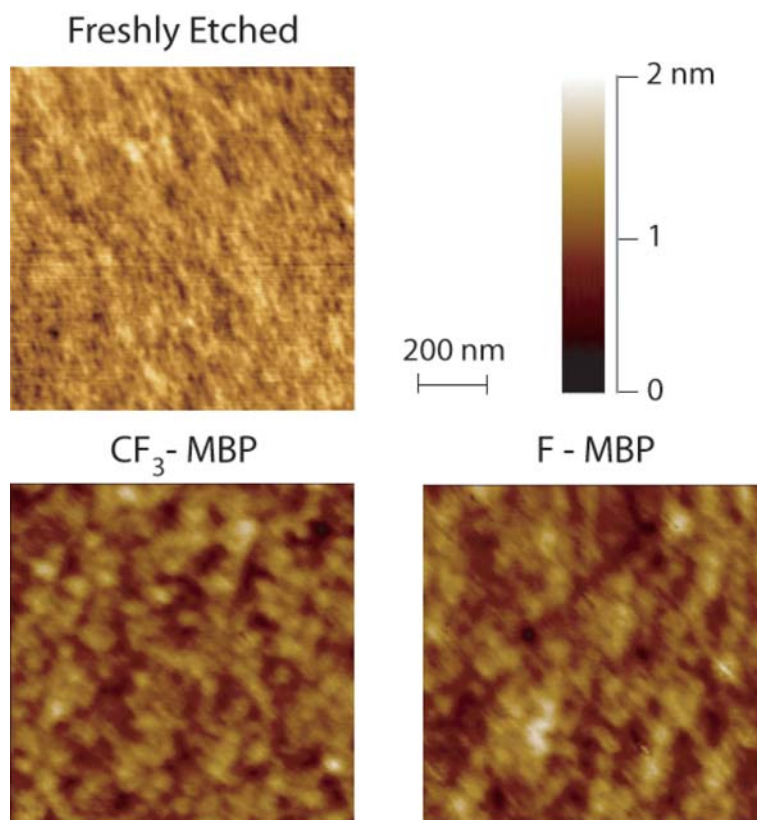


Figure A.1: Tapping mode AFM images of Freshly Etched, CF_3 -MBP and F-MBP coated GaAs surfaces. The RMS roughness was quantified by scanning over $1 \times 1 \mu\text{m}^2$ surface areas. For freshly etched, $\text{RMS} = 2.8 \text{ \AA}$, for CF_3 -MBP 3.0 \AA and F-MBP 3.2 \AA .

Surface coating	RMS Roughness (\AA)
Native Oxide	2.3
Freshly Etched	2.8
H-MBP	3.6
CH_3 -MBP	3.1
OH -MBP*	3.4
F-MBP	3.2
CF_3 -MBP	3.0

The RMS roughness of the native GaAs was increased after the oxide stripping by HCl from 2.3 \AA to 2.8 \AA . Nevertheless, the roughness of the samples with a molecular layer averaged 3.3 \AA . To test the effect of the solvents in the grafting reaction, a freshly etched GaAs was immersed into a reactor without molecules. In this case, the resulting roughness was comparable to the freshly etched shown on table. Despite the slight

increase of roughness by depositing the molecular layer, the coated surfaces suggest to be formed by ordered molecular monolayers. (* these measurements were carried out by K. Adlkofer [105])

A.1.2 Ellipsometry

Ellipsometry was employed to measure the thickness of the self-assembled molecular layer. For this reason, initially, the freshly etched GaAs optical parameters (n_{GaAs} and k_{GaAs}) were extracted by ellipsometry. These optical parameters are obtained by measuring the ellipsometric parameters (Δ and Ψ) on an air/GaAs interface. It is worth noting, for GaAs n_{GaAs} and k_{GaAs} were very sample dependent. To account for the thickness of the added organic molecular layer, Δ_{SAM} and Ψ_{SAM} of the air/SAM/GaAs system was measured. For organic molecules, $n_{SAM} = 1.5$, $k_{SAM} = 0$ was assumed (usual values for organic molecules) [106]. Introducing Δ_{SAM} , Ψ_{SAM} , n_{GaAs} , k_{GaAs} , n_{SAM} and k_{SAM} into the non-linear equations of ellipsometry (see section 2.3.2), the thickness of the organic layer could be acquired. The results are presented on the next table.

Molecule	Thickness (Å)
H-MBP	11
CH ₃ -MBP	10
OH-MBP*	12
F-MBP	10
CF ₃ -MBP	11

Homogenous thicknesses were obtained with different mercapto-biphenyls. Provided that the length of the molecules is $\simeq 11.5$ Å (see section 2.1.1), the results indicate that the molecular layer forms a molecular monolayer. (* these measurements were carried out by K. Adlkofer [105])

A.1.3 Contact Angle

Contact angle measurements are performed to all different X-terminated biphenyl-thiol to account for the surface free energy. The Owens and Wendt's method was used after measuring the static contact angle of water (H₂O), diodomethane (CH₂I₂) and glycerol (C₃H₈O₃). Although the method only requires too make use of two different

Appendix

liquids, here three liquids were employed to confirm our observations. The following table summarizes the contact angle outcomes. *

Surface	Static			Dynamic	
	Water	Diodomethane	Glycerol	Advancing	Receding
Freshly Etched	41°	18°	41°	46°	17°
H-MBP	77°	34°	70°	85°	62°
CH ₃ -MBP	77°	46°	71°	89°	63°
OH-MBP	60°	26°	43°	64°	26°
F-MBP	71°	32°	67°	88°	59°
CF ₃ -MBP	80°	40°	70°	88°	74°

By introducing the data to Owens and Wendy's equation, eq. 2.3 of page 13, the surface free energy for each organic monolayer was calculated. The results are presented in the following table.

	Total Surface free Energy γ [mNm ⁻¹]	Dispersive component γ_d [mNm ⁻¹]	Polar component γ_p [mNm ⁻¹]
Freshly Etched	54	27	27
H-MBP	41	37	3
CH ₃ -MBP	36	31	5
OH-MBP	50	37	13
F-MBP	42	37	5
CF ₃ -MBP	39	35	3

Different surface free energy were obtained by functionalizing GaAs surface with the different mercapto compounds. CH₃-MBP monolayers on GaAs show the highest advancing and receding water contact angles. Furthermore, CH₃-MBP surfaces have the lowest total surface free energy and the lowest polar component of the surface free energy γ_p . This indicates that, of all different molecules, CH₃-MBP is the most suitable to make GaAs surfaces hydrophobic.

In conclusion, the halogen components of the headgroup forming F-MBP and CF₃-MBP molecules do not affect the kinetics and the quality of the self-assembled monolayers on GaAs (to our sensitivity limit). The quality of the films is comparable to the one formed by the rest of the MBP family.

*The data of Dynamic contact angle are shown for completeness but, in this section, are not used to calculate the surface free energy.

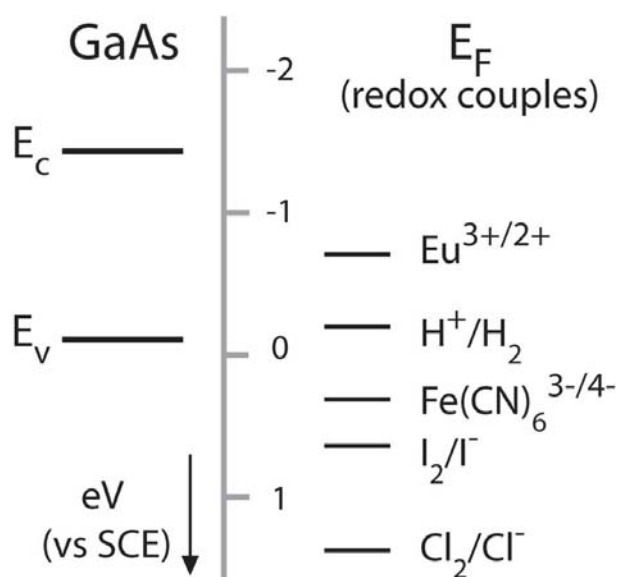


Figure A.2: Chart representing the energetic relationship between the Fermi level of different redox couples (right) and the bands of GaAs (left). The reference energy scale (vs Ag/AgCl reference electrode) is given in electron-volts [eV]. By tuning the U_{bias} , the bands of the semiconductor move accordingly. Positive changes of U_{bias} shift the semiconductor bands downwards.

A.2 Electron Transfer between Redox Couples and Semiconductors

As demonstrated by Memming [107], electron transfer between a semiconductor and a redox system can only take place between levels of the same energy. Thus, it is necessary to set the energy of the redox couple with respect to the semiconductor band structures. This is done by means of a reference electrode. In this way, the Fermi level of semiconductor can be related to the standard redox potential of the redox couple through the standard Columel potential [108]. Fig. A.2 shows the relationships between GaAs bands and different redox couples [43]. The scale-bar indicates the energy in [eV] with respect of the Ag/AgCl reference electrode. By applying an additional external bias potential (U_{bias}), E_c and E_v move accordingly with respect to the electrolyte potential. For positive changes of U_{bias} , the semiconductor bands move downwards.

Gerischer [44] and Marcus [53] developed a theory of the electron transfer currents between semiconductor and redox pairs. Different currents may arise. For example, anodic currents (electrons entering the semiconductor) occur if oxidation of reduced electrolyte species through the conduction band (involving electrons) or reduction of the oxidized species through the valence band (involving holes) takes place. In the framework of this theory, the interfacial currents for the conduction band (c) and the valence band (v) can be written as

$$\begin{aligned}
 j_c^+ &= eh_c^+ N_c c_{red} & j_c^- &= ek_c^- n_s c_{ox} \\
 j_v^+ &= eh_v^+ N_v c_{ox} & j_v^- &= ek_v^- p_s c_{red}.
 \end{aligned}
 \tag{A.1}$$

Here, N_c and N_v represent the effective density of states (cm^{-3}) at the conduction and valence band, respectively, c_{red} and c_{ox} the concentrations of the reduced and oxidized species of the redox couple (cm^{-3}), respectively, and k_i is the electron or h_i is the hole exchange rate constants ($\text{cm}^4 \text{s}^{-1}$). n_s and p_s are the surface concentrations of electrons and holes of the semiconductor, respectively.

As the number of available electrons and holes at the surface depends on the band bending, ϕ_{BB} , given the Boltzmann distribution,

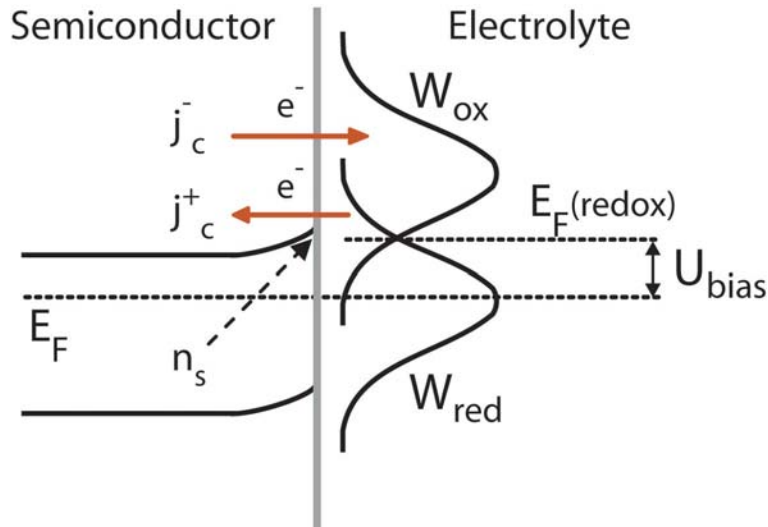


Figure A.3: Scheme representing different physical parameters involved in interfacial electron transfer between redox couple and conduction band of a semiconductor. Set by the U_{bias} potential vs a reference electrode, the conduction band of the semiconductor and the redox couples are brought in a defined energetic relationship. The overlapping (convolution) between the density of states of electrons in the conduction band (n_p) and the density of states of the redox couple in the oxidized (W_{ox}) or reduced (W_{red}) states determines the current density across the interface. Anodic currents density (j_c^+) occurs when reduced ions of redox couple (W_{red}) transfer electrons to the semiconductor. Cathodic current density (j_c^-) arises when oxidized ions are reduced by electrons of the semiconductor. Analogous physics occurs at the valence band. There, the exchanged carriers are holes instead of electrons.

$$n_s = n_0 e^{-\frac{e\phi_{BB}}{kT}} \quad p_s = p_0 e^{\frac{e\phi_{BB}}{kT}} \quad (\text{A.2})$$

where n_0 and p_0 are the bulk concentrations of electrons and holes, determined by the doping level and

$$\phi_{BB} = U_{bias} - U_{fb}$$

the final current will *exponentially* depend on the bias potential U_{bias} or the flat band potential U_{fb} . Theoretically, 60 mV/decade (of current) is the maximum response achievable, i.e. the Nernst response.

Nonetheless, electron-transfer reactions do not change the band bending ϕ_{BB} . In cases where electron-transfer reaction is experimentally observed to change the band bending, the structure of the Helmholtz layer must be modified either by charging the surface, changing the polarity or modifying the density of the surface states [51].

The predictions of the theory rely on the stability and reversibility of the interfacial processes. Irreversible electrochemical reactions may involve the bands of the semiconductor and the surface states, as well. Nevertheless, in irreversible processes, the states of the semiconductor bands, surface states and the energetic relation between ion species and the semiconductor might be undefined. Therefore, the applicability of the presented theory is valid mainly for reversible processes.

A.3 Lipid Bilayers on GaAs coated with OH-MBP Monolayers

Impedance spectroscopy is used to investigate the formation and the properties of lipid layers on GaAs coated with OH-terminated biphenyls. As shown on the contact angle data A.1.3, monolayers of OH-MBP molecules exhibit the highest polar component of the surface free energy of the family of MBP molecules, indicating the highest degree of hydrophilicity. This is why, these monolayers are the most promising candidates for the formation of lipid bilayers on bulk GaAs electrodes.

Experimental Procedure

Analogously as done on chapter 7, the stability of the GaAs electrodes coated with OH-MBP monolayers was checked by impedance spectroscopy over a wide frequency range (100 kHz - 100 mHz). Equivalent circuit 'Model A' of chart 7.1 fitted the entire impedance spectra with errors below 2%. The electrochemical stability was confirmed as the total interface resistance (R_p) and the total interface capacitance (C_p) remained constant at $R_p = 1.3 \pm 0.05 \text{ M}\Omega \text{ cm}^2$ and $C_p = 1.8 \text{ }\mu\text{Fcm}^{-2}$ for more than 6-8 hours at the current minimum potential $U_{bias,j=0} = -400 \text{ mV}$.

Separately, unilamellar vesicles of 60 mol% of neutrally charged lipids (DMPC) and 40 mol% Cholesterol were prepared as described on section 2.2.4. The lipids were mixed and sonified in 10 mM PBS and 100 mM NaCl electrolyte to form unilamellar vesicles.

Results and Discussion

Figure A.4 shows the Bode plot of the impedance spectrum of the GaAs surface coated with OH-MBP monolayers in contact with the electrolyte (blue, +). The solid line depicts the result of the non-linear fit of the experimental data with Model A of chart 7.1 on page 74. In this case $R_p = 4 \text{ M}\Omega\text{cm}^2$ and $C_p = 1.8 \text{ }\mu\text{Fcm}^{-2}$. On the same figure A.4, the impedance spectrum of the interface after depositing the lipid layer on the OH-MBP coated GaAs surface are also depicted (blue, o). Model B of chart 7.1 was employed to account for the electrical properties of the lipid layer. The continuous line is the result of the fitting, too. In numbers, the $R_p = 2.5 \times 10^5 \text{ }\Omega\text{cm}^2$, $C_p = 2.3 \text{ }\mu\text{Fcm}^{-2}$, $R_{PT} = 9.1 \times 10^2 \text{ }\Omega\text{cm}^2$, $C_m = 0.79 \text{ }\mu\text{cm}^{-2}$, $W_m = 9.3 \times 10^4 \text{ }\Omega\text{cm}^2$.

The lipid membrane capacitance C_m (see chapter 7 for proof) was the half of the one observed for a lipid monolayer on section 7.1. In fact, if $\epsilon_m = 2.2$ (usual for lipid molecules), the thickness of the lipid layer is $d_m = 24 \text{ \AA}$, indicating that the lipid layer is a lipid bilayer.

Nevertheless the electrochemical **stability** of the surface was **limited**. The Warburg resistance could not be kept constant after some hours and the quality of the OH-MBP monolayer/GaAs system were gradually degraded (data not shown). The samples were stable for 2-4 hours. There are several reasons for it. First, the electrochemical stability of GaAs coated with OH-MBP monolayers was sensibly lower than CH_3 -MBP monolayers on GaAs. This is caused by the poorer quality of OH-MBP

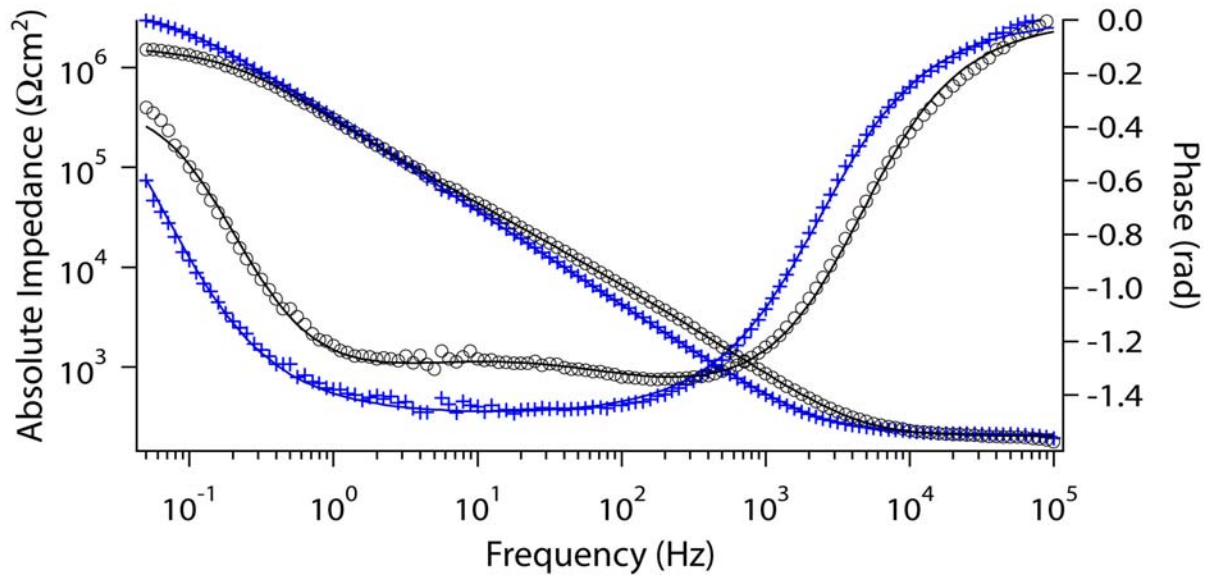


Figure A.4: Impedance spectra (Bode Plot) of before (blue, +) and after (black, o) lipid layer deposition on GaAs electrodes coated with OH-MBP monolayers. The impedance spectrum were taken at $U_{bias} = -400$ mV and non-linearly fitted with the equivalent circuits shown in figure 7.1. For lipid-free surface, Model A was employed (blue). For lipid coated surface Model B (black) yielded a membrane capacitance of $C_m = 0.79$ μcm^{-2} , which corresponds to the capacitance of a lipid bilayer.

monolayers with respect to CH_3 -MBP monolayers. And secondly, lipid bilayers require being in contact with water at both sides of the layer, as lipid bilayers are formed mainly thanks to the hydrophobic force.

A.4 Salt Concentration Sensitivity on 2DEG Devices coated with CH_3 -MBP Monolayers

Sensing of salt concentration measurements on 2DEG devices coated with CH_3 -MBP monolayers were carried out to provide supporting arguments to the charging mechanism responsible for the pH sensitivity of section 5.2.

Experimental Procedure

The experiment consisted in measuring, as a function of the electrolyte pH, the changes of surface potential caused by changes of salt concentration. To stabilize the electrolyte pH, 1 mM PBS was added to all solutions. The set of different solutions consisted of

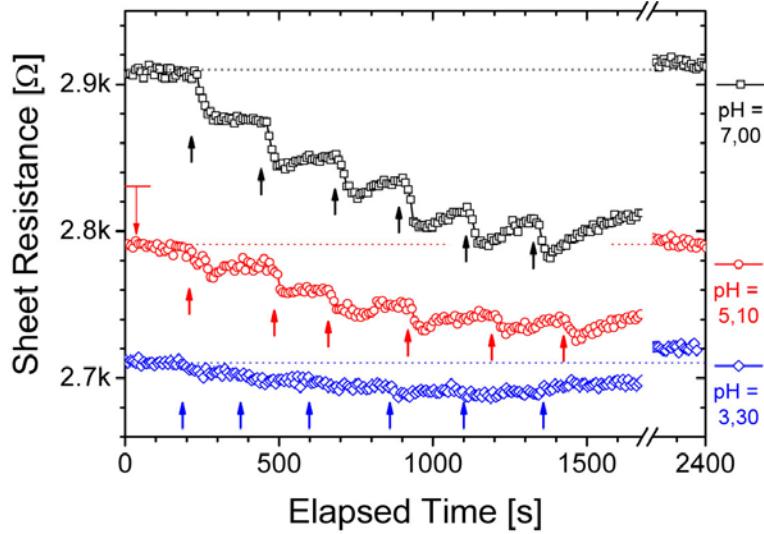


Figure A.5: Raw data showing the response of the Sheet resistance (R_{sh}) of the 2DEG devices coated with $\text{CH}_3\text{-MBP}$ monolayers to changes of NaCl concentration in the electrolyte at different pH values and at $U_{bias} = -400$ mV. The arrows indicate the moment of the new salt concentration injection and the last value taken to average R_{sh} . Three series of 3 mM, 10 mM, 30 mM, 100 mM, 300 mM and 1 M of NaCl were injected at pH 7, 3.30 and 5.1, in sequence on the same sample. To demonstrate the reversibility of the experiment, the last measurements are performed at the initial 3 mM NaCl. The clear influence of the pH to the response upon changes of salt concentration indicates that the surface charging mechanism is controlled by the pH.

1 mM, 3 mM, 10 mM, 30 mM, 100 mM, 300 mM, and 1 M of NaCl for every pH. As changes in salt concentration shift the electrolyte pH (see equation 2.1), the corresponding solution was titrated with either HCl or NaOH to reach the desired pH.

Experimental Observations and Discussion

Figure A.5 shows the response of R_{sh} as a function of time for a set of 3 experiments on the same sample. The salt concentration was changed in sequence at a fixed pH. Each set of R_{sh} vs time corresponds to fix pH value. Each plateau reflects the value of R_{sh} that achieved at 3 mM, 10 mM, 30 mM, 100 mM, 300 mM and 1 M of NaCl in sequence. To check the reversibility of the experiment, the first salt concentration condition (3 mM of NaCl) was tested in the end. The same sample was examined at pH = 7, 3.3 and 5.1 (in this order). The arrows mark the moment at which the new salt injection took place and the last measuring point was taken. As a sensible drift occurred at high salt concentration (1 M NaCl), this measurement is not considered.

As discussed in section 5.2.2, the stability of the 2DEG device ensured that changes in

R_{sh} corresponded to changes of surface potential. To quantify the changes in surface potential caused by the salt concentration, a potential sweep calibration curve was carried out (data not shown), that yielded a slope of $1.79 \pm 0.2 \text{ k}\Omega\text{V}^{-1}$, regardless of the pH and the salt concentration.

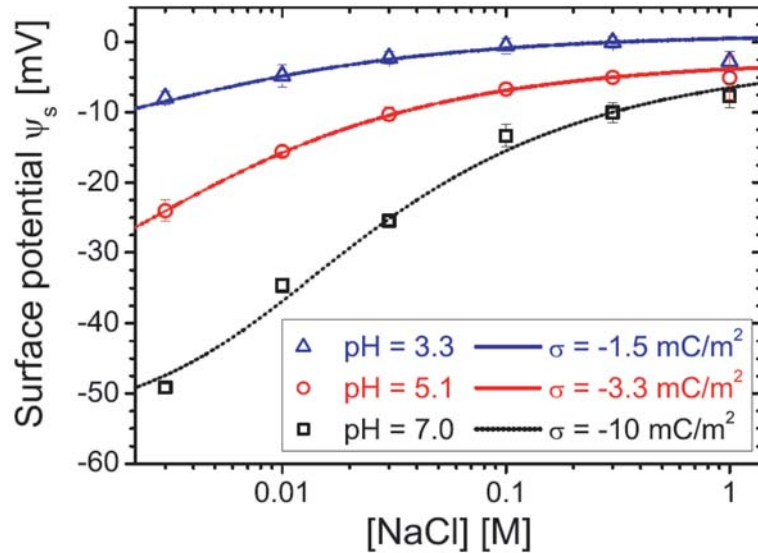


Figure A.6: Relationship between the surface potential, ψ_s , and NaCl concentration on 2DEG devices coated with CH_3 -MBP monolayers. The spots correspond to the average of the experimental data extracted from figure A.5 with its corresponding errors. The continuous lines correspond to the fitting the experimental data with equation A.3. The model supposes that the surface charge density σ_i remains constant irrespective to the salt concentration. The resulting values of σ_i are presented in the box.

Figure A.6 depicts the relationship between salt concentration and surface potentials (dots) at different pH of the electrolyte, extracted from Fig A.5. For pH = 3.3, the surface potential was less affected by the changes in salt concentration than for pH = 7.0. This indicated that at pH = 3.3 the surface was closer to the point of zero charge than at pH = 7.0.

To gain further insight to the charging mechanism observed on the salt dependent measurements, the present experimental data (dots on figure A.6) were fitted with different models.

Supposing that the electrostatic ion-ion and ion-surface interaction is dominant and considering that the chemical potential remains constant all over the electrolyte (Poisson-Boltzmann theory), the Grahm equation

$$\sigma_i = \sqrt{8\epsilon\epsilon_0KT} \sinh\left(\frac{e\psi_\delta}{2KT}\right) \left([M^+]_\infty + [D^{2+}]_\infty(2 + e^{\frac{-e\psi_\delta}{KT}})\right)^{\frac{1}{2}} \quad (\text{A.3})$$

provides the relationship between the ψ_δ (ζ -potential), the salt concentration of monovalent (M^+) and divalent (D^{2+}) ions, and the total charge density of the surface, σ_i . Note that the measured surface potential with the 2DEG devices, ψ_s , may differ from the ζ -potential because of the presence of adsorbed ions at the Stern layer (see figure 3.3).

In addition, because of the charge neutrality, the charge densities must fulfil

$$\sigma_{diffuse} + \overbrace{\sigma_{ads}}^{\sigma_i} + \sigma_0 = 0. \quad (\text{A.4})$$

Here $\sigma_{diffuse}$ is the total charge of the Gouy-Chapman layer and σ_{ads} the charge of the Stern layer. σ_0 consists, in principle, of the sum of the charge density of the semiconductor and the charging originated by the pH. To relate the surface potential ψ_0 with the salt concentration, σ_i needs to be derived.

As a first attempt to theoretically quantify σ_i , the site-binding model that accounts for the protination and deprotination of the possible GaAs oxides at the defects of the self-assembled monolayer was employed [78]. To conveniently model the surface charge, the SAM's defect density on GaAs (effective surface area), the reactivity constants of bare GaAs with the aqueous ions of the electrolyte, K_a and K_b (described in equations 5.3 and 5.4) need to be known. Regardless of the fact that these values are, up to our knowledge, experimentally unobtainable and that such mechanism would induce electrochemical instability, the model could not fit the tendency of the data presented in Fig. A.6 [32], even by inserting different set of values for each parameter. Positive surface potential arose from the existence of positive charge densities. In conclusion, the result provides a supporting argument to discard the protination-deprotination reaction as a charging mechanism.

The second scenario is based on the adsorption of ions on the Stern layer. The Stern Layer is formed by the adsorption of ions on the surface either by electrostatic interaction or specific adsorption, as described by the Stern Model [46]. The model provides the charge density of adsorbed ions, σ_{ads} (equation 3.4 on page 23). Even though this term was not included into the charge balance equation (eq. A.4), the experimental

data of figure A.6 could not be fitted, either.

Surprisingly, the experimental results of figure A.6 could be fitted when the surface charge σ_i was considered to remain constant and *independent* to the salt concentration. The fitting from this model are represented by the solid lines of figure A.6, from which the total surface charge density, σ_i , is extracted for each pH value (inset of the figure).

In fact, Ohki et al. [109] demonstrated the correct prediction of the Stern model in accounting for the aggregation of charged vesicles as a function of the salt concentration, or Eisenberg et al. [110] in quantifying the adsorption of cations on negatively charged lipid membranes. On solid surfaces, Rossetti et al. [111] made use of the predictions the Stern model to influence (through the presence or absence of Ca^{2+} ions) the attraction and/or repulsion between TiO_2 and negatively charged lipid vesicles to the surface. In addition, on H-terminated diamond surfaces (hydrophobic), Härtl et al [9] claim the validity of the Stern model by demonstrating a direct correlation between surface potentials (ψ_s) measured on diamond-based field effect transistors and ζ -potentials by electrokinetic measurements.

The reason for such discrepancy between the model and the experimental observations is not straightforward. This result would mean that there is a strong charge contribution σ_0 from an unconsidered effect that dwindles any possible changes of σ_{ads} (Stern Model) to negligible. Different causes can be attributed. Firstly, the model employed to fit the data did not account for the potential drop across the Stern layer. Secondly, the constant drift obtained in our experimental measurements (Fig. A.5) made impossible a precise quantification of the surface potential. And thirdly, additional counter ions could be adsorbed through an unaccounted mechanism. Although the effect of salt concentration is evident, a more developed ion adsorption model, further simulations and an improved performance of the 2DEG device are necessary to better understand the current problem.

Bibliography

- [1] F. Patolsky, G. F. Zheng, and C. M. Lieber. Nanowire-based biosensors. *Analytical Chemistry*, 78(13):4260–4269, 2006.
- [2] Y. Cui, Q. Q. Wei, H. K. Park, and C. M. Lieber. Nanowire nanosensors for highly sensitive and selective detection of biological and chemical species. *Science*, 293(5533):1289–1292, 2001.
- [3] E. Katz and I. Willner. Biomolecule-functionalized carbon nanotubes: Applications in nanobioelectronics. *Chemphyschem*, 5(8):1085–1104, 2004.
- [4] P. Bergveld. Thirty years of isfetology - what happened in the past 30 years and what may happen in the next 30 years. *Sensors and Actuators B-Chemical*, 88(1):1–20, 2003.
- [5] L. Bousse, N. F. Derooij, and P. Bergveld. Operation of chemically sensitive field-effect sensors as a function of the insulator-electrolyte interface. *Ieee Transactions on Electron Devices*, 30(10):1263–1270, 1983.
- [6] G. Steinhoff, M. Hermann, W. J. Schaff, L. F. Eastman, M. Stutzmann, and M. Eickhoff. ph response of gan surfaces and its application for ph-sensitive field-effect transistors. *Applied Physics Letters*, 83(1):177–179, 2003.
- [7] B. Baur, J. Howgate, H. G. von Ribbeck, Y. Gawlina, V. Bandalo, G. Steinhoff, M. Stutzmann, and M. Eickhoff. Catalytic activity of enzymes immobilized on algan/gan solution gate field-effect transistors. *Applied Physics Letters*, 89(18), 2006.
- [8] J. A. Garrido, A. Hardl, S. Kuch, M. Stutzmann, O. A. Williams, and R. B. Jackmann. ph sensors based on hydrogenated diamond surfaces. *Applied Physics Letters*, 86(7), 2005.

Bibliography

- [9] A. Hartl, J. A. Garrido, S. Nowy, R. Zimmermann, C. Werner, D. Horinek, R. Netz, and M. Stutzmann. The ion sensitivity of surface conductive single crystalline diamond. *Journal of the American Chemical Society*, 129(5):1287–1292, 2007.
- [10] E. Sackmann. Supported membranes: Scientific and practical applications. *Science*, 271(5245):43–48, 1996.
- [11] H. Hillebrandt, G. Wiegand, M. Tanaka, and E. Sackmann. High electric resistance polymer/lipid composite films on indium-tin-oxide electrodes. *Langmuir*, 15(24):8451–8459, 1999.
- [12] H. Hillebrandt, M. Tanaka, and E. Sackmann. A novel membrane charge sensor: Sensitive detection of surface charge at polymer/liquid composite films on indium tin oxide electrodes. *J.Phys.Chem. B*, 106:477–486, 2002.
- [13] O. Purrucker, H. Hillebrandt, K. Adlkofer, and M. Tanaka. Deposition of highly resistive lipid bilayer on silicon-silicon dioxide electrode and incorporation of gramicidin studied by ac impedance spectroscopy. *Electrochimica Acta*, 47(5):791–798, 2001.
- [14] M. Tanaka and E. Sackmann. Polymer-supported membranes as models of the cell surface. *Nature*, 437(7059):656–663, 2005.
- [15] M. Tanaka and E. Sackmann. Supported membranes as biofunctional interfaces and smart biosensor platforms. *Physica Status Solidi a-Applications and Materials Science*, 203(14):3452–3462, 2006.
- [16] M. Tanaka, A. P. Wong, F. Rehfeldt, M. Tutus, and S. Kaufmann. Selective deposition of native cell membranes on biocompatible micropatterns. *Journal of the American Chemical Society*, 126(10):3257–3260, 2004.
- [17] M.J. Howes and D.V. Morgan. *Gallium Arsenide*. The Willey Series in Solid State Devices and Circuits. John Wiley & Sons, 1985.
- [18] G. Ashkenasy, D. Cahen, R. Cohen, A. Shanzer, and A. Vilan. Molecular engineering of semiconductor surfaces and devices. *Accounts of Chemical Research*, 35(2):121–128, 2002.
- [19] A. Vilan and D. Cahen. How organic molecules can control electronic devices. *Trends in Biotechnology*, 20(1):22–29, 2002.

- [20] P. Allongue and S. Blonkowski. Corrosion of iii-v-compounds - a comparative-study of gaas and inp .2. reaction scheme and influence of surface-properties. *Journal of Electroanalytical Chemistry*, 317(1-2):77–99, 1991.
- [21] P. Allongue and S. Blonkowski. Corrosion of iii-v-compounds - a comparative-study of gaas and inp .1. electrochemical characterization based on tafel plot measurements. *Journal of Electroanalytical Chemistry*, 316(1-2):57–77, 1991.
- [22] S. R. Lunt, G. N. Ryba, P. G. Santangelo, and N. S. Lewis. Chemical studies of the passivation of gaas surface recombination using sulfides and thiols. *Journal of Applied Physics*, 70(12):7449–7465, 1991.
- [23] S. R. Lunt, P. G. Santangelo, and N. S. Lewis. Passivation of gaas surface recombination with organic thiols. *Journal of Vacuum Science & Technology B*, 9(4):2333–2336, 1991.
- [24] K. Adlkofer, E. F. Duijs, F. Findeis, M. Bichler, A. Zrenner, E. Sackmann, G. Abstreiter, and M. Tanaka. Enhancement of photoluminescence from near-surface quantum dots by suppression of surface state density. *Physical Chemistry Chemical Physics*, 4(5):785–790, 2002.
- [25] A. Ulman. Self-assembled monolayers of 4-mercaptobiphenyls. *Accounts of Chemical Research*, 34(11):855–863, 2001.
- [26] K. Adlkofer, W. Eck, M. Grunze, and M. Tanaka. Surface engineering of gallium arsenide with 4-mercaptobiphenyl monolayers. *Journal of Physical Chemistry B*, 107(2):587–591, 2003.
- [27] K. Adlkofer, A. Shaporenko, M. Zharnikov, M. Grunze, A. Ulman, and M. Tanaka. Chemical engineering of gallium arsenide surfaces with 4'-methyl-4-mercaptobiphenyl and 4'-hydroxy-4-mercaptobiphenyl monolayers. *Journal of Physical Chemistry B*, 107(42):11737–11741, 2003.
- [28] S. Lubber, K Adlkofer, U. Rant, A. Ulman, A. Götzhäuser, M. Grunze, D. Schuh, M. Tanaka, M. Tornow, and G. Abstreiter. Liquid phase sensors based on chemically functionalized gaas/algaas heterostructures. *Physica E*, 21:1111–1115, 2004.
- [29] J.F. Kang, A. Ulman, S. Liao, R. Jordan, G. Yang, and G. Liu. Self-assembled rigid monolayers of 4'-substituted-4-mercaptobiphenyls on gold and silver surfaces. *Langmuir*, 17:95–106, 2001.

Bibliography

- [30] A. Ulman. Formation and structure of self-assembled monolayers. *Chemical Reviews*, 96(4):1533–1554, 1996.
- [31] P. Allongue and H. Cachet. Photocapacitance study of n-gaas electrolyte interfaces. *Berichte Der Bunsen-Gesellschaft-Physical Chemistry Chemical Physics*, 91(4):386–390, 1987.
- [32] S. Luber. *III-V Semiconductor Structures for Biosensor and Molecular Electronics Applications*. PhD thesis, Walter Schottky Institute, Technische Universität München, 2006.
- [33] R.M.A. Azzam and N.M. Bashara. *Ellipsometry and polarized light*. North Holland Personal Library. Elsevier North Holland, Amsterdam, 1977.
- [34] F. M. Fowkes. Determination of interfacial tensions, contact angles, and dispersion forces in surfaces by assuming additivity of intermolecular interactions in surfaces. *Journal of Physical Chemistry*, 66(2):382–&, 1962.
- [35] D. K. Owens and R. C. Wendt. Estimation of surface free energy of polymers. *Journal of Applied Polymer Science*, 13(8):1741–&, 1969.
- [36] F. M. Fowkes. Attractive forces at interfaces. *Industrial and Engineering Chemistry*, 56(12):40–&, 1964.
- [37] S. M. Sze. *Semiconductor Devices: Physics and Technology*. John Wiley & Sons, New York, 1985.
- [38] R. Cohen, L. Kronik, A. Shanzer, D. Cahen, A. Liu, Y. Rosenwaks, J. K. Lorenz, and A. B. Ellis. Molecular control over semiconductor surface electronic properties: Dicarboxylic acids on cdte, cdse, gaas, and inp. *Journal of the American Chemical Society*, 121(45):10545–10553, 1999.
- [39] C.J. Palmström and D.V. Morgan. Metallization for gaas devices and circuits. In M.J. Howes and D.V. Morgan, editors, *Gallium Arsenide. Materials, Devices and Circuits*, pages 195–261. Wiley, Norwich, UK, 1985.
- [40] L. J. Brillson, R. Z. Bachrach, R. S. Bauer, and J. McMenamin. Chemically-induced charge redistribution at al-gaas interfaces. *Physical Review Letters*, 42(6):397–401, 1979.

- [41] W. E. Spicer, P. W. Chye, P. R. Skeath, C. Y. Su, and I. Lindau. New and unified model for schottky-barrier and iii-v insulator interface states formation. *Journal of Vacuum Science & Technology*, 16(5):1422–1433, 1979.
- [42] D. Bolmont, P. Chen, V. Mercier, and C. A. Sebenne. Electron-states at abrupt metal-gaas(110) interfaces. *Physica B & C*, 117(MAR):816–818, 1983.
- [43] G. Horowitz, P. Allongue, and H. Cachet. Quantitative comparison of fermi level pinning at gaas/metal and gaas/liquid junctions. *Journal of the Electrochemical Society*, 131(11):2563–2569, 1984.
- [44] H. Gerischer. *Physical Chemistry an Advanced Treatise*, volume IX A / Electrochemistry of *Physical Chemistry*. Academic Press, New York, 1970.
- [45] J. Israelachvili. *Intermolecular and Surface Forces*. Academic Press Limited, London, second edition edition, 1991.
- [46] O. Stern. The theory of the electrolytic double shift. *Zeitschrift Fur Elektrochemie Und Angewandte Physikalische Chemie*, 30:508–516, 1924.
- [47] H. Gerischer and W. Mindt. The mechanisms of decomposition of semiconductors by electrochemical oxidation and reduction. *Electrochimica Acta*, 13:1329–1341, 1968.
- [48] P.H.L. Notten, J.E.A.M. van der Meerakker, and J.J. Kelly. *Etching of III-V Semiconductors: an electrochemical approach*. Elsevier Advanced Technology, Oxford, 1991.
- [49] H. Gerischer. The impact of semiconductors on the concepts of electrochemistry. *Electrochimica Acta*, 35(11-12):1677–1699, 1990.
- [50] K. Adlkofer, M. Tanaka, H. Hillebrandt, G. Wiegand, and E. Sackmann. Electrochemical passivation of gallium arsenide surface with organic self-assembled monolayers in aqueous electrolytes. *Applied Physics Letters*, 76(22):3313–3315, 2000.
- [51] W. Schmickler. *Grundlagen der Elektrochemie*. Vieweg Lehrbuch. Vieweg & Sohn Verlagsgesellschaft, Braunschweig/Wiesbaden, 1996.
- [52] I. Uhlendorf, R. Reinekekoeh, and R. Memming. Analysis of the hydrogen formation at gaas electrodes by impedance spectroscopy investigations. *Berichte Der Bunsen-Gesellschaft-Physical Chemistry Chemical Physics*, 99(9):1082–1090, 1995.

Bibliography

- [53] R.A. Marcus. Chemical and electrochemical electron-transfer theory. *Annual Reviews of Physical Chemistry*, 15(155), 1964.
- [54] K. Siemoneit, R. Reineke-Koch, A. Meier, and R. Memming. Fast processes at semiconductor-liquid interfaces: reactions at gas electrodes. *Electrochimica Acta*, 45(28):4577–4589, 2000.
- [55] B. A. Cornell, V. L. B. BraachMaksvytis, L. G. King, P. D. J. Osman, B. Raguse, L. Wiczorek, and R. J. Pace. A biosensor that uses ion-channel switches. *Nature*, 387(6633):580–583, 1997.
- [56] S. Gritsch, P. Nollert, F. Jahnig, and E. Sackmann. Impedance spectroscopy of porin and gramicidin pores reconstituted into supported lipid bilayers on indium-tin-oxide electrodes. *Langmuir*, 14(11):3118–3125, 1998.
- [57] C. Steinem, A. Janshoff, H. J. Galla, and M. Sieber. Impedance analysis of ion transport through gramicidin channels incorporated in solid supported lipid bilayers. *Bioelectrochemistry and Bioenergetics*, 42(2):213–220, 1997.
- [58] M. Stelzle, G. Weissmuller, and E. Sackmann. On the application of supported bilayers as receptive layers for biosensors with electrical detection. *Journal of Physical Chemistry*, 97(12):2974–2981, 1993.
- [59] M. Rentschler and P. Fromherz. Membrane-transistor cable. *Langmuir*, 14(2):547–551, 1998.
- [60] J.R. MacDonald. *Impedance Spectroscopy*. John Wiley & Sons, Inc., 1987.
- [61] G. Wiegand. *Fundamental principles of the electric properties of supported lipid membranes investigated by advanced methods of impedance spectroscopy*. PhD thesis, Technische Universität München, 1999.
- [62] G. S. Popkirov and R. N. Schindler. A new impedance spectrometer for the investigation of electrochemical systems. *Review of Scientific Instruments*, 63(11):5366–5372, 1992.
- [63] G. S. Popkirov and R. N. Schindler. Optimization of the perturbation signal for electrochemical impedance spectroscopy in the time-domain. *Review of Scientific Instruments*, 64(11):3111–3115, 1993.

- [64] G. Wiegand, K. R. Neumaier, and E. Sackmann. Fast impedance spectroscopy: General aspects and performance study for single ion channel measurements. *Review of Scientific Instruments*, 71(6):2309–2320, 2000.
- [65] G. Cevc, editor. *Phospholipids Handbook*. Marcel Dekker, New York, 1993.
- [66] J. E. B. Randles. Kinetics of rapid electrode reactions. *Discussions of the Faraday Society*, 1:11–19, 1947.
- [67] C. Ho, I. D. Raistrick, and R. A. Huggins. Application of ac techniques to the study of lithium diffusion in tungsten trioxide thin-films. *Journal of the Electrochemical Society*, 127(2):343–350, 1980.
- [68] H. O. Finklea, D. A. Snider, J. Fedyk, E. Sabatani, Y. Gafni, and I. Rubinstein. Characterization of octadecanethiol-coated gold electrodes as microarray electrodes by cyclic voltammetry and ac-impedance spectroscopy. *Langmuir*, 9(12):3660–3667, 1993.
- [69] J. R. Macdonald. Power-law exponents and hidden bulk relation in the impedance spectroscopy of solids. *Journal of Electroanalytical Chemistry*, 378(1-2):17–29, 1994.
- [70] K. S. Cole and R. H. Cole. Dispersion and absorption in dielectrics i. alternating current characteristics. *Journal of Chemical Physics*, 9(4):341–351, 1941.
- [71] D. de Levie. On the impedance electrodes with rough interfaces. *J. Electroanal. Chem*, 261:1, 1989.
- [72] D. L. Koch and A. S. Sangani. The ac electrical-impedance of a fractal boundary to an electrolytic solution. *Journal of the Electrochemical Society*, 138(2):475–484, 1991.
- [73] B. LindholmSethson. Electrochemistry at ultrathin organic films at planar gold electrodes. *Langmuir*, 12(13):3305–3314, 1996.
- [74] W. P. Gomes and D. Vanmaekelbergh. Impedance spectroscopy at semiconductor electrodes: Review and recent developments. *Electrochimica Acta*, 41(7-8):967–973, 1996.
- [75] Z. Hens and W. P. Gomes. On the diffusion impedance at semiconductor electrodes. *Journal of Physical Chemistry B*, 101(30):5814–5821, 1997.

Bibliography

- [76] J. H. Sluyters and J. J. C. Oomen. On the impedance of galvanic cells .2. experimental verification. *Recueil Des Travaux Chimiques Des Pays-Bas-Journal of the Royal Netherlands Chemical Society*, 79(8):1101–1110, 1960.
- [77] H. Hillebrandt. *Design of polymer supported lipid membranes on indium-tin-oxide (ITO) semiconductor electrodes for biosensoric applications*. PhD thesis, Technische Universität München, 2001.
- [78] P. Bergveld and A. Sibbald. *Analytical and Biomedical Applications of Ion-Selective Field-Effect Transistors*. *Comprehensive Analytical Chemistry*, volume XXIII. Elsevier Science, New York, 1988.
- [79] S. Roy Morrison. *Electrochemistry at semiconductor and oxidized metal electrodes*. Plenum Press, New York u.a., 1980.
- [80] P. Allongue and H. Cachet. Band-edge shift and surface-charges at illuminated n-gaas aqueous-electrolyte junctions - surface-state analysis and simulation of their occupation rate. *Journal of the Electrochemical Society*, 132(1):45–52, 1985.
- [81] K. Adlkofer and M. Tanaka. Stable surface coating of gallium arsenide with octadecylthiol monolayers. *Langmuir*, 17(14):4267–4273, 2001.
- [82] W.M. Siu and R.S.C. Cobbold. Basic properties of the electrolyte-sio₂-si system: Physical and theoretical aspects. *IEEE Trans. Electron Devices*, 26:1805–1815, 1979.
- [83] H. Hillebrandt and M. Tanaka. Electrochemical characterization of self-assembled alkylsiloxane monolayers on indium-tin oxide (ito) semiconductor electrodes. *Journal of Physical Chemistry B*, 105(19):4270–4276, 2001.
- [84] K. Marinova, R.G. Alargova, N.D. Denkov, O.D. Velev, D.N. Petsev, I.B. Ivanov, and R.P. Borwankar. Charging of oil-water interfaces due to spontaneous adsorption of hydroxyl ions. *Langmuir*, 12:2045–2051, 1996.
- [85] R. Schweiss, P.B. Welzel, C. Werner, and W. Knoll. Dissociation of surface functional groups and preferential adsorption of ions on self-assembled monolayers assessed by streaming potential and streaming current measurements. *Langmuir*, 17:4304–4311, 2001.
- [86] Y.M. Chan, R. Schweiss, C. Werner, and M. Grunze. Electrokinetic characterization of oligo- and poly(ethylene glycol)-terminated self-assembled monolayers on gold and glass surfaces. *Langmuir*, 19:7380–7385, 2003.

- [87] H. Kreuzer, R. L. Wang, and M. Grunze. Hydroxide ion adsorption on self-assembled monolayers. *JACS*, 125:8384–8389, 2003.
- [88] R. Zangi and Jbfn Engberts. Physisorption of hydroxide ions from aqueous solution to a hydrophobic surface. *Journal of the American Chemical Society*, 127(7):2272–2276, 2005.
- [89] M. G. Cacace, E. M. Landau, and J. J. Ramsden. The hofmeister series: salt and solvent effects on interfacial phenomena. *Quarterly Reviews of Biophysics*, 30(3):241–277, 1997.
- [90] F. Hofmeister. Zur lehre von der wirkung der salze. *Arch. Exp. Pathol. Pharmacol.*, 1888.
- [91] W. Kunz, J. Henle, and B. W. Ninham. 'zur lehre von der wirkung der salze' (about the science of the effect of salts): Franz hofmeister's historical papers. *Current Opinion in Colloid & Interface Science*, 9(1-2):19–37, 2004.
- [92] Y. Marcus. *Ion Solvation*. Wiley, Chistester, 1985.
- [93] L. Onsager and N.N.T. Samaras. The surface tension of debye-hückel electrolytes. *Journal of Chemical Physics*, (2):528, 1934.
- [94] T. M. Chang and L. X. Dang. Recent advances in molecular simulations of ion solvation at liquid interfaces. *Chemical Reviews*, 106(4):1305–1322, 2006.
- [95] J. P. Dilger, S. G. A. McLaughlin, T. J. McIntosh, and S. A. Simon. Dielectric-constant of phospholipid-bilayers and the permeability of membranes to ions. *Science*, 206(4423):1196–1198, 1979.
- [96] M. Montal and P. Mueller. Formation of bimolecular membranes from lipid monolayers and a study of their electrical properties. *Proceedings of the National Academy of Sciences of the United States of America*, 69(12):3561–3566, 1972.
- [97] J. Requena and D. A. Haydon. Vanderwaals forces in oil-water systems from study of thin lipid films .2. dependence of vanderwaals free-energy of thinning on film composition and structure. *Proceedings of the Royal Society of London Series a-Mathematical Physical and Engineering Sciences*, 347(1649):161–177, 1975.
- [98] A. L. Plant. Self-assembled phospholipid alkanethiol biomimetic bilayers on gold. *Langmuir*, 9(11):2764–2767, 1993.

Bibliography

- [99] C. A. Keller, K. Glasmaster, V. P. Zhdanov, and B. Kasemo. Formation of supported membranes from vesicles. *Physical Review Letters*, 84(23):5443–5446, 2000.
- [100] E. Sackmann and R. Lipowski. *Structure and Dynamics of Membranes*. Handbook of Biological Physics. Elsevier, Amsterdam, The Netherlands, 1995.
- [101] R. Verger, M. C. E. Mieras, and G. H. Dehaas. Action of phospholipase a at interfaces. *Journal of Biological Chemistry*, 248(11):4023–4034, 1973.
- [102] K. Balashev, N. J. DiNardo, T. H. Callisen, A. Svendsen, and T. Bjornholm. Atomic force microscope visualization of lipid bilayer degradation due to action of phospholipase a(2) and humicola lanuginosa lipase. *Biochimica Et Biophysica Acta-Biomembranes*, 1768(1):90–99, 2007.
- [103] C. Leidy, O. G. Mouritsen, K. Jorgensen, and N. H. Peters. Evolution of a rippled membrane during phospholipase a(2) hydrolysis studied by time-resolved afm. *Biophysical Journal*, 87(1):408–418, 2004.
- [104] W. Geyer, V. Stadler, W. Eck, M. Zharnikov, A. Golzhauser, and M. Grunze. Electron-induced crosslinking of aromatic self-assembled monolayers: Negative resists for nanolithography. *Applied Physics Letters*, 75(16):2401–2403, 1999.
- [105] K Adlkofer. *Engineering Bulk and Nanostructured GaAs with Organic Monomolecular Films*. PhD thesis, Technical University of Munich, 2004.
- [106] R.C Weast. *Handbook of Chemistry and Physics*. Cleveland, The Chemical Rubber Co., 1970.
- [107] R. Memming. *Electroanalytical Chemistry. A Series of Advances.*, volume 11. Dekker, New York, 1979.
- [108] A.J. Bard and L.R. Faulkner. *Electrochemical methods*. Wiley Interscience, New York, 1980.
- [109] S. Ohki, N. Duzgunes, and K. Leonards. Phospholipid vesicle aggregation - effect of mono-valent and divalent ions. *Biochemistry*, 21(9):2127–2133, 1982.
- [110] M. Eisenberg, T. Gresalfi, T. Riccio, and S. McLaughlin. Adsorption of mono-valent cations to bilayer membranes containing negative phospholipids. *Biochemistry*, 18(23):5213–5223, 1979.

- [111] F. F. Rossetti, M. Bally, R. Michel, M. Textor, and I. Reviakine. Interactions between titanium dioxide and phosphatidyl serine-containing liposomes: Formation and patterning of supported phospholipid bilayers on the surface of a medically relevant material. *Langmuir*, 21(14):6443–6450, 2005.

Bibliography

Acknowledgements

This thesis would not have been possible without the help and dedication of many persons from and outside the Technical University of Munich, to whom I would very pleasantly like to thank.

Prof. Matthias Rief is to be thanked for taking part of the examining committee. As a head of our Biophysik Department E22, I kindly appreciate his understanding about our laboratory move to University of Heidelberg by facilitating my stage in Munich.

My biggest gratitude is to **Prof. Motomu Tanaka** for being my supervisor and seriously taking responsibility for teaching me different aspects of scientific work and introducing me to such a challenging scientific field, as surface biophysics is. I sincerely appreciate Motomu's sharp and constant critical eye on my work as well as his priority in forming me as an independent researcher.

I honestly appreciate the interest of **Prof. Gerard Abstreiter** from the Walter Schottky Institute (TU München) and, particularly, of the sub-group leader **Prof. Marc Tornow** (Technische Universität Braunschweig) in investigating the possibilities of GaAs as a biosensor. Together with **Dr. Sebastian Luber**, we started the first biosensing experiments using their 2-Dimensional-Electron-Gas devices and our surface chemistry. Sebastian and I spent loads of hours discussing our pH sensitivity experiment. The work became a main block of our both theses as well as a publication. To this FCB sufferer, and good friend, I am very glad to have shared all this time with him! I would also like to thank **Max Bichler** for his immediate disposition to provide new solutions to aspects related to materials and **Angelika Stumpf** for patiently teaching and helping me with the underpinnings of sample fabrication. I sincerely enjoyed to have worked with such always receptive staff of WSI!

The functionalization of GaAs surface with mercapto-biphenyl molecules has been the key to the realization of this work. For this reason, I would like to thank **Prof. Abraham Ulman** (Polytechnic University of New York, USA) and **Prof. Michael Grunze** (Ruprecht-Karls-Universität Heidelberg) for the synthesis of the compounds, fruitful suggestions in surface chemistry and their participation in the discussion of the pH sensitive experiment.

The study of counter-ion sensitivity would not have been possible without the proposals of **Dr. Dominik Horinek** and **Prof. Roland Netz** (TU München). My grateful thanks to them as they have always been open to receive me, patiently explain the the-

oretical issues and introducing me to such a relevant research topic in biophysics. To Prof. Roland Netz, I also appreciate his sincere disposition to be part of the examining committee of my doctoral work.

From the Ruprecht-Karls-Universität Heidelberg, **Dr. Michael Himmelhaus** and **Dr. Svetlana Stoycheva** are to be thanked for their joint dedication to develop a new strategy to measure molecular layers on GaAs with FTIR, and **Dr. Michael Zharnikov** for the HRXPS and NEXAFS measurements on the GaAs functionalized with fluorinated biphenyl compounds.

The success of the doctoral research of **Dr. Klaus Adlkofer** in the preparations and characterization of the self-assembled monolayers on GaAs was a solid departing point for this work. Klaus was the person to introduce me to the topic and to all contacts in the university. My honest gratitude to him. Later, **Tom Kaindl** and I continued to broaden the characterization techniques of molecular films on GaAs. Especially to cite are the FTIR measurements and the GID strategy to measure the 2D crystal structure of molecular monolayers at the ESRF in Grenoble. I am very grateful to have shared all these ideas and time with him.

The members of Motomu group cannot be forgotten. Altogether, we formed a solid gang build up from daily struggles and friendship. Here, I would like to acknowledge **Dr. Stefan Kaufmann**, **Dr. Olliver Purrucker** and **Dr. Florian Rehfeldt** and the international Post Doctoral researchers **Dr. Fatima Al-Ali**, **Dr. Andreea Pasc-Banu** and **Dr. Rafael Oliveira** for uncountable tiny things. To **Dr. Fernanda Rossetti**, I also give my thanks for accurately and patiently correcting a big part of this thesis. The PhD students of the group, **Jochen Oelke** and **Thomas Schubert**, who also helped in correcting this thesis, **Emmanuel Schneck**, **Peter Seitz** and **Murat Tutus** are to be said that I have been very glad to have had them as colleagues!

The members of E22 are to acknowledge for the relaxed and fantastic atmosphere. I particularly thank the technicians **Monika Rusp** and **Gabriele Chmel** for their immediate disposition for help at any time.

My sincere and personal gratitude is to **Prof. Dag Winkler** from Chalmers Tekniska Högskola (CTH) in Göteborg, Sweden. Dag was the first person to introduce me to research and who relied on me by opening as many doors as he could.

My Parents and **my brother Abel** deserve my highest thanks. With their unconditional and constant support, I could complete with all my satisfaction this doctoral work.